An Investigation of Thermal Springs throughout Arizona: Geochemical, Isotopic, and Geological Characterization, Arizona Basin and Range Province

Diane S. Love, Brian F. Gootee, Joseph P. Cook
Michael K. Mahan and Jon E. Spencer
Arizona Geological Survey

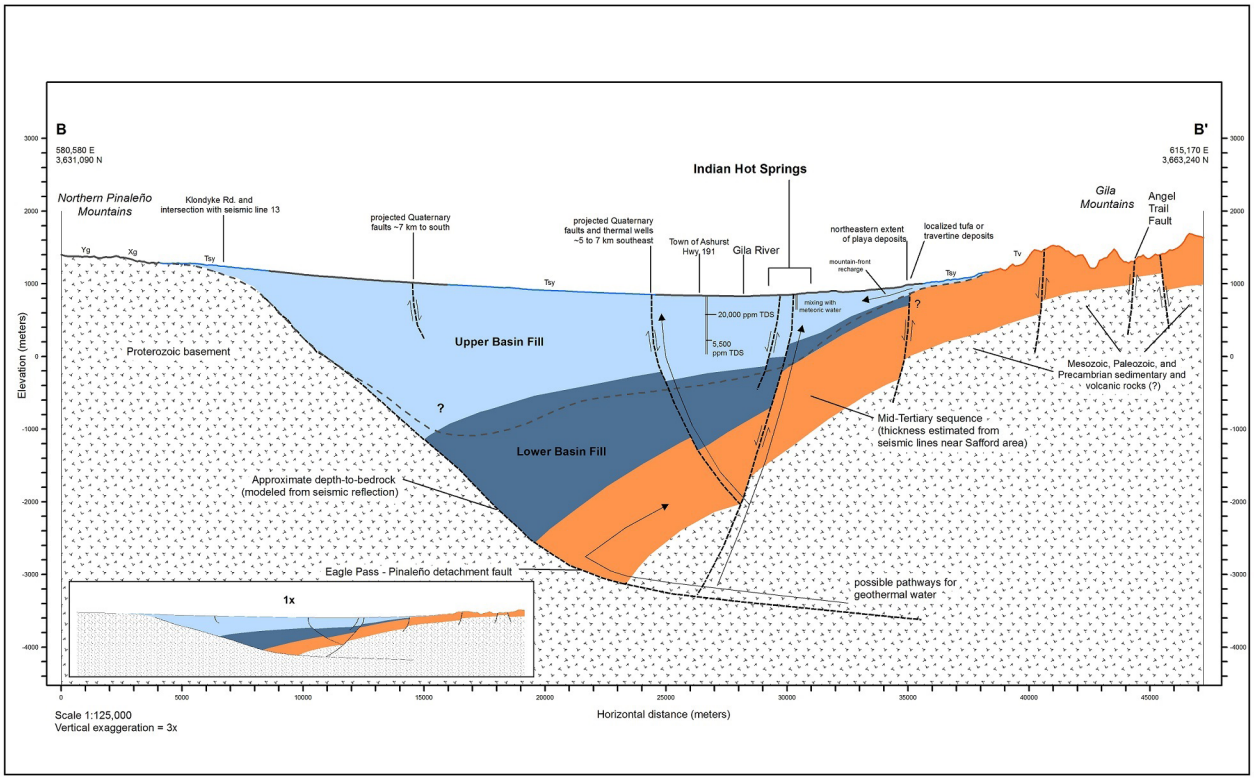

Geologic Cross Section across Safford Basin, Cactus Flat to Buena Vista Hot Springs

OPEN-FILE REPORT OFR-14-06

August 2014

Arizona Geological Survey

www.azgs.az.gov | repository.azgs.az.gov

Arizona Geological Survey

M. Lee Allison, State Geologist and Director

Manuscript approved for publication in August 2014
Printed by the Arizona Geological Survey
All rights reserved

For an electronic copy of this publication: www.repository.azgs.az.gov
Printed copies are on sale at the Arizona Experience Store
416 W. Congress, Tucson, AZ 85701 (520.770.3500)

For information on the mission, objectives or geologic products of the Arizona Geological Survey visit www.azgs.az.gov.

This publication was prepared by an agency of the State of Arizona. The State of Arizona, or any agency thereof, or any of their employees, makes no warranty, expressed or implied, or assumes any legal liability or responsibility for the accuracy, completeness, or usefulness of any information, apparatus, product, or process disclosed in this report. Any use of trade, product, or firm names in this publication is for descriptive purposes only and does not imply endorsement by the State of Arizona.

Recommended Citation: An Investigation of Thermal Springs throughout Arizona: Geochemical, Isotopic, and Geological Characterization, Arizona Basin and Range Province, 2014, Love, D.S., Gootee, B.F., Cook, J.P., Mahan, M.K. and Spencer, J.E., Arizona Geological Survey Open-File Report -14-06, 129 p.

An Investigation of Thermal Springs throughout Arizona: Geochemical, Isotopic, and Geological Characterization, Arizona Basin and Range Province

Prepared by
Diane S. Love, PG
Brian F. Gootee
Joseph P. Cook
Michael K. Mahan
Jon E. Spencer

Arizona Geological Survey
416 West Congress Street
Tucson, Arizona 85701

Prepared for
U.S. Department of Energy
Under the National Geothermal Data System Supplemental Project
Contract DE-EE0002850

June 2014

Acknowledgements

Land owners throughout the project area are thanked for their cooperation and helpfulness and for extending permission to sample thermal wells and springs on private properties and information relating to those hot springs. Thank you goes out to Kathy Gardner representing Potters Ranch; Pat Talley, Mark Sifferman Clark Hill PLC, Dave Headstream CBRE Land Services Group representing Castle Hot Spring; Jerry Cullision property owner of Radium Hot Spring; Elston Grubaugh, General Manager at Wellton-Mohawk Irrigation and Drainage District; Joe Dixon at the Arizona State Land Department; BLM Safford Field Office; Michael Stevens at Eden Hot Springs (Indian Hot Spring); and Phil Wisely for Cofer Hot Spring.

In addition, our gratitude is extended to Bob Rogers and Ron Day of the Mule Shoe Ranch Nature Conservancy for their hospitality; Pima County Natural Resources, Parks and Recreation for allowing sampling at the Agua Caliente Warm well; and the National Park Service for permission to sample at Ringbolt Spring in the Lake Meade Recreational Area.

Special thanks go out to those who assisted with guidance and research information relating to geochemical analysis and data interpretation. Chris Eastoe at the University of Arizona laboratory was instrumental in providing isotopic analyses for Carbon-14, Tritium, and $^{18}O/^{16}O$ and $^{2}H/^{1}H$ isotopes. Alan Rigby at the University of Utah's Dissolved and Noble Gas Laboratory provided analyses for Helium and noble gases and much appreciated insight into gas theory. Diego Hernandez at the Strontium Isotope Lab in the Department of Geology & Geophysics at the University of Utah provided analysis for $^{87}Sr/^{86}Sr$. Turner Laboratory in Tucson, Arizona, provided laboratory services for groundwater general chemistry analyses.

This research was supported by the U.S. Department of Energy's Geothermal Technologies Office an Office of Energy Efficiency & Renewable Energy program, under Award No. DE-E0002850.

Cover Photo: Agua Caliente Regional Park, Tucson, Arizona

Disclaimer: *"This report was prepared as an account of work sponsored by an agency of the United States Government. Neither the United States Government nor any agency thereof, nor any of their employees, makes any warranty, express or implied, or assumes any legal liability or responsibility for the accuracy, completeness, or usefulness of any information, apparatus, product, or process disclosed, or represents that its use would not infringe privately owned rights. Reference herein to any specific commercial product, process, or service by trade name, trademark, manufacturer, or otherwise does not necessarily constitute or imply its endorsement, recommendation, or favoring by the United States Government or any agency thereof. The views and opinions of authors expressed herein do not necessarily state or reflect those of the United States Government or any agency thereof."*

Table of Contents

1. INTRODUCTION 1
Background 3
Objective of Study 4
Previous Investigations in Areas of Interest 5
Basin and Range 6
Clifton-San Francisco River 7
Safford-San Simon 8
Tucson Basin 10
Yuma 11
Transition Zone 11
Colorado Plateau 13
2. PHYSIOGEOLOGY 14
Regional 14
Structure 16
Geology 17
Pre-Cenozoic Rocks 17
Cenozoic Rocks 17
Basin-Fill Deposits 18
3. HYDROGEOLOGY 19
Climate 19
Regional Hydrology 19
Occurrence of Groundwater 19
Groundwater Flow System 20
General Chemical Character of the Groundwater 20
Geothermal Groundwater 21
Variation with Depth 23
4. GEOCHEMISTRY 24
Dissolved Species General Chemistry 24
Light Stable Isotopes 25
Groundwater Geochronology 26

Stable Radiogenic Isotopes 27
Noble Gases 28
5. SAMPLING AND ANALYSES (GENERAL) 30
Permissions and Permits 30
Field Collection Methods 30
Analytical Methods 32
6. GEOCHEMISTRY RESULTS 35
Physical Parameters 35
Major-Ion Geochemistry 36
Cations 36
Anions Chloride, Fluoride, and Sulfate 38
Dissolved Gases 38
Alkalinity 40
Sulfide and Silica 41
Stable Isotope Chemistry 41
Tritium 41
14 Carbon 42
Light Stable Isotopes 45
Oxygen and Hydrogen Isotopes 45
Strontium 48
Noble Gases 50
Helium Dating 50
Other Noble Gases 51
7. GEOTHERMOMETRY 53
Ternary Diagrams 53
Tcsh 54
Tclb 55
Tcfb 56
Tnkm 57
Piper 59
Silica 60

Xkms 61
Xkmc 62
Liquid Geothermometers Report 63
8. GEOLOGICAL MAPPING 65
8.1 Pinaleño Mountains-Safford Basin Geologic Investigation 65
Geologic setting of the Cactus Flat, Buena Vista and Indian Hot Springs, Safford Basin 65
Cactus Flat Hot Springs 68
Buena Vista Hot Springs 71
Indian Hot Springs Area 73
References - Pinaleño Mountains 74
8.2 Geohydrology of Agua Caliente Warm Spring, northeastern Tucson basin, Arizona 77
Introduction 77
Geologic setting 77
Hydrology 77
Agua Caliente Warm Spring 78
Structural Geology of Agua Caliente Hill 79
Catalina detachment fault 81
Conclusion 84
References - Agua Caliente 86
8.3 Geology of Hooker's Hot Spring, Galiuro Mountains, southeastern Arizona 88
Introduction 88
Regional geology 88
Geology of the Hooker's Hot Spring area 89
Geohydrology of the Hooker's Hot Spring area 92
References Cited 94
Appendix. Hooker's Hot Spring map unit descriptions 95
9. DISCUSSION 97
Summary 97
Mapping 97
Characterization of Thermal Springs 99
Clifton Area 100

Safford Area 101
Willcox Area 102
Yuma 103
Kaiser and Cofer Hot Springs 104
Ringbolt 104
Castle Hot Spring 105
Tonopah 105
Agua Caliente Tucson 106
Conclusion 106
10. REFERENCES 108

TABLES

Table 4.1 Helium abundances and isotopic ratios in different reservoirs
Table 5.1 Thermal Spring Locations and Permissions
Table 5.2 Analytics
Table 6.1 Summary of Field Physical Parameters
Table 6.2 Summary of Results for Metals
Table 6.3 Summary of Results for Anions Chloride, Fluoride, and Sulfate
Table 6.4 Summary of Results for Dissolved Gases
Table 6.5 Summary of Results for Alkalinity
Table 6.6 Summary of Results for Sulfide and Silica
Table 6.7 Summary of Results for Tritium in Thermal Springs and Wells
Table 6.8 Summary of Carbon 14 in Groundwater from Select Thermal Springs and Wells
Table 6.9 Dissolved Inorganic Carbon Sources for δ13C in Groundwater
Table 6.10 Summary of Results for δ 18Oxygen and δ Deuterium Isotopes
Table 6.11 Summary of Results for Strontium and 87Sr/86Sr Isotopes
Table 6.12 Summary of Results for Helium Isotopes
Table 6.13 Summary of Results for Other Noble Gases
Table 7.1 Liquid Geothermometry Report (temperatures in degrees C)
Table 8.2.1 Agua Caliente Warm Spring Surrounding Wells and Lithology

FIGURES

Figure 1.1 DOE NGDS Supplemental Project Sample Location Map
Figure 4.1 Strontium isotopes in sedimentary rocks throughout Phanerozoic time
Figure 6.1 δ18O and δD plotted against the SMOW and LMWL trend lines
Figure 6.2 Deviating of δ18O values of Pleistocene and Holocene Groundwater in Arizona
Figure 6.3 Plot of Strontium versus $^{87}Sr/^{86}Sr$ for Springs and Wells in Arizona
Figure 7.1 Tsch – SO_4-CL-HCO_3 Ternary
Figure 7.2 Tclb – Chloride-Lithium-Boron Ternary
Figure 7.3 Tcfb – Chloride Fluoride-Boron Ternary
Figure 7.4 Na-K-Mg Ternary
Figure 7.5 Piper Trilinear
Figure 7.6 SiO2-K/Mg Geothermometry
Figure 7.7 K-Mg-Ca Geothermometry
Figure 8.1.1 Geologic Map of the Pinaleño Mountains and Safford Basin including Cactus Flat, Buena Vista, and Indian Hot Springs
Figure 8.1.2 Geologic Cross Section A-A' Across Safford Basin, Cactus Flat to Buena Vista Hot Springs
Figure 8.1.3 Geologic Cross-section B-B' across Safford Basin, Northern Pinaleño Mountains to Indian Hot Springs
Figure 8.2.1. Geologic map of the southwestern flank of Agua Caliente Hill
Figure 8.2.2. Geologic map of the northeastern corner of Tucson basin
Figure 8.2.3. Cross sections of the northeastern corner of Tucson basin
Figure 8.2.4 Water Wells in the Area Surrounding Agua Caliente Park
Figure 8.2.5. Cross Sections A-A' and B-B' located on Figure 8.2.4 showing geologic structure
Figure 8.3.1. Geologic map of the Hooker's Hot Spring area
Figure 8.3.2. Geologic cross sections of the Hooker's Hot Spring area

APPENDICES

APPENDIX A: NPS IRMA PERMIT AND ANNUAL REPORT

APPENDIX B: Laboratory Reports

APPENDIX C: Summary of Results Tables

APPENDIX D: Powell and Cumming (2010) Geothermometry Workbook

1. INTRODUCTION

Under the Department of Energy (DOE) National Geothermal Data System (NGDS) (Contract DE-EE0002850) Supplemental Data project to discover new geothermal data, the Arizona Geological Survey (AZGS) investigated the geochemical makeup of groundwater from select thermal springs and wells during late 2012 through 2013. In addition, the related geological context was investigated to evaluate potential groundwater transport mechanism(s) and heat source(s) relevant to geothermal energy production. Chemical analysis of thermal groundwater may be used to estimate subsurface temperatures by applying chemical geothermometry techniques, thus attempting to specify reservoir temperatures and to model possible sources of heat. An exploration program that integrates geochemical indicators of aquifer geometry and temperature with geology, geophysics, well targeting and well testing is likely to lower the cost of building sufficient confidence in resource conceptual models capable to commit to a generation capacity and plan well targets for development (Powell and Cumming, 2010). This report is intended to discuss the geochemistry and geology in relation to the select hot springs and wells sampled throughout Southern Arizona. This report presents the data and our interpretation to the extent of our limited understanding of geochemistry and complex factors that contribute to the geothermometry. It is meant to provide data for geothermal experts and others interested in pursuing additional interpretation.

The geothermometry model devised by Tom Powell and William Cumming (Powell and Cumming, 2010) supports many of the common graphic analyses of water chemistry used to interpret hot spring and thermal well groundwater in geothermal exploration and development. The model provides geochemistry interpretative tools with proven value in exploring and characterizing the properties of both volcanic and forced-convection geothermal reservoirs. Cross-plots and ternary diagrams are generated from measured concentrations of chemical species using formulas based on equilibrium reactions and empirical relationships. These geochemistry interpretation tools help integrate geothermal geochemistry with geoscience data in building resource conceptual models directed at geothermal exploration and development (Powell and Cumming, 2010). The Powell and Cumming geothermometry model was used to interpret geochemistry data collected for this project. The report summarizes our findings and presents supporting data in various tables and ternary diagrams.

The investigation field work was divided into two parts for data acquisition:

1) Investigating thermal groundwater at 20 proposed hot springs throughout Arizona to acquire new geochemical, isotopic, and temperature data; calculation of water geothermometry based on analyses; and, speculation on a model for heat sources.
2) Construction of a detailed geologic map at three locations–Agua Caliente Warm Spring Park, Hooker's Hot Spring, and the eastern Pinaleño Mountains-Safford Basin region to define potential thermal water transport mechanism(s) and heat source(s); construction of geologic cross sections; and, speculation of geologic context of geothermal heat source(s).

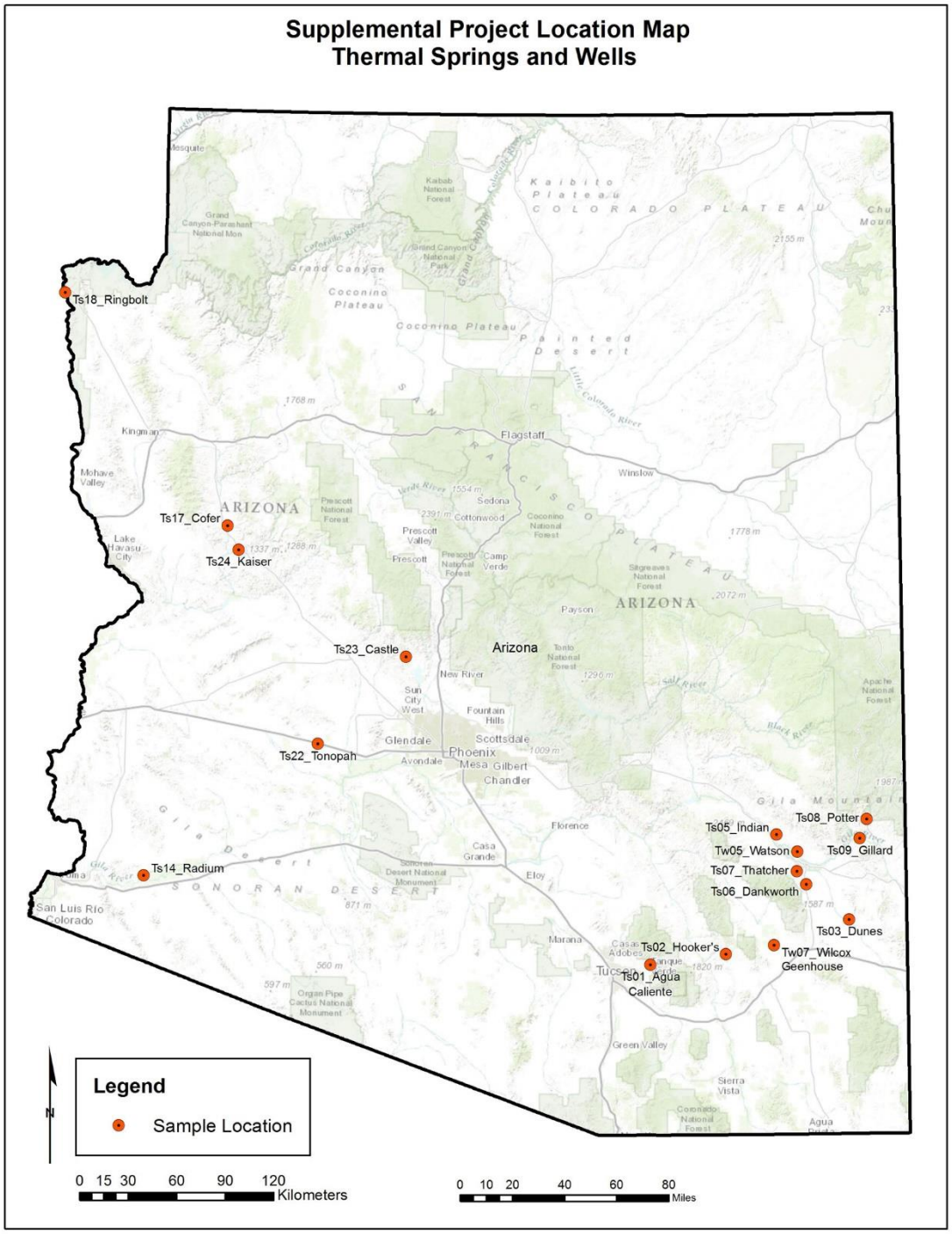

Figure 1.1 DOE NGDS Supplemental Project Sample Location Map

The AZGS identified 20 thermal springs and related wells with historical data indicating temperatures above 35°Celsius (C) at which to collect groundwater samples for geochemical and isotopic analyses. Only 16 springs and wells were actually sampled (Figure 1.1), several were dry, and one secluded thermal spring was eliminated where access time and budget prohibited inclusion.

The AZGS reviewed existing reports on the geologic setting surrounding thermal springs in Arizona to evaluate potential geothermal source scenarios and identify springs that might reflect thermal attributes for an area. Previous reports for these areas were reviewed to provide insight into the geothermal resource. Geochemical and isotopic analyses along with measured physical parameters provided data required for most geothermometry models, while the geological map surveys and field investigations were used to evaluate faulting as a potential groundwater transport conduit from deep-seated heat sources. Appropriate analytics were chosen to incorporate results into the Powell and Cumming geothermometry modeling workbook (Powell and Cumming, 2010).

Background

The earliest known work devoted solely to thermal water was U. S. Geological Survey Bulletin 701, "Geothermal Data of the U. S." by Darton (1920). About that same time, the first papers were published on Arizona hot springs. Everit (1925) wrote about Clifton hot springs; Buehrer (1927) wrote about Castle Hot Spring; and Knechtel (1935) about Indian Hot Spring. In 1937 Stearns, Stearns, and Waring (1965) compiled "Thermal springs in the United States" which was revised and expanded nearly 30 years later. Between the mid-1930s and the mid-1960s, only a few heat-flow and geothermal studies were published in the United States. Basic heat-flow research was carried out the latter part of this period, but it was not done specifically to aid geothermal exploration (Witcher, 1982).

Publications related to thermal waters of Arizona did not appear until the late 1960s and after. Haigler (1969) listed 32 selected thermal springs and wells in Arizona in a volume devoted to the mineral and water resources of the state. Wright (1971) was the first to examine in some detail the thermal waters of southern Arizona. He concluded that occurrences of thermal springs and wells are related to structural elements of the Basin and Range province. Other early papers were written by Harshbarger (1972); Norton and Gerlach (1975); Norton, Gerlach, DeCook, and Sumner (1975); Dellechaie (1975); and Swanberg, Morgan, Stoyer, and Witcher (1977) (Witcher 1982).

Efforts to explore and develop high-temperature geothermal resources (capable of power production) began in the Southwest in the early 1970s after the first energy crisis. In response to the American involvement in the Yom Kippur War in 1973 in the Middle East, the Organization of Arab Petroleum Exporting Countries (OAPEC) reduced their petroleum production and proclaimed an embargo on oil shipments to the United States and the Netherlands, the main supporters of Israel. The embargo and OAPEC limitations on oil production sparked an international energy crisis. Americans faced high price hikes and fuel shortages, causing lines to form at gasoline stations around the country. A revived interest in geothermal energy occurred in 1977 when the search for low- to moderate-temperature

geothermal resources got underway in Arizona. Funding for this work came from the U. S. Department of Energy, Division of Geothermal Energy, and for two concurrent years from the U. S. Department of Interior, Bureau of Reclamation (Witcher, 1982). A comprehensive report was published by Witcher and Stone (1982) to bring together in a single volume current knowledge and basic data on geothermal energy resources in the State of Arizona. Since that time, numerous other works were published by Witcher and Stone, and others throughout Arizona. Most of these reports and data are available electronically through the AZGS and the National Geothermal Data System (NGDS).

Interest in developing geothermal resources has re-emerged in recent years with new projects proposed and new drilling performed. In 2010, the DOE provided funding through the AASG NGDS Supplemental Data project to collect new data through field investigations to identify geothermal resources throughout the U. S. in an effort to produce clean energy and reduce fossil fuel reliance. The DOE set priorities for power plant development, on-site electrical production (aka distributed generation), and direct-use applications (focusing on space and district heating for cities). Under the AASG NGDS project, existing and new geothermal data from all 50 states were brought together and exposed through the NGDS for worldwide internet access.

Arizona currently utilizes low and intermediate temperature geothermal resources for Aquaculture, greenhouses, recreation, district heating, and space heating. Although geothermal hot spring resorts and spas have operated in Arizona for decades, the utilization of geothermal resources are rather modest considering Arizona's overall energy use. Potential geothermal resources can be found throughout the Basin and Range Province in southern Arizona, where expressions of geothermal anomalies are exposed at the surface as warm to hot springs and thermal wells with temperatures exceeding 35 degrees Celsius (°C) [100 degrees Fahrenheit (°F)] in select areas. Over 45 thermal springs have been identified throughout central and southern Arizona. Thermal springs in Arizona are defined as having temperatures at least 10°C above mean ambient air temperature (MAT) for warm springs and wells (Druit, 1976), and 15°C above MAT for hot springs and wells.

Objective of Study

The main focus of this project is to provide additional new geochemistry data for potential geothermal sources and to investigate related geology in three areas where thermal water surfaces as hot springs in the Basin and Range Province in Arizona. All data will be made available online for open access. Thermal groundwater from springs along the basin margins may be transported from deep Paleozoic bedrock through faulting, or fractures and joints associated with fault zones, from deep basin aquifers by circulation, convection, or a mixture of both processes. Specific suites of geochemical analyses combined with isotopic analysis can indicate probable origin(s) for deep sources of thermal waters. Since many of the thermal springs selected are for the most part separated by significant distances, or in some cases are within the same basin, each case will be discussed on either an individual basis or as a

group within a common reservoir system. Geologic context is approached in the same manner and discussed with the associated thermal spring(s).

In addition to groundwater, surface geology and structure were investigated at three locales with hot spring activity to better understand the geologic context associated with thermal waters in southern Arizona. Increased permeability within fault systems provides conduits for circulation of geothermal fluids. Future geothermal development depends on precise and accurate location of such fluid flow pathways in order to assess geothermal resource potential and increase the likelihood of drilling successful geothermal wells. A geothermal analysis to locate potential geothermal fields would look for 1) fault zones that are ideally oriented for slip or dilation under ambient stress conditions, 2) areas with a high spatial density of fault intersections, and 3) lithologies capable of supporting dense interconnected fracture networks. Areas in which these characteristics are concomitant with both elevated temperature and fluids are probable upflow zones where economic-scale, sustainable temperatures and flow rates are most likely to occur (Siler, 2014).

During this investigation, the geology of the following three areas was investigated:

- Along the southeastern Catalina Mountains metamorphic core complex and detachment fault in the area of Agua Caliente warm spring (temperatures <50°C) along the basin margin;
- The complex geology of a young volcanic zone abutting Hooker's Hot Spring (temperatures > 50°C) where basin fill is faulted against bedrock; and
- Areas of enhanced recharge along the eastern Pinaleño Mountains and the western Safford-San Simeon Basin to document facies changes and faulting that may favor discharge of thermal waters. The contact between the Safford Basin and the Pinaleño Mountains to the west is associated with a lineament and fault zone that is not well understood. The Safford area is known for its numerous hot springs.

The purpose of this report is to present groundwater chemistry data results for select springs and attempt to define the structural geometry providing a potential mechanism of transport for thermal groundwater at Agua Caliente Warm Spring, Hooker's Hot Spring, and the Pinaleño-Safford area hot springs.

Previous Investigations in Areas of Interest

In a lineament study by Lepley (1978), it appeared that the northeast (N40-60°E) striking lineaments have a significant relationship with areas of high geothermal potential. Field observations in the volcanic field immediately west of Springerville, Arizona, tend to support the importance of this northeast direction. Cinder cones appear to be aligned along relic fissure vents striking N40-45°E (Hahman, 1978). Another apparently important lineament direction is N40-45°W. Favorable geothermal energy areas seem to occur in the vicinity of intersections of the northeast and northwest lineaments. The

geothermal anomalies could result from favorable ground reparation of the basement complex. These lineament intersections could have numerous, deeply penetrating fractures extending considerable depths into the earth's crust. Groundwater in the intermontane basins could easily circulate to great depths, become heated, and rise along these fractures. This action would cause cycling of the groundwater in aquifers, creating a convection cell or cells similar to one inferred in the Tucson Basin (Witcher, 1982).

Basin and Range

Hahman (1978) investigated the development of successful economic exploration techniques for the location, evaluation and development of low- to moderate-temperature geothermal resources for use by the general public and private industry. The program compiled and published a comprehensive geothermal energy resource map of the state of Arizona, 1:500,000 scale. Most of the favorable areas on this map were situated in the Basin and Range physiographic province. Preliminary investigations indicated that low- to moderate-temperature geothermal energy would be available for use at most of the populated areas in the Arizona Basin and Range province (Hahman, 1978). The resulting geothermal map produced from this effort was the initial attempt to present the knowledge to date (1978) on the geothermal energy potential of the State of Arizona. Water geochemical geothermometers are reasonably accurate at designating the minimum range for the geothermal reservoir temperatures—the result of mixing of non-thermal water with thermal water prior to the water reaching the sample site. Measured thermal gradients were considered the most accurate (Hahman, 1978).

Giardina and Conley (1978) conducted a survey of records from numerous thermally anomalous water wells in the southern portion of the Basin and Range province of Arizona that indicated most of these wells are less than 300 meters (m) deep. The temperature and depth data of most of the shallow wells produce abnormally high computed thermal gradients that are inconsistent with considerably lower gradients in deeper wells. Thermal water moving vertically from deep-heated crustal rock along faults into Tertiary, Quaternary, and Recent sediments and then moving outward horizontally in these sediments from fault zones, appears to be the most probable mechanism effecting the identified thermal gradient anomalies. A significant number of these anomalies appear to have thermal gradients potentially adequate for non-electrical energy uses. Those portions of aerially large anomalies exhibiting abnormally high gradients equal to or greater than 60°C/km below the shallow alluvial Cenozoic sediments, may be closest to fault zones emitting thermal water. Localities containing such sites offer some degree of selectivity for initial geological, geophysical, and geochemical exploratory programs designed to evaluate the geothermal energy potential.

Specific parameters relating to the source of heat and the mode of occurrence of the identified thermal gradient anomalies remain speculative; however, a synthesis of conclusions derived from geology and geohydrology studies (Hahman, 1978; Hem, 1970) indicate that the most probable sources of the shallow heat concentrations found in the Basin and Range province may be summarized as follows:

1. Upward convection of thermal water along fault zones; primary source of heat not known but possibly due to heated shallow crust.
2. Heat generated by late Quaternary dikes and sills intruded into Cenozoic sediments.
3. Heat produced from the exothermic hydration of anhydrite within basins containing extensive evaporite deposits.

Thermal water is closely associated with major fault zones (Hahman, 1978; Waring, 1965). Stearns and others (1937) believe that thermal springs throughout the entire Basin and Range province are closely associated with major fault lines. Hem (1970) suggested that the hot springs and wells in the Coolidge Dam area result from ground-water movement along faults in the Tertiary and Pleistocene valley-fill deposits (Giardina and Conley, 1978).

Witcher and Stone (1982) published a single volume, then current knowledge (as of 1982), and basic data on geothermal energy resources in the State of Arizona. Their thorough report covered background and historic data for specific areas of investigation, thermal aspects of Arizona, and exploration methods.

Clifton-San Francisco River

The lower San Francisco River area lies in the transition zone on the southern margin of the Colorado Plateau and extensive Quaternary basaltic volcanism associated with high regional conductive heat flow (>2.0 HFU) (Witcher, 1981b). The structure in the Clifton area is dominated by two regional, northwest- and northeast-striking fault sets. Numerous dikes, intra-formational shear zones and breccia zones are found in the area. Most of these features follow the northwest-northeast structural fabric of the area. Controlled Source Audio-frequency Magnetotelurics (CSAMT) cross-sections were performed in 2007 by Zonge Engineering of Tucson, Arizona. The results of their work confirmed the presence of a major, previously unmapped fault on the east side of the San Francisco Canyon, in the area of the Clifton hot springs orifices and other thermal features, and a number of other smaller paralleling faults, both synthetic and antithetic to the major fault. The structural interpretations from the geophysics by the Zonge team confirmed the detailed outcrop mapping by David Brown & Associates. It appears this fault has formed a keystone graben under the San Francisco River, controlling the local geothermal system (Brown, 2007). Work performed during 1950s-1970s indicated the total thermal flow into the San Francisco River could be over a thousand gallons per minute (Brown, 2007). There are many springs in the basin, most of which discharge less than 100 gallons per minute. One spring, about 10 miles northeast of Clifton, discharged around 200 gallons per minute (gal/min) (Mann, 1980). Most springs issue from the contact between basalt flows or underlying silt and clay deposits. Insufficient data exists to determine whether a continuous groundwater system exists or if the area is made-up of several discontinuous systems.

Where the Gila River cuts through the Gila Mountains southwest of Clifton, lies Gillard Hot Spring, reported to be the hottest spring in Arizona, at 80° to 84°C (Witcher, 1981a). The output of hot, saline water from the springs (TDS 1200-1500 mg/l) is sufficient to raise the temperature of Gila River water about 2°C (3.6°F), and raise the chloride content of the river from 25 mg/l upstream from the springs to 30 mg/l below the springs (Hem, 1970; Witcher, 1981a).

Eagle Creek Hot Springs may be on the same fault zone as Clifton hot springs (Witcher, 1981a). Eagle Creek springs discharge water at about 42°C of a mixed sodium bicarbonate-chloride type.

Safford-San Simon

The crust of southeast Arizona is highly anisotropic and is dominated by a west-northwest to northwest structural grain which is superimposed on an older northeast grain (Swan, 1982 and Silver, 1978). This anisotropicity originated during the Precambrian. During the Mesozoic, probable reactivation of west-northwest structures (Titley, 1976) may have uplifted the Mogollon Highland (Coney, 1978, Turner, 1962, Elston, 1958). Significant erosion during that same period removed Paleozoic and pre-late Cretaceous rocks to expose Precambrian basement (Elston, 1958), consisting of the Pinal Schist and large granitic batholiths (Silver, 1978). The Safford area lies astride the Mesozoic Mogollon Highland. (Witcher, 1982).

The Safford basin, in Graham County, contains at least four proven and potential geothermal reservoirs of less than 1.2 km depth and three inferred moderate- to high-temperature reservoirs less than 2.5 km depth (Arizona Geothermal Commercialization Team, 1979). Studies by Witcher (1979b, 1981a,b, 1982) and Hahman and others (1980) focused on characterizing the nature and extent of geothermal anomalies in the Safford area (Harris, 1998). One of the surface manifestations of geothermal reservoirs is the presence of hot springs and hot artesian wells. The relation of natural hot springs and hot wells to water quality in the upper Gila River was discussed in Harris (1998).

Indian Hot Spring, northwest of Safford, produces about 1000 liters per minute of water at 45 to 48°C (Witcher, 1981a). The water is a sodium chloride type and travertine (calcium carbonate) deposits are present at the springs. TDS ranges from 2,570 mg/l to 3,004 mg/l. A high level of sulfate in the spring water indicates the presence of gypsum in the sediments. Indian Hot Spring is on an alignment of faults trending NW on the north side of the Gila River flood plain. This zone of faulting extends from Bylas to northwest of Safford and is thought to be responsible for an alignment of hot springs and hot wells in that area (Witcher, 1981a). Traces of fault segments and associated deformation of sedimentary units are exposed at several localities (Houser, 1990; Houser and others, 1985).

Several thermal wells have temperatures > 30°C near Buena Vista (northeast of Safford). One of these is known to have artesian flow at about 800 gallons per minute (gpm). The 49.5°C water discharges from around the base of a pump installed over a 24-inch surface casing. Another artesian well northwest of Safford and north of Thatcher flows at an estimated 500 gpm at 43.5°C from an open surface casing. A

shallow geothermal resource at 30 to 50°C is found in a basin-fill reservoir of sand and gravel to 215 m depth beneath Buena Vista. The top of the reservoir is formed by a confining clay and silt unit whose base ranges from 105 m deep at Sanchez Monument to less than 46 m deep northeast of the Monument near the Gila River. Apparently this thermal water originates from upward leakage along fractures and structure in an underlying bedrock structural bench.

A study of soil mercury anomalies in western Safford Basin, frequently associated with high temperature hydrothermal systems (>150°C), was conducted in an area having wells with anomalous temperatures to delineate the extent of the anomaly, identify potential structure control of a probable convective system, and test the applicability of soil mercury on a probable low temperature (<100°C) geothermal system. These mercury anomalies overlie a major fault zone interpreted from seismic-reflection surveys (Kruger and others, 1995). An inferred structural intersection of northeast-trending basement faults (lineations) with the high angle basin-bounding fault zone coincided with the elevated soil mercury levels and heat flow anomalies. The highest soil mercury anomalies trend east-northeast suggesting structure control with that orientation. Repetitious Pleistocene faulting on the fault zone may have created and sustained open fracture permeability at depth. All the above factors point toward a hydrothermal convection system possibly controlled by basement structure (Witcher, 1982).

The Pinaleño Mountains, a mid-Tertiary metamorphic core complex (Davis and Coney, 1979), defines the western boundary of the Artesia area in the Safford Basin. This range reaches an altitude over 3,000 m (10,000 feet) and receives significant precipitation (>76.2 cm/year). The impressive mountain front is dissected by several linear canyons which are deeply eroded into gneiss and mylonitic gneiss. These canyons coincide with major northeast striking fault zones displaying minor left-lateral strike-slip movement (Thorman, 1981). Mylonitic foliation in the gneiss dips gently north to northeast near the base of the Pinaleño Mountains and it dies out rapidly into the range (Thorman, 1981). A large displacement high angle Basin and Range fault zone is interpreted from gravity data by Wynn (1981). This fault zone forms the western boundary of the Safford basin, which may contain up to 3 km (Oppenheimer and Sumner, 1981) of post mid-Miocene basin filling sediments (Scarborough and Pierce, 1978). Pleistocene tectonic activity along the fault zone is observed in multiple and composite fault scarps displacing Pleistocene geomorphic surfaces up to 30 m (Morrison and others, 1981). A faulting re-occurrence interval of 100,000 years was estimated by Menges and others (1982) (Witcher, 1982).

While a low angle fault is not observed in the Pinaleño Mountains adjacent to Artesia, outcrops of mylonitic gneiss at the base of the Pinaleño Mountains suggest that a fault is preserved in the Safford basin basement. A mid-Tertiary age for cataclasis of the gneiss is unconfirmed (Thorman, 1981), but low-angle Miocene faults are observed at Eagle Pass (Blacet and Miller, 1978) and near Gillespie Mountain (Thorman, 1981) on the northwest and southeast ends, respectively, of the Pinaleño Mountains. (Witcher, 1982). Because the Pinaleño Mountains are a metamorphic core complex, a low angle fault, overlain by highly deformed pre-Basin and Range tectonism (pre-late Miocene) rocks, is tentatively

inferred in the Safford basin basement. Such a fault zone may contain significant fracture permeability and may receive recharge from the Pinaleño Mountains via northeast trending basement fault zones.

The residual aeromagnetic map of Arizona (from Sauck and Sumner, 1974) illustrating major geophysical lineaments shows that only one out of 15 thermal springs is located farther than 30 km from major geophysical lineaments (Witcher and Stone, 1983). The single exception, Hookers Hot Spring, lies astride the Morenci lineament. The apparent association of hot-spring activity with aeromagnetic linears is probably not coincidental. These aeromagnetic anomalies probably represent ancient, deep-seated crustal structures that allow deep flow of ground water (Witcher and Stone, 1983).

Tucson Basin

The Tucson Basin is a single intermontane basin in the Basin-and-Range Province of southeastern Arizona. The basin is a northwest-trending, alluvium-filled valley surrounded by mountain ranges. These mountains are underlain by the Catalina core complex, which is one of dozens of metamorphic core complexes in the North American Cordillera. Coney (1980a) described metamorphic core complexes as "a group of generally domal or archlike, isolated uplifts of anomalously deformed, metamorphic and plutonic rocks overlain by a tectonically detached (faulted) and distended unmetamorphosed cover." Metamorphic core complexes consist of a heterogeneous older metamorphic-plutonic basement overprinted by lineation, foliation, and gneissic fabrics (Coney, 1980b), faulted, and generally overlain by younger basin sedimentary rocks and volcanics.

The Catalina detachment fault separates ductile deformed gneissic rocks of the lower plate from brittle deformed plutonic and sedimentary rocks of the upper plate. The fore-range rises from the basin to mid elevations; it consists of foliated lineated gneiss and is dissected by numerous canyons and ridges. These features are thought to correspond to antiforms and synforms, i.e., to undulations in the surface of the Catalina fault (Dickinson, 1991). Detailed study of rock types, folding, faulting and joints across the Catalina Mountains indicates numerous faults, folds, and joint patterns (Peterson, 1968; Suemnicht, 1977; Janecke, 1986; Young, 1988). Several large scale lineaments have been inferred that are probably fractures, both parallel and transverse to lineation in the gneiss. Faults and fractures are potential conduits for downgradient movement of recharge water and upwelling of thermal waters.

Olson (1982) and Morbacher (1984) used chemical and isotopic data in groundwater in the foothills of the Santa Catalina Mountains to distinguish two mechanisms of mountain-front recharge. These studies identified two isotopically and chemically distinct classes of groundwater. Both studies suggested that one class receives recharge from the infiltration of mountain streams at the basin margin, and the other class received recharge directly from fractures in the crystalline mountain mass (Olson, 1982; Mohrbacher, 1984). The two classes of water were mapped with relation to the global meteoric water line which represents the relationship between hydrogen and oxygen isotope ratios in natural terrestrial

waters, expressed as a worldwide average. The spring waters data plotted above the line and more closely resembled the deeply circulated, fracture-flow water of previous studies.

Yuma

Stone et al. (1980) conducted a preliminary assessment of the Yuma area geothermal potential. The Yuma study area is located in the extreme southwest corner of Arizona. The Yuma area contains three separate ground-water reservoirs, the Fortuna Basin, the San Luis Basin, and the Yuma Trough. The Yuma study area (Stone, 1980) falls within the Mojave-Sonora Megashear (Anderson and Silver, 1979).The basins and ranges are superimposed over the 150+ km wide megashear with California and Arizona basins and ranges paralleling the trend of the earlier structure. Gravity highs in the Fortuna Basin, magnetic highs, and fault trends coincide with the above-normal temperature gradients, thus providing specific targets for more definitive exploration. Because of intensive ground-water studies and nuclear power plant siting studies in the area, data on subsurface conditions for this area are much more extensive than for most basins in Arizona. There are at least 35 wells with recorded discharge temperatures in excess of 30°C, even with extensive infiltration of irrigation waters. Temperature gradient studies are also hampered by the mixing of irrigation water with groundwater (Stone, 1980).

Proximity of the Salton Trough to the Yuma area makes this a favorable geothermal area. The strong northwest structural trend through this area is seen in the lineaments and in the gravity and magnetic maps. This trend is a reflection of involvement in the Gulf of California-Salton Trough system, an active transform fault system along two major plate boundaries to the west and southwest of Yuma. It is possible that active tectonism of the Salton Trough-Gulf of California system periodically reactivates fracture permeability in the basement, allowing convective transfer of heat to shallow depths, and thick insulating basin-fill sediments permit the accumulation of this heat energy (Stone, 1981). Extensive irrigation and pumping practices have resulted in extensive infiltration of irrigation waters mixing with groundwater in the Yuma area to such an extent that variations in chemical composition are useless in detecting geothermal fluids that may be leaking upwards from a deep reservoir (Stone, 1980). Published and estimated heat flow from the periphery of the Yuma area is normal for the Basin and Range Province. These values may or may not be indicative of heat flow throughout the entire region. Presently, the only positive indication of a potential geothermal resource in the Yuma area is the occurrence of an area of high thermal gradients coincident with a fault-bounded horst block and a "warm" anomaly (Stone, 1981).

Transition Zone

The boundary of the Mojave section of the Basin and Range Province in northwest Arizona is arbitrary, but in general lies between the Bill Williams River-Lake Alamo-Santa Maria River to the south and the Colorado River to the north. The Mojave section is within a transition zone that has characteristics of both the Basin and Range and the Colorado Plateau. Most of this transition zone resembles the Basin

and Range geology because it has incurred volcanism and igneous intrusion. Prior to mid-Tertiary volcanism and plutonism, the Mojave section was structurally high. Precambrian basement consists of predominantly Precambrian granitic to granodioritic gneiss, which intrude high grade metavolcanic rocks (Witcher and Stone, 1982). Kaiser Hot Spring, Cofer Hot Spring, and Ringbolt Hot Spring below Hoover Dam are located in the Mojave section.

Kaiser Hot Spring discharges from a 25 m-wide breccia zone striking N45°W. The breccia zone is in Precambrian granitic rocks underlying the silicic flows and flow breccias of the Kaiser Spring-Elephant Head volcanic field (Goff, 1979; Moyer, 1982). Temperatures are reported to be around 37°C.

Castle Hot Spring is the highest temperature hot spring in the Transition Zone northwest of Phoenix (Swanberg and others, 1977). Although the chemistry of the water is similar to other hot springs within the Transition Zone, its purity, high sulfate, and high fluorine (Mariner and others, 1977) are anomalous. The geologic setting of Castle Hot Spring consists of a Precambrian basement of granite and schist that is overlain by Miocene age volcanic rocks. The emergence of Castle Hot Spring and several other related springs is controlled by the fault contact between the basement and volcanic rocks (Sheridan et al., 1980). The generalized stratigraphy of the area consists of Precambrian schist and granitic rocks overlain unconformably by 300-450 m of basaltic lavas and rhyolitic tuffs which are in turn overlain by approximately 120 m of latitic epiclastic breccia and lava flows (Sheridan et al., 1979). Hydrothermal alteration is widespread within the volcanic rocks.

Toward the end of the volcanic cycle, large-scale, NW-trending normal faults formed a series of horsts and grabens. Large listric faults allowed sheets of Precambrian granite to come to rest on top of volcanic rocks along the Castle fault system. This structural setting controls the location of the major high-temperature springs and wells in this system (Sheridan et al., 1980). The thermal system is a steady-state low-temperature hydrothermal resource. Chemical geothermometry and mixing models indicate a maximum reservoir temperature of 100°C. The size of the resource is much more extensive than previously recognized. This regional geothermal system may extend along the entire southeastern flank of the Bradshaw Mountains. The heat source is not well specified, but may be due to a shallow source related to radioactive heating or to an abnormally high geothermal gradient. The information presented favored heating by the geothermal gradient due to deep circulation (Sheridan et al., 1980).

Thermal springs occur on both side of the Colorado River below Hoover Dam. Three springs occur on the east side of the river, including Ringbolt in the Lake Mead Recreation Area, with an estimated composite flow rate of 70 L/sec with individual springs that discharge from 2 to 14 L/sec. Temperatures of the springs range from 32° to 58°C. The springs discharge sodium chloride water from faults and fractures in mid-Tertiary volcanic rocks which comprise Black Canyon (McKay, 1981).

Colorado Plateau

The Springerville area in Apache County was a site-specific target for geothermal exploration on the basis of moderate to high chemical geothermometers, proximity of young volcanics and intersection of regional lineaments defined by the alignment of young volcanics in the White Mountain volcanic field (Stone, 1980). A USGS program focused on the area between Springerville and Alpine. Previous data were reviewed and the geothermal reservoir appeared to be of sufficient magnitude to warrant further evaluation. In the Springerville area, volcanism had been nearly continuous from 32 m.y. to at least 10,000 years ago. Rock chemistry showed that volcanic activity occurred in three distinct pulses, suggesting renewed episodes of partial melting in the mantle. The cause of periodic melting events is unknown, but is probably related to global plate tectonics. Geochemical evidence, locally anomalous silica concentrations in the groundwater indicative of high heat flow, supported the probability of a geothermal resource in the Springerville area. Geophysical surveys indicated that a mantle upwarp or shallow, low-velocity zone exists beneath the area. Aubele and Crumpler (1978) placed a lower age limit of >10,000 years on all volcanism in their study area. Crumpler confirmed the suspected WNW and NE orientation of fissures and the alignment of cinder cones along the fissures. Lineaments intersect in the White Mountain volcanic field and undoubtedly have a dynamic influence on continuing magma generation and volcanism in the region.

2. PHYSIOGEOLOGY

Regional

The state of Arizona is divided into two main physiographic provinces divided by a transition zone. The Colorado Plateau province lies across the northeast portion of the state. The landforms that characterize this province are broad plains, plateaus, buttes and mesas. These features have been formed by differential erosion of resistant and nonresistant sedimentary rocks. The Basin and Range province covers the southwest portion of the state. The complex lithologies and overall structure of the Basin and Range province are the result of a long history of tectonic activity that commenced during the Precambrian, over one billion years ago. The physical features visible today— north, northwest and northeast trending mountain ranges and sediment-filled intermontane basins—are the result of the most recent complex tectonic activity that commenced approximately 14 million years ago and may continue in some places. The Colorado Plateau, when compared to the Basin and Range, is tectonically stable (Hahman, 1978).

The Basin and Range disturbance in late Cenozoic was responsible for the formation of the modern landscape of Arizona. The Basin and Range disturbance was the latest in a series of tectonic episodes that have deformed the region since the late Mesozoic era. During the Laramide orogeny, spanning from late Cretaceous to early Eocene, northeast-southwestward directed compression resulted in folding, thrust faulting and basement uplift (Drewes, 1976, 1978; Davis, 1978). Intermediate to silicic volcanism and plutonism accompanied compression. Many Laramide plutons contain significant disseminated copper-molybdenum mineralization. The region was quiescent from the end of the Laramide orogeny, from 50 m.y. until the beginning of the Oligocene at about 38 m.y. (Damon and Mauger, 1966; Livingston and others, 1968; Damon, 1968; Epis and Chapin, 1975; Gilluly, 1956; Hayes, 1970). Detritus from eroded "Laramide" mountains formed the lower members of the Pantano Formation and other early to middle Oligocene, coarse-grained, clastic deposits found throughout the region (Shafiqullah and others, 1978).

Since the beginning of the Oligocene, the region has been subjected to three episodes or stages of tectonism (Shafiqullah and others, 1976; Damon and others, 1978). The first Stage, a period of heating and crustal melting, lasted throughout the Oligocene and was characterized by intermediate to silicic volcanism, emplacement of granitic plutons, and evolving cauldron complexes. The Stage 1 volcanic rocks range in composition from rhyolite to diorite. Stage 2 covers the 12 m.y. transition between the magmatism of Stage 1 and rifting of Stage 3. Stage 2 represents a transition from silicic to basaltic volcanism during a time of complex tectonism. This stage also involved a shift from thin-skin rotation of the crust to continental rifting. Stage 3, the Basin and Range tectonic event, encompasses the last 12 m.y. ending approximately 6 m.y. in Arizona, during which thin, brittle crust was rifted. This stage is also characterized by mantle-related basaltic volcanism. The Basin and Range tectonic event is still in progress and is characterized primarily by basaltic volcanism (Shafiqullah and others, 1978).

Stage 1 magmatic activity progressed from small eruptions of intermediate composition lavas to massive effusions of rhyolitic ash-flow tuffs over hundreds of square kilometers. Much of southeastern Arizona was blanketed with such flows from eruptive centers in the Chiricahua Mountains (Marjaniemi, 1968), the Tucson-Roskruge mountains (Bikerman, 1968; Eastwood, 1970), the Galiuro Mountains (Creasey and Krieger, 1978), and the Santa Rita Mountains (Drewes, 1972). In the Chiricahua Mountains alone, about 400 cubic kilometers (km^3) of rhyolitic lavas and ash-flow tuffs were erupted from either cauldron complexes, fissure systems or isolated vents. The Turkey Creek caldera in the Chiricahua Mountains is the best exposed and described of these complexes (Marjaniemi, 1968). This caldera is about 20 km in diameter and contains a sub-volcanic pluton. Coarse-grained, granitic plutons were intruded at many places in southeastern Arizona either before or simultaneously with eruption of ash-flow tuffs. In addition, gneissic core complexes such as the Tortolita-Santa Catalina-Rincon Mountains were created or reactivated (Damon et al., 1963; Mauger et al., 1968; Creasey et al., 1977). During Stage 1, the crust was heated in some areas with possible attendant melting and extension. This crustal extension is evidenced by north to north-northwest trending dikes, veins and plutons (Rehrig and Heidrick, 1976) and the inception of low-angle, normal faulting of a similar trend. Other structural adjustments during this stage were primarily local, such as the collapse of calderas and the rise of resurgent domes (Shafiqullah, et al., 1978).

The present-day physiography in Arizona's Basin and Range Province, characterized by mountains and basins, was formed primarily by large-scale normal faulting during the Basin and Range tectonic event 14 to 6 m.y. (Scarborough and Peirce, 1978). Structural movement resulted in a series of upthrown and downthrown blocks throughout a large region in Arizona and nearby States. Block faulting altered previous drainage patterns, and the subsiding areas became depositional sites for locally derived sediments. Concurrent with this faulting, erosion and subsequent deposition of basin fill sculptured the mountains and formed the basins and valleys that now exist. The mountains consist mainly of consolidated intrusive and metamorphic rocks of Precambrian, Mesozoic, and Tertiary age. Volcanic and sedimentary rocks of Tertiary age also are common in many ranges. Volcanic and sedimentary rocks of Paleozoic and Mesozoic age occur in parts of a few ranges, but are less abundant. Most basins in the study areas contain alluvial deposits and volcanic rocks of late Cenozoic age (Wilson et al., 1969).

The study area includes the Basin and Range province characterized by generally north- to northwest-trending mountains separated by wide alluvial basins that form a regional topography of alternating mountains and valleys. Altitudes range from 150 feet (ft) above sea level near Yuma to more than 11,000 ft above sea level in the Central Highlands. Although a common geologic structure prevails throughout the Basin and Range province, physical differences exist between the Central Highlands and the Basin and Range lowlands.

The Basin and Range mountain ranges are small, deeply dissected, and rimmed by large pediments. The valleys in the northwestern and southeastern parts of the Basin and Range lowlands are characterized by long, north-trending valleys and mountains that are approximately equal in areal extent. The valley

floors range in altitude from less than 200 ft above sea level to about 4,000 ft in the Willcox basin in the southeast, with adjacent mountains rising as much as 6,000 ft above the valley floors.

In contrast to the Basin and Range lowlands, the Central Highlands are mountainous and contain shallow intermontane basins that occupy only a small part of the total area. With the exception of Verde and Big Chino Valleys, the basins commonly contain little more than thin sequences of alluvium along stream and river corridors.

Structure

Understanding the structural geology of a geothermal area is important. Most geothermal systems are controlled by faulting. The faults act as both subsurface barriers and subsurface pathways for fluid movement. Hot springs, geysers, rock alteration, and ancient hot spring deposits are usually found associated with faulting. The location of dikes, intrusives, shear zones and breccia zones are also important. These features tend to follow the local structural fabric and can intrude into existing fault zones and provide additional fluid pathways (Brown, 2007). Faults and fractures are also potential conduits for downgradient movement of recharge water. Concentrations of thermal features can commonly be found at the intersection of two or more structural features. Intersecting faults can create stress shadows resulting in open conduits in fault zones that can allow fluids to ascend to the surface, or ascend to an intervening shallow thermal aquifer, where they can be intercepted by a drill hole. Therefore, understanding the structural geology and locating the “thermal” faults are of uppermost importance for successful geothermal exploitation (Brown, 2007).

Structural disturbances resulting in faulting, flexing, erosion, deposition of sediments, and volcanic activity have taken place intermittently and with variable intensity throughout the geologic history of the Basin and Range Province (Wilson and Moore, 1959). Most of the faulting occurred between 30 and 6 m.y. (Morrison, 1969). The alternating mountains and valleys of the province are the result of large-scale faulting. The depression of some blocks and subsequent deposition of detritus derived from adjacent uplifted blocks produced the present day landforms (Giardina and Conley, 1978).

Faulting can create good vertical permeability for deep circulation of water. High-angle faults can displace permeable rocks to sufficient depth for significant heating by normal heat flow from the earth's interior, whereas low-angle faults can displace impermeable rock over permeable rock, creating a "structural trap" reservoir. Low-angle faults in Arizona are frequently characterized by impermeable zones at or near the fault plane that may overlie fractured and permeable rock. Rock geometries resulting from tectonic movement, post and syntectonic sediment deposition, and erosion may create favorable combinations of potential reservoir rocks and cap rocks to form "stratigraphic traps". Similar traps may also form during volcanism where eruptions result in mud flows and impermeable tuff overlying permeable volcanic sequences. Impermeable "cap rocks" are as important as the occurrence of permeable rock. With a cap rock acting as an aquitard, heat will be conserved in a deep reservoir as

leakage out of the reservoir will occur only along vertical fracture zones or faults and limit flows (Witcher, 1981a).

Geology

Pre-Cenozoic Rocks

Pre-Cenozoic rocks present in the Basin and Range major mountain ranges are divided into intrusive, metamorphic, and volcanic rocks. Intrusive rocks of Precambrian age include granite, quartz monzonite, granodiorite, quartz diorite, and locally, gabbro. Metamorphic rocks of Precambrian age include phyllite, mica-schist, chlorite-schist, amphibolite, and gneiss. These rocks are most abundant in the Central highlands and adjacent areas where they partially bound several major basins and are found in the largest ranges having the highest altitudes (Wilson and Moore, 1959). Intrusive and volcanic rocks of Mesozoic age are scattered throughout the central, western, and southwestern parts of the study area. Isolated outcrops of Paleozoic rocks occur in west-central Arizona (Shafiqullah and others, 1980). Sedimentary rocks of Mesozoic age and continental origin are found in southeastern Arizona. The rocks were structurally deformed, intruded by magmas, and overlain by younger sedimentary rocks during the late Mesozoic and early Cenozoic (Paleocene) as a result of the Sevier and Laramide orogenies. Rocks formed during the Laramide orogeny are extensive and include rich porphyry copper deposits in parts of south-central Arizona (Wilson et al., 1969; Shafiqullah et al., 1980).

Cenozoic Rocks

Three major geologic events followed the Laramide orogeny during the Cenozoic Era: (1) the Mid-Tertiary Orogeny, which was accompanied by calc-alkaline volcanism and plutonism and the accumulation of sediments; (2) the Basin and Range disturbance, which was accompanied by andesitic-basaltic volcanism, block faulting, basin formation, and sedimentation; and (3) maximum basin filling, which was followed by minor uplift, river system integration and erosion, and development of terraces along major rivers (Scarborough and Peirce, 1978).

The Mid-Tertiary Orogeny was characterized by crustal melting, plutonism, and extrusion of intermediate to silicic lavas. The volcanic rocks formed during the orogeny are extensive and are predominantly andesitic, rhyolitic, and dacitic in composition. Rhyolitic volcanic rocks form most of the Chiricahua Mountains and parts of the Galiuro and Winchester Mountains in the southeast, the Superstition Mountains area near Phoenix, and the Tucson and Roskruge Mountains near Tucson. Intermediate volcanic rocks, transitional in chemical composition between mafic and felsic rocks, form large parts of the Galiuro and Winchester Mountains and are predominant in the Sand Tank Mountains near Vekol Valley and adjacent areas of the Tohono O'odham Indian Reservation (formerly Papago Indian Reservation) in south-central Arizona (Scarborough and Peirce, 1978.)

Following the Mid-Tertiary Orogeny, thick sequences of pre-Basin and Range sedimentary rocks of Tertiary age were deposited in places. These rocks of continental origin range from boulder conglomerate to mudstone and generally are well indurated. The rocks are moderately deformed, faulted, and tilted and generally are found at the basin margins in fault contact with older and younger rocks. These pre-Basin and Range sedimentary rocks are present in many basins beneath younger less-consolidate basin fill (Laney and Hahn, 1986).

Basin-Fill Deposits

Most of the rocks comprising alluvial basins in the study area were deposited after the Basin and Range disturbance and are Quaternary to late Tertiary in age. The basins were created in response to an east-northeast to west-southwest regional extension field that resulted in a network of north- to northwest-trending horsts and grabens bounded by high-angle normal faults. The subsidence of these grabens and subsequent erosion resulted in late Cenozoic basin-fill deposits that exceed thicknesses of 8,300 ft (Scarborough and Peirce, 1978).

Basin-fill deposits include clastic sediments, evaporites, interbedded volcanic rocks, stream alluvium, and flood-plain deposits. These deposits occur as distinct beds of sand and gravel and as poorly sorted interbedded clayey silt, sand, and gravel, locally interbedded with volcanic rocks. Deposits near the basin margins commonly are fanglomerate or alluvial sand and gravel that grade laterally into silt, clay, and evaporites near the center of the basin. The amount of fine-grained silt and clay deposits and evaporites that lie in basin centers accumulated in internal or restricted drainage environments. Deposition of the basin fill was controlled primarily by tectonic processes. Erosion of up-thrown areas and concurrent deposition of sediments resulted in the basin-ward increase in fine-grained sediments and occurrences of the thick, fine-grained deposits in the deepest structural parts of the basins. The transition from coarse-grained to fine-grained deposits generally occurred near fault boundaries, but vary due to size of the drainage area, amount of precipitation on the drainage area, relief of the depositional area, structural movement, and shifting of the stream channels during deposition. Many places likely abruptly changed from closed to open systems. Development of integrated or through-flowing drainage also influenced grain-size distribution (Robertson, 1991). On the basis of source area, particle size, age, composition, and degree of cementation, the basin-fill deposits are informally divided into three general units: (1) lower basin fill, (2) upper basin fill, and (3) stream alluvium (Pool, 1986).

3. HYDROGEOLOGY

Climate

The climate of the region is semi-arid, with hot, dry summers and mild winters. Temperatures commonly rise to over 35°C during the summer and fall below freezing in the winter. Southern Arizona receives much of its precipitation during the months of July and August when intense, short-duration thunderstorms are common. A rainy period also extends from December to March, and is characterized by gentle rains and cooler temperatures. The driest months are April, May and June. Mean annual precipitation ranges from less than 0.25 ft near Yuma to more than 0.8 ft in the higher altitudes of the central and eastern highlands. Precipitation is highly variable and in any given year may depart greatly from the mean (Robertson, 1991). Alluvial aquifers in the desert southwest are generally thought to be recharged along washes near mountain fronts where precipitation is high. At lower elevations, where precipitation is less intense, evaporation and transpiration are believed to largely restrict groundwater infiltration.

Regional Hydrology

In southeastern Arizona, the regional groundwater flow system closely parallels the direction of the surface-water drainage. Groundwater in areas north and south of the Gila River generally flows toward the Gila and along the Gila River drainage. Groundwater in basins that adjoin the Colorado River flows toward the river, and groundwater in a few individual basins along the international boundary flows southward into Mexico. The intrusive and metamorphic rocks and most of the volcanic rocks that separate the basins, generally, are impermeable and transmit little, if any, water. Where basins are hydraulically interconnected, groundwater moves from the basin of higher altitude to the basin of lower altitude. Basins are hydrologically interconnected where the alluvium overlying the consolidated or other impermeable rocks along groundwater divides is saturated (Robertson, 1991). Most of the basins in the study area are connected hydraulically; only the Willcox basin is internally drained.

Occurrence of Groundwater

Groundwater occurs in the study area in rocks of all principal types: intrusive, metamorphic, and volcanic rocks; pre-Basin and Range sedimentary rocks of Tertiary age; and basin-fill sediments. The water-bearing properties of these rocks, however, vary widely. Well yields range from a few gallons per minute (gal/min) to more than 6,000 gal/min (Robertson, 1991). The water-bearing characteristics of the intrusive, metamorphic, and volcanic rocks are dependent on localized joint fractures and weathering characteristics. In general, well yields of intrusive and metamorphic rocks are limited to a few gal/min. Volcanic rocks, which can be more porous and fractured, may yield more water and serve as local sources, but, like intrusive rocks, their water-yielding properties are generally limited. Volcanic rocks are the source for the municipal water supply for the city of Kingman (Gillespie and Bentley, 1971),

and groundwater flow through fractured volcanic rocks has been reported on the Tohono O'odham Nation (formerly the Papago Indian Reservation) (Heindl, 1967). Although the intrusive, metamorphic, and volcanic rocks generally contain little water, they may indirectly influence the hydraulic conductivity or recharge of the alluvial aquifers. Intrusive granitic rocks are more likely to weather to permeable quartz-rich sandy soils, whereas volcanic rocks are more likely to weather to tight clayey deposits. The weathering process, therefore, may form deposits of differing hydraulic conductivity or deposits that may enhance or preclude infiltration.

Groundwater Flow System

Depth to the water table varies widely throughout the study area, but in all basins is greater near the mountain fronts. Depth to water near the mountains is typically 300 to 800 ft or more and decreases basinwards, partially due to elevation change. Groundwater moves perpendicular to the mountain fronts toward the basin axis, where it either discharges or blends with existing underflow. The hydraulic gradient of the water table resembles that of the land surface, but is somewhat gentler. Groundwater velocities are on the order of a few feet to a few tens of feet per year. Velocities generally are greater near the mountain fronts, where gradients are steeper and permeabilities are higher than those in the interior of the basins (Robertson, 1991).

Groundwater generally occurs under unconfined conditions, but confined conditions may exist where extensive fine-grained facies of the basin-fill deposits are present and form an aquitard. Confined conditions and flowing wells, some of which discharge more than 600 gal/min, are found extensively in the eastern part of the study area in the Safford basin, the Benson area, lower San Pedro Valley, San Bernardino Valley and San Simon Valley. Confined conditions also exist in Verde Valley (Owen-Joyce and Bell, 1983).

General Chemical Character of the Groundwater

The groundwater in the Basin and Range basins, as indicated by dissolved-solids and trace-element content, generally is of suitable chemical quality for most purposes but is not without some problems. Dissolved-solids concentrations range from an average of less than 500 milligrams per liter (mg/l) in 11 of the 28 southern basins to more than 3,000 mg/l in basins along the Gila and Colorado Rivers, and above 10,000 mg/l in the Safford basin. In several basins, the groundwater contains large concentrations of the trace elements fluorine, chromium, arsenic, lead, boron, or selenium that exceed standards established for public supply or certain agricultural uses (Robertson, 1991). In the recent study, *A Summary of Salinities in Arizona's Deep Groundwater* (Gootee, Mahan, and Love, 2012), a total of 270 water-quality well records were retrieved based on a defined salinity criteria. The search identified a total of 22 wells below 800 m depth with salinity greater than 10,000 mg/l total dissolved solids (TDS), 34 wells below 800 m depth with salinity less than 10,000 mg/l TDS, and 214 wells less than 800 m

depth with salinity greater than 5,000 mg/l TDS. Water with salinity above 5,000 mg/l is considered non-potable and not suitable for drinking water.

Geothermal Groundwater

Many reports have been written on research conducted during the 1970s and later on geothermal resources in Arizona. There have been many research efforts throughout Arizona in areas that exhibit geothermal anomalies as thermal springs and wells, each resulting in site specific theories as to heat source, groundwater source, structure, and, when warranted, evaluation of groundwater mixing. Some previous studies pertinent to the study area are summarized below to illustrate different ideas on geothermal groundwater sources and characteristics, but the research studies are by no means limited to these summaries.

Numerous wells in southern Arizona discharge thermal water contained in bedrock, sand and gravel aquifers stacked within, and below extensive silt and clay aquitards. Thermal well and spring groundwater temperatures can range from 30° to 50°C or higher (Witcher, 1982). The often artesian geothermal resource appears to be characterized chiefly by a conductive thermal regime in basin fill sediments, although hydrothermal convective systems apparently exist below the silt and clay in a few areas (Witcher, 1982).

In the Tucson Basin, tritium was measured in groundwater from approximately 30 wells in the early 1990s (Lindquist, 1992). Bomb pulse tritium concentrations were measured up to 14 tritium units (TU) adjacent to the Rillito River and contributing drainages in the basin (Cunningham et al., 1998). In several springs adjacent to the Catalina detachment fault, values range from below detection to 8.2 TU. Pashley (1966) postulated that water rises along the Catalina detachment fault plane. However, the tritium and stable-isotope values do not clearly indicate a common source of water. Along the northeastern edge of the Tucson Basin in the Catalina Mountain foothills, many springs emerge from igneous-sedimentary contacts, but this is not a consistent pattern and the fault contact in many areas is hidden beneath basin-fill. Since tritium data did not correlate well, it was postulated that fractures may be an important control on spring location and age of water. The apparent variation in relative age could be attributed to fractures of varying size, length and orientation.

The use of $\delta^{18}O$ and δD to identify sources of water and altitude of precipitation is well established. In the Tucson basin, summer and winter precipitation have different moisture sources, each with distinctive stable isotope composition. A comprehensive long-term collection of δD and $\delta^{18}O$ data in precipitation and groundwater for Tucson areas corroborates the findings of earlier studies (Kalin, 1994). The weighted average δD values of summer and winter precipitation were –38 and –58 parts per thousand (‰), respectively. Winter δD values clustered between –60 and –80 ‰. Summer values had a much wider range, from –5 to –110 ‰. Several areas within basin groundwater had relatively low δD (–65 ‰) values. Kalin (1994) suggested that in these areas groundwater is derived principally from

mountain-front recharge. Many studies support the hypothesis that winter precipitation is the dominant source of groundwater recharge to the basin, and one study (Kalin, 1994) suggests that areas with relatively low δD values represent areas recharged by mountain precipitation (Cunningham, 1998). Olson (1982) and Morbacher (1984) reported δD and $\delta^{18}O$ in groundwater near the Santa Catalina Mountain front and confirmed a bimodal distribution of isotopic values. Olson (1982) identified two distinctive chemical classes of water, one of which he interpreted as shallow recharge through infiltration of mountain streams, and the other as deeply circulated mountain precipitation. Stable isotopes confirm that these two water types are distinct and support the interpretation of the origin of each water type. Mohrbacher's (1984) interpretation of the source of each water type agreed with Olson's (1982). In addition, he reported $\delta^{18}O$ values in a few spring waters from the Santa Catalina Mountains that were similar to those of the deeply circulated, fracture-flow recharge water (Cunningham, 1998).

Within the Gila River drainage area, several hot springs are known to produce salty water. Clifton hot springs are a typical fault-controlled, sodium chloride dominated system. The hot springs emerge from the bottom and edges of the San Francisco River, where the river has eroded down to intercept hot fluids ascending through fault zones. These springs issue thermal water at temperatures up to 49°C from Tertiary volcanic rocks. Total dissolved solids (TDS) are up to 14,548 mg/l and chloride range from 5,800 mg/l to 6,500 mg/l (Witcher, 1981a). Having very high chloride content is usually a good indicator that there is a hot water resource. Using pre-existing data and industry accepted geothermetric calculations, the predicted geothermal reservoir temperatures range from about 130°C to as high as 180°C. The wide range in chloride contents along with the predicted high subsurface temperatures suggested a fracture controlled and inhomogeneous geothermal reservoir (Witcher, 1979b). The springs were reported as having high magnesium content, presenting problems concerning geothermometry interpretation because the solubility of magnesium carbonates is very low at higher temperatures (Mariner, et al., 1977). Deuterium and chloride data suggested that the spring discharges were mixes of hot and cold water. The preliminary chemical geothermometry studies of the Clifton hot springs pointed toward a high temperature reservoir that is greater than 150°C. Total dissolved solids of 25,000 to 50,000 mg/l or greater are likely in the reservoir (Witcher, 1979c). Eagle Creek Hot Spring, thought to be on the same fault zone as Clifton hot springs, discharges water at about 42°C with TDS < 1000 mg/l. The water is of a mixed sodium bicarbonate-chloride type (Witcher, 1981a).

A group of springs and wells, located between Springerville and Alpine on the Colorado Plateau, have SiO_2 geothermometers in the range of 80°-90°C. Since the average SiO_2 geothermometer for the Colorado Plateau is 53.4°C (Swanberg and Morgan, 1978/1979), and all other SiO_2 geothermometers in the study area cluster around this average, the higher values were distinctly anomalous.

Variation with Depth

The extent of mixing of waters within the aquifers is not known, but the chemistry of waters in the recharge and discharge areas suggest that vertical variations are less important than lateral variations. The variation in the water chemistry within basins appears to be a function more of the flow path than of mixing (Anderson, 1995). Feth et al. (1964) showed that the chemistry of shallow and deep circulating springs could be related to the mineralogy and weathering of surrounding source rocks and to the equilibrium with secondary minerals. Garrels (1967) also used solute ratios to predict compositions of the igneous rocks; however, observed groundwater chemistry of the recharge area did not seem to reflect all aspects of the primary rock composition. Large silica concentrations suggested that hydrolysis of primary silicates is a major process, and, in a slowly fluxing system, the formation of secondary clay minerals would be expected. Analyses of springs also provide indirect evidence of a magnesium carbonate phase. Springs that emerge near recharge areas commonly have compositions similar to recharge waters. Spring discharge waters are often controlled by fault or fracture systems, which may provide a direct route from recharge to discharge, diminishing residence and reaction times. The walls of fracture systems may become coated with precipitates, which can inhibit the reactions of the silicates (Anderson, 1995).

4. GEOCHEMISTRY

Dissolved Species General Chemistry

Water chemistry is used to determine reservoir temperatures (geothermometers) and subsurface physic-chemical processes (boiling and mixing relations). Geochemical tracers are chemically inert, non-reactive, conserved constituents, and once added to the fluid phase, remain unchanged and can be used to infer source characteristics. The tracers commonly used in geothermometry include chloride (Cl), boron (B), rubidium (Rb), cesium (Cs), and helium (He). Geoindicators are chemically reactive, non-conservative species and respond to changes in environment. These are used to infer the physico-chemical processes during ascent of thermal waters to the surface.

Physical parameters, including field pH measurement and sample temperature, are used to determine changes to sample chemistry between field and lab. Conductance, measured in the field and in the lab, is used for quality control since conductance reported in microSeimens per cm (µS/cm) is usually about 100 times the sum of cations or anions (in mg/l) (Hem, 1970).

The following descriptions of dissolved species and their sources are taken from Powell and Cumming (2010). Isotope and Noble gases description sources are as cited.

Calcium (Ca), an alkaline earth, ionizes readily and forms a number of moderately soluble compounds such as carbonates, fluoride, hydroxides, and phosphates. Weathering of plagioclase and dissolution of calcite, and probably dolomite, are widespread sources of calcium in all basins. The ferromagnesian minerals of the pyroxene and amphibole groups are minor sources. Gypsum and anhydrite, although not as widespread, are the most prolific sources where they occur in playas and evaporate bedding.

Magnesium (Mg), also an alkaline earth, behaves geochemically differently from Ca. Mg is not found in feldspars, but is incorporated in ferromagnesian minerals during early crystallization of magmas.

Sodium (Na), together with lithium (Li), potassium (K), Rb, and Cs, is part of the alkali metal group. Na is also found with Ca in silicate minerals. Because of its smaller charge, however, Na does not tend to be incorporated in the higher temperature ferromagnesian minerals. The most widespread source of sodium is the weathering of feldspars. Halite (NaCl), where present in the basin fill, can cause large concentrations of solute sodium.

Potassium (K) forms minerals that are the last to crystallize from cooling magmas. K-feldspar is formed near the final stages of crystallization and is the major source of K in solution. Micas and feldspathoids also contain K and may contribute. Although K is nearly as abundant as Na in the rocks, unlike Na, it is present in groundwater in relatively small concentrations.

Chloride (Cl) is a member of the halogen family. Cl, the ionized form, is enriched in the last fraction of cooling magmatic liquids and vapors; consequently, alkali rocks, pegmatites, volcanic emanations, and hydrothermal solutions are characterized by large concentrations of Cl (Rankama and Sahama, 1950). Ore deposits or hydrothermal deposits are sources of chloride in most basins. Owing to the high solubility of most Cl compounds, particularly halite, the compounds are concentrated in evaporites or playa deposits. Whether they predate the basins or were formed during basin deposition, deposits of halite, if present, are the source of all large magnitude Cl concentrations.

Sulfur (S) has properties of a non-metal and forms binary covalent compounds with metals and oxides with oxygen. In high-temperature volcanic and hydrothermal environments, S is present as sulfides, but when exposed to the atmosphere or oxygenated with water during weathering, the sulfides are oxidized to sulfates. The sulfates are moderately soluble and can be concentrated in evaporites and playa deposits as gypsum ($CaS0_4$-$2H_20$) or anhydrite ($CaS0_4$). These deposits are the sources of large sulfate concentrations found in some basins. Ore deposits or hydrothermal deposits are likely sources of sulfate in most basins.

Carbon (C) is a non-metal. It occurs in the reduced form as methane and organic carbon and in the oxidized form as carbon dioxide. Carbon dioxide (CO_2) is in a stable form where it occurs primarily as the bicarbonate ion in dilute waters. The principal source of carbon is soil-gas CO_2 produced by respiration of plants. Paleozoic carbonate rock may be an additional source.

Silicon (Si) is a metalloid showing properties of both metals and non-metals. Plagioclase, followed by K-feldspar and the ferromagnesian silicate minerals, are the major sources of dissolved silica in the groundwater. Quartz, because of its low solubility, and volcanic glass because of a general paucity in most basin fill, are not major sources.

Light Stable Isotopes

The light stable isotopes (LSIs) of C, hydrogen (H), oxygen (O), nitrogen (N), and S (CHONS) are the most utilized isotopes in groundwater hydrology. Their mass numbers are low and all are stable – being neither radioactive nor daughter products of a radioactive parent (radiogenic). Large mass differences between isotopes in each system, such as ^{18}O and ^{16}O, allow fractionation of isotopes by biogeochemical processes, evaporation, and exchange reactions between water and minerals (Hurst, 2010).

Isotopic Oxygen and Deuterium (D) ($\delta^{18}O$ and δD). Atmospheric water derived from the ocean is depleted in the heavy stable isotopes of oxygen and hydrogen. The isotopic composition of precipitation depends on the fraction of water remaining in the air mass from which the rain or snow is derived, the first precipitation being the richest in heavy isotopes (Ellis and Mahon, 1977). The isotopic ratios of oxygen and hydrogen in water are expressed as differences (delta values) from a seawater standard, the Vienna Standard Mean Ocean Water (SMOW), in terms of per mil (‰). The Vienna SMOW is a water standard defining the isotopic composition of ocean water. Craig (1961) showed that $\delta\ ^{18}O$ and δD

values of normal, minimally re-evaporated precipitation lie along or near the line $\delta D=8*\delta^{18}O+10$ ‰. This line is the global meteoric water line and represents the relationship between oxygen and hydrogen isotope ratios in natural terrestrial waters, expressed as a worldwide average. Precipitation occurring under cooler conditions (at higher latitudes and altitudes) is has lower δD values and plots to the left (above) of the meteoric line. Water that has evaporative loss due to longer exposure at the surface, especially at low humidity, plots to the right of the meteoric line (Gat and Gonfiantini 1981). The use of $\delta^{18}O$ and δD to identify sources of groundwater and altitude of precipitation is well established (Cunningham et al., 1998).

Groundwater Geochronology

Commercially available methods for determining the geologic age of groundwater rely on either tritium (^{3}H) for qualitative ages or radiocarbon dating (^{14}C), if numerical ages are required. Both are cosmogenic – produced by nuclear interactions in the atmosphere – and each has its place in geochronologic analysis of groundwater (Hurst, 2010).

Tritium (^{3}H). Tritium, with a half-life of 12.43 years, decays to Helium-3 (^{3}He). Prior to atmospheric nuclear bomb testing in the 1950s, tritium's natural average concentrations ranged from approximately 2 to 8 TU (tritium units) (Motzer, 2005), but varied with season and location. Above-ground nuclear weapons tests in the late 1950s and early 1960s introduced a large spike of tritium and other radioisotopes into the atmosphere (Eriksson, 1965). Following atmospheric testing of nuclear weapons, levels of tritium rose to 500 TU, and to more than 1,000 TU by the mid-1960s, but have been decreasing due to radioactive decay, the cessation of atmospheric detonations of thermonuclear devices, and removal through rainfall (Hurst, 2010). Because groundwater tritium concentrations reflect atmospheric tritium levels when the water was last in contact with the atmosphere, tritium can be used to date groundwater recharge in geologically young groundwater. Measurement of tritium in rainfall was not systematic until after the onset of atmospheric testing of thermonuclear weapons, so only an approximation of the natural level of tritium in the environment can be made based upon limited measurements that were made prior to the 1950s. However, in the period of three half-lives (1963 to 2000), tritium concentrations have been reduced by a factor of 8, and with no further atmospheric nuclear weapons tests, tritium will continue to drop to near natural background levels. Usage of tritium for age dating groundwater recharge is approaching an expiration date (Motzer, 2005).

Carbon (^{14}C). The carbon radioisotope, ^{14}C (radiocarbon), with a half-life of 5,730 years, is used to date groundwater up to 50,000 years old (Hurst, 2010). ^{14}C can be used as a dating tool for materials that contain carbon compounds derived from atmospheric CO_2 either by simple mixing processes or by carbon exchange. The half-life of roughly 6,000 years is ideal for dating of reservoirs that are a few centuries to tens of thousands of years old. For groundwater, this means that ^{14}C dating can be applied to aquifers that contain water formed during periods that reach well into the past glacial time. ^{14}C is a widely used tool to establish chronologies for groundwater flow systems and climate records for the

Holocene and Pleistocene. It is considered to be the most important tool for age dating of 'old' groundwater. Local groundwater with ^{14}C concentrations >100 percent modern carbon (pmC), indicates the presence of anthropogenic "bomb carbon" (Webb et al., 2008) in groundwater that was recharged since ~1950.

Stable Radiogenic Isotopes

Strontium (Sr). The stable strontium isotopes ^{86}Sr and ^{87}Sr are used in groundwater investigations. Although delta notations are sometimes employed, it is more common to see the actual isotope ratios ($^{87}Sr/^{86}Sr$) reported. The isotopes of strontium are stable; however, ^{87}Sr is also radiogenic, the abundance increasing over geologic time due to radioactive decay of the rubidium isotope ^{87}Rb. Rb+ substitutes for K+ in K-bearing minerals like muscovite, biotite, lepidolite, K-feldspar, and in some clay and evaporate minerals.

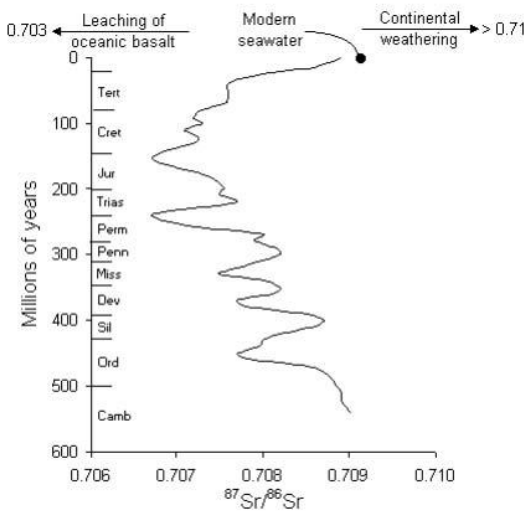

Figure 4.1 Strontium isotopes in sedimentary rocks throughout Phanerozoic time
(modified from Veizer, 1989) (Clark and Fritz, 1997).

Strontium has four stable isotopes: ^{84}Sr, ^{86}Sr, ^{87}Sr, and ^{88}Sr. Sr^{2+} substitutes Ca^{2+} in granitic minerals including plagioclase, feldspar, K-feldspar, hornblende, biotite, and muscovite. Both Rb and Sr are incompatible in silicate magmatic systems during early stages of fractional crystallization— Rb more strongly. Ideally, a granite melt begins to crystallize and accumulate an assemblage of plagioclase and hornblende (i.e., tonalite or diorite), low in K (and hence Rb) but high in Sr (as this substitutes for Ca) and proportionally enriches the melt in K and Rb. This then causes orthoclase and biotite, both K-rich minerals into which Rb can substitute, to precipitate later in the crystallization process. The resulting Rb-Sr ratios and Rb and Sr abundances of both the whole rocks and their component minerals will be markedly different. This allows a different rate of radiogenic strontium to evolve in the separate rocks

and their component minerals as time progresses with a degree of differentiation, the highest ratios exceeding ten in pegmatites, while the lowest ratios are close to zero in carbonates and Ca-rich plutonic rocks.

Most of Phanerozoic time (the past 540 million years) is characterized by a general decrease in marine $^{87}Sr/^{86}Sr$ (Figure 4-1) due at least partly to increasing activity along mid-ocean spreading ridges and interaction of sea water with low $^{87}Sr/^{86}Sr$ basalt that hosts hydrothermal vents on the sea floor. The late Cenozoic increase in $^{87}Sr/^{86}Sr$ in marine sediments has been attributed to climate cooling and increased rates of continental weathering by glaciation (Faure, 1991). This rapid and steady increase through the Pliocene and Pleistocene provides a high-resolution dating tool for sedimentary rocks. The strong variation in $^{87}Sr/^{86}Sr$ through Phanerozoic time and between rock types provides for strong contrasts between differing geological terrains. Modern seawater has $^{87}Sr/^{86}Sr = 0.709$ (Faure, 1991), which is intermediate between ^{87}Sr-depleted ocean basalts (~0.703) and ^{87}Sr-enriched continental rocks (0.710 to 0.740). In spite of the complex history of strontium in the upper crust, the $^{87}Sr/^{86}Sr$ ratio should be significantly greater than that in the upper mantle (Faure, 1986).

Noble Gases

Helium (He). Regional and local trends in the crustal occurrence of mantle volatiles provide insight into the coupling between mantle-crust tectonics, heat and mass exchange between the mantle and crust, and the occurrence and distribution of economic resources such as ore minerals and oil, gas, and geothermal fluids. Mantle-derived volatiles in the crust are traceable through Helium isotopic compositions of hydrologic fluids. Once injected into a crustal-fluid system, mantle He will be continuously diluted with radiogenic helium-4 (^{4}He) acquired from radioactive decay of uranium and thorium, which is abundant in Earth's crust relative to the mantle. Therefore, in addition to providing information regarding the heat source (mantle heat sources and magmas derived from the mantle carry more Helium-3 (^{3}He), He isotopic compositions in near-surface aqueous solutions also provide a measure of the mantle He flux and the integrated permeability-fluid pressure gradient (flow rate) through the crust (Kennedy, Christenson, van Soest, 2010).

The ^{4}He is a light, non-radioactive isotope of helium. Some of the ^{4}He found in the terrestrial atmosphere is a relic of atmospheric and underwater nuclear weapons testing in the 1960s. Most of this comes from the decay of ^{3}H, which decays into ^{4}He with a half-life of 12.3 years. Additionally, some nuclear reactors (land or ship) periodically release some ^{4}He and ^{3}He into the atmosphere. The ^{4}He content of deep groundwater frequently exceeds the expected level in equilibrium with atmospheric helium ($^{3}He/^{4}He$) by orders of magnitude. This excess helium originates from the α-decay of U and Th and of their daughter nuclides in the aquifer material, as well as from the ^{4}He release from deeper rock layers of the Earth's crust. This results in a diffusional flux of the crustal helium that penetrates various groundwater aquifers during migration before eventually entering the atmosphere. Thus, the quantity

of excess helium accumulated in groundwater bears information on the groundwater mean-residence time.

He isotope ratios ($^3He/^4He$) are reported relative to the atmospheric value (1.39×10^{-6}) in the R/Ra notation:

$$(^3He/^4He)_{R/R_A} = (^3He/^4He)_{sample} \ / \ (^3He/^4He)_{atmosphere}$$

The ratio (R) of ^3He to ^4He is often used to represent ^3He content. R usually is given as a multiple of the present atmospheric ratio (Ra) (Rigby, 2014). Helium-4 (^4He) is created by radiogenic production (decay of U/Th-series elements). The continental crust has become enriched with those elements relative to the mantle and thus more ^4He is produced in the crust than in the mantle (Figure 4.1).

Table 4.1 Helium abundances and isotopic ratios in different reservoirs

Source	He Concentration	$^3He/^4He$	R/R_{air}
Atmosphere	5.24 ppmv	$1.38*10^{-6}$	1
Surface Water	$4.5*10^{-8}$ cm^3STPg^{-1}	$\sim 1*10^{-6}$	~1
Crustal Fluids	10^{-7} to 10^{-4} cm^3STPg^{-1}	$\sim 10^{-8}$ to $<10^{-10}$	0.007 to 0.022
Mantle He	Up to $2.7*10^{-5}$ cm^3STPg^{-1}	1 to $3*10^{-5}$	7 to 21

Note: $R=^3He/^4He$ (Clark and Fritz, 1997)

The other noble gases [N, Argon (Ar), Neon (Ne), Krypton (Kr), and Xeon (Xe)] in the continental crust are generally at low concentrations and dominated by radiogenic components. The two main reservoirs of noble gases in the Earth are the atmosphere and the mantle. Noble gases in the atmosphere have uniform isotope ratios and provide a good reference against which mantle values can be compared.

5. SAMPLING AND ANALYSES (GENERAL)

Permissions and Permits

The AZGS developed a list of 30 select thermal springs based on high-end temperatures and accessibility with a goal to sample 20 thermal springs or wells. Private property owners or managers were contacted to obtain permission to access these thermal springs (Table 5.1). A permit was obtained to sample Ringbolt Hot Spring from the National Park Service, Lake Meade Recreational Area, Permit #LAME 2012, SCI-0021 (Appendix A). The Investigator Annual Reports presenting investigation methods and findings were submitted to the National Park Service as required (Appendix A). Permissions were also obtained to sample the Agua Caliente warm well (Pima County Natural Resources, Parks and Recreation) and Hooker's Hot Spring (Mule Shoe Ranch Nature Conservancy). Three springs were on Morenci mine properties and access was not permitted. Several springs were reported as dry and a few thermal wells visited were capped. The list was revised as necessary to replace those wells and springs that could not be sampled. The complete list of proposed and sampled springs with ownership contact for permissions are listed in Table 5.1 (springs proposed but not sampled are greyed-out). The locations of sampled thermal springs and wells are mapped in Figure 1.1.

Field Collection Methods

The AZGS developed a Sample and Analysis Plan (SAP) to provide consistent sample collection by specifying methods, identifying thermal wells and springs for sample collection, providing sample IDs and listing analytics for each sample. Duplicate samples were collected one per every ten groundwater samples collected. Pre-cleaned sample containers appropriately preserved for specific analysis were supplied by the laboratory (Table 5.2). Field sheets were used to record sample ID, date, location in Lat/Long degrees, elevation, and physical parameters.

One groundwater sample was collected from each of the selected thermal springs or wells with reported temperatures at least 10°C above mean ambient air temperature. Water samples for general chemistry analytics were collected using pre-cleaned laboratory-supplied bottles. Bottles for analytical methods requiring preservatives were prepared by the laboratory. Where necessary, a peristaltic pump was used to extract spring water from as close to the source as possible. In the case of thermal well sampling, wells casings were evacuated using the installed pump to produce fresh groundwater for sample collection. Well samples were collected at the sampling spigot. All sample bottles were stored in ice during transport and shipping if required by the analytical method. The analytical methods and bottle size and type are listed in Table 5.2.

For dissolved noble gases measurement, the samples were collected in copper tubes. Copper tube samples are collected by establishing a pump-generated flow-cell from the source through an inline copper tube, and sealing the tube off using refrigeration type clamps. The peristaltic pump mechanism was placed on the outlet end of the copper tube for a relatively undisturbed sample volume.

Table 5.1 Thermal Spring Locations and Permissions

No.	"Popular" or USGS Spring Name	County	Land Owner-ship Type	Owner Name	Access Request Status
Ts01	**Agua Caliente Warm Spring**	Pima	Pima County	Pima County	Pima County contacted to obtain access. Permission granted; aqueous sample collected from artesian well head.
Ts02	**Hooker's Hot Spring**	Cochise	Private	Nature Conservancy	Letter Sent, permission granted. Call Bob Rogers to schedule; aqueous spring sample collected.
Ts03	**Hot Well Dunes**	Graham	BLM	Safford BLM	Hot Well Dunes BLM office in Safford provided permission to collect a sample from the "formerly" artesian Hot Well Dunes. The BLM staff will turn the pump on for sample collection; aqueous spring sample collected.
Ts05	**Indian Hot Spring (Eden)**	Graham	Private	Indian springs Ranch Inc.	Letter Sent, permission granted; aqueous spring sample collected.
Tw05	**Watson Well**	Graham	BLM	Debbie Morris, Safford BLM	Debbie Morris reported that the well, following capping, continues to discharge to approximately 1 gpm to pool. Spring sample collected from upgradient pond source.
Ts06	**Roper Hot Springs (Dankworth Pond)**	Graham	AZ Game & Fish	State of Arizona	No Letter sent, State permission granted. Roper Lake spring piped; aqueous spring sample collected at source at Dankworth Pond.
Ts07	**Thatcher South**	Graham	Municipal	Town of Thatcher	Mike Payne, Town of Thatcher, stated the Well had been capped several years previously. Collected sample from an alternate flowing spring south of Thatcher.
Tw07	**Willcox Greenhouse**	Cochise	Private	Jacques Vanderlelidj	Phoned. Permission granted to sample at Greenhouse thermal well; aqueous spring sample collected.
Ts08	**Potter Hot Spring**	Greenlee	Private	June Potter Palmer	Letter Sent, permission granted; aqueous spring sample collected.
Ts09	**Gillard Hot Spring**	Greenlee	BLM	Dept of Interior	No Letter sent, Federal land. Contacted BLM. Permission granted; aqueous spring sample collected.
Tw14	**Radium Hot Spring**	Yuma	Private	Jerry Cullison	Letter Sent, permission granted; aqueous spring sample collected.
Ts17	**Cofer Hot Spring**	Mohave	BLM	Dept of Interior	Supervisor Paul Wisely granted permission contingent on the analytical results are submitted as a record; aqueous spring sample collected.
Ts18	**Ringbolt Hot Spring**	Mohave	NPS, Lake Mead Nat. Rec . Area	Dept of Interior	Permit application submitted with National Park Service. Permission granted; aqueous spring sample collected.
Tw22	**Tonopah Well**	Maricopa	Private		Permission granted (Property Manager)
Ts23	**Castle Hot Spring**	Yavapai	Private	Pat Talley	Letter Sent, Permission granted from Dave Headstream (CBRE)- aqueous spring sample collected
Ts24	**Kaiser Hot Spring**	Mohave	Private	Charles & Mildred Shipp Trust	Letter Sent, Permission granted; aqueous spring sample collected.

Proposed springs and wells listed below not sampled.					
04	Salado Springs	Apache	Private	Tri-State/TEP/ SRP-AG Improv	Letter Sent, No Response
10	Antelope Spring	Cochise	Private	Jack Telles [Telles Enterprises]	Letter Sent, permission granted, Informed that the Spring is Dry last 4-5 years.
11	Mescal Warm spring	Gila	Private	San Carlos Apache	Letter Sent, No Reply, follow-up calls to tribe attny general and legal counsel, no reply
12	Coolidge Dam Warm spring	Pinal	Private	San Carlos Apache	Letter Sent, No Reply, follow-up calls to tribe attny general and legal counsel, no reply
13	Grapevine Spring	Graham	State Trust	Arizona Land Department	Letter Sent, permission granted, "Temporary Right of Entry" issued (Oct 1 - Dec 31/2012). Spring was not located, may have been dry.
15	Clifton Hot Spring	Greenlee	Private	Freeport McMoran	Letter Sent, permission denied
16	Eagle Creek Hot spring	Greenlee	Private	Freeport McMoran	Letter Sent, permission denied
19	Seep	Greenlee	Private	Freeport McMoran	Letter Sent, permission denied
20	Pioneer Spring	Gila	BLM	Dept of Interior	Spring dry, no flow or nearby springs
21	Warm spring [Tom Niece Spring]	Graham	BLM	Dept of Interior	Spring dry, no flow or nearby springs
25	Hannah Hot Spring	Greenlee	Apache-Sitgreaves National Forest	Dept of Interior	Removed from sampling plan due to access constraints.
26	Roosevelt Dam Springs	Maricopa	Tonto National Forest	Dept of Interior	No Letter sent, Federal land. Permission requested. No springs found.
27	Verde Hot spring	Yavapai	Tonto National Forest	Dept of Interior	River too high to cross. Inaccessible.
28	Buena Vista hot well	Graham	BLM	Safford BLM	Dry, no flow. No adjacent prospects.

Analytical Methods

Each groundwater sample was collected and analyzed for physical parameters, general chemistry anions, dissolved gases, metals and silica (SiO_2) for silica thermometry to identify end members, quantify mixing parameters, and estimate source temperatures. A combination of isotope analyses were performed on thermal water samples: $^{18}O/^{16}O$ ratio and deuterium (^{2}H) to evaluate the significance of meteoric water in geothermal water; ^{14}C analysis to evaluate the age of the meteoric water component; $^{87}Sr/^{86}Sr$ to determine if geothermal waters were derived from deep, Proterozoic bedrock; and $^{3}He/^{4}He$ analysis to determine if faults or fractures are allowing mantle-derived He to enter groundwater. These

analyses should enable qualitative characterization of thermal water systems and evaluation of their heat-source potential.

Physical parameters were measured in the field using a handheld Hanna 991301 pH/EC/TDS/T Multiparameter Meter with HI1288 probe for temperature, conductivity, pH, and TDS and recorded on the field sheets. Physical parameters for aqueous samples were also measured in the laboratory for alkalinity by method SM2320B, specific conductance by method SM2510B, pH and temperature by method SM4500-H+B.

Table 5.2 Analytics

Analysis	Method	No.	Container	Preservative	Laboratory
Cations + silica	Method 300/SM2320B/ SM4500 Si-D	1	500-ml plastic bottle	No preservative	Turner Labs
Anions (Metals)	Method 200.7/200.8/ 245.1	1	250-ml plastic bottle	HNO_3	Turner Labs
CH_4	RSK 175	3	50-ml VOAs with septa seal cap	HCl	Turner Labs
CO_2	RSK 175/D5504-08	3	50-ml VOAs with septa seal cap	No preservative	Turner Labs
H_2S	Calculation	1	1-Liter plastic bottle	NaOH | ZnAC	Turner Labs
$^{18}O/^{16}O$	Finnigan Delta S	1	included w/ 3He (tritium)	No preservative	U of AZ, Dept of Geoscience
$^{2}H/^{1}H$	Finnigan Delta S	1	included w/ 3He (tritium)	No preservative	U of AZ, Dept of Geoscience
^{3}He (tritium)	tritium dating	1	500 ml LDPE	No preservative	U of AZ, Dept of Geoscience
^{14}C	radiotopic age/CSM	2	500 ml LDPE	filter/refrigerate	U of AZ, Dept of Geoscience
$^{87}Sr/^{86}SR$	isotopic analysis	1	125-mL LDPE bottle	No pres/acid washed	U of Utah, Noble Gas Lab
$^{3}He/^{4}He$/Noble gases	isotopic method	1	Copper tubing sample	No preservative	U of Utah, Noble Gas Lab

General chemistry analyses were performed by Turner Labs of Tucson, Arizona. ICP metals B, Ca, Cs, iron (Fe), Li, Mg, K, Rb, and Na were analyzed by EPA method E200.7. Anions Cl, fluorine (F), and sulfate (SO_4) were analyzed by ion chromatography using EPA method E300. Sulfide (S^{-2}) was analyzed by method SM4500-SF and silica as SiO_2 by method SM4500-Si D. Hydrogen sulfide as S (H_2S) was determined by calculation.

Prepared samples were analyzed for dissolved gases CO_2 using a gas chromatograph equipped with a thermal conductivity detector (TCD) and for methane (CH_4) using a gas chromatograph equipped with a flame ionization detector (FID). The amount of carbon dioxide and methane in the original sample was

calculated using Henry's Law. This method was performed with guidance from EPA test method RSKSOP-175. The CO_2 and CH_4 analyses were performed by ALS Environmental in Simi Valley, California.

To evaluate groundwater characteristics related to age and source, several isotopic analyses plus rubidium and cesium were performed on each sample.

The $^{18}O/^{16}O$ ratio, $^{2}H/^{1}H$, and tritium analyses were conducted to evaluate the significance and age correlation of meteoric water in geothermal water. Analysis for ^{14}C was conducted to evaluate the age of the meteoric water component. These analyses were conducted by the University of Arizona, Department of Geoscience, Geophysics Laboratory.

Analysis for $^{87}Sr/^{86}Sr$ was conducted to determine if geothermal waters were derived from deep, Proterozoic bedrock. Analysis for Rb and Ce was performed for use in the Powell and Cummings (2010) geothermometry worksheets and ternary plots. These analyses were conducted by the University of Utah, Department of Geology and Geophysics lab in Salt Lake City, Utah.

Analyses for dissolved noble gases were conducted by the University of Utah Dissolved and Noble Gas Laboratory. The majority of the lab's research involves isotopic measurements of noble gases for groundwater age dating and thermometry. Analysis for noble gases, including ^{3}He—a stable isotope—was conducted to determine if faults or fractures at springs associated with high-angle normal faults or volcanics (magma source) are allowing mantle-derived helium to enter groundwater. The thermal water sample for dissolved noble gases analysis was extracted from copper collection tubes by the lab using an extraction line. Under a high-vacuum, closed system, the water is transferred from the copper tube into a large stainless steel flask. The flask is heated while a smaller flask is chilled. This creates a flux of gas from the large flask into the small flask. The small flask is then sealed before being transferred to the mass spectrometry input line.

Analysis for other noble gases included nitrogen, argon, neon, krypton, and xenon by use of a quadrupole mass spectrometer (MS). The quadrupole mass spectrometer uses four, parallel, charged rods that isolate specific ions with given mass/charge ratios. Different electrical charge's radio frequencies allow different ions to pass through the quadrupole to a detector. The quadrupole MS is used to quickly determine the abundance and isotopic analysis of most atmosphere gases using a Stanford Research SRS – Model RGA 300 quadrupole mass spectrometer. Measurements for all gases except helium are made using this instrument. These include: $^{28}N_2$, ^{36}Ar, ^{40}Ar, ^{20}Ne, ^{22}Ne, ^{78}Kr, ^{84}Kr, ^{86}Kr, ^{126}Xe, ^{129}Xe, ^{131}Xe, ^{132}Xe, ^{134}Xe, ^{136}Xe. Like the quadrupole, the sector-field mass spectrometer uses ions' mass/charge ratios, but in this case, a magnet is used to deflect the ions into separate detectors— Mass Analyzers Products – Model 215-50 Magnetic Sector Mass Spectrometer. This is used to precisely measure abundances of ^{3}He and ^{4}He. An electron multiplier is used to measure low-abundance ions with high-precision, while a Faraday cup measures more abundant ions.

6. GEOCHEMISTRY RESULTS

Laboratory analytical reports are included as Appendix B. Data is presented in the Summary of Results Tables (Appendix C) and in the Powell and Cumming geothermometry workbook (Appendix D) and summarized herein. Analytical results are summarized below and the complete data tables 6.1-6.11 are included as Appendix C. The aqueous chemistry results were also entered into the Powell and Cumming (2010) geothermometry model (Section 7) to provide insight as to thermal water sources and its value to geothermal exploration.

Geochemistry data were added to the Arizona Aqueous Chemistry Data collection as interoperable interchange data for the NGDS repository, providing online accessibility and interoperability for web map services (AZGS, 2014). Well and spring feature headers were provided under the NGDS project and cross referenced with chemistry observations using FeatureURIs.

Physical Parameters

Physical parameters were collected in the field at each location prior to collecting the groundwater sample for laboratory analysis. Field measured physical parameters are summarized in Table 6.1.

Table 6.1 Summary of Field Physical Parameters

Label	Field pH	Field Temperature (°C)	Field Conductivity (µS/cm)	Total Dissolved Solids (mg/l)
Ts01	7.92	31.1	1,110	560
Ts01	7.82	31.5	970	500
Ts02	9.24	44.6	490	250
Ts02	9.15	47.8	610	na
Ts25	9.24	44.6	490	250
Ts06	8.94	35.5	1,790	900
Ts03	8.56	37.5	1,960	970
Tw07	9.52	40.3	420	230
Ts09	7.56	>60	3,040	1,520
Ts07	8.08	36.4	13,420	6,690
Tw05	7.85	31.4	5,333	2,680
Tw14	7.57	50.5	4,740	2,350
Ts18	7.56	48.7	4,860	2,430
Ts17	7.31	32.6	1,590	790
Ts08	6.47	46.6	19,820	9,740
Ts05	7.57	44.4	5,690	2,960
Tw22	8.74	30.1	650	320
Ts23	8.12	40.0	1,260	630
Ts24	7.62	33.9	1,330	660

The pH values ranged from 6.47 to 9.52 with all but one sample being alkaline (pH >7.0). Hot springs with boiled geothermal solutions typically have a neutral to alkaline pH, and low dissolved gas content. On the other hand, hot springs that effuse geothermal solutions that have been cooled by conduction on the way to the surface, generally have a lower pH because they have not lost their dissolved CO_2 and H_2S (Fridriksson and Ármannsson, 2004).

Field measured temperatures ranged from 31.1°C to greater than 50°C at two locations —Radium Hot Spring (50.5°C) and Gillard Hot Spring (>60°C). Temperatures were consistent with previously reported temperatures (Witcher, various) for those springs and wells.

Field measured conductivity ranged from 420 to 19,820 µS/cm. Conductivity is the measure of a solution's ability to carry an electric current. This ability depends on the ions present and on temperature. Total dissolved solids (TDS) ranged from 230 to 9,740 mg/l. TDS and conductivity are related by *TDS (mg/l) = conductivity (mS/cm)* • *K mg/l / µS/cm* (where *K* is an empirical constant ranging from 0.5-0.9, depending on the ions in solution and the temperature). Results are consistent with this assumption.

Major-Ion Geochemistry

Aqueous major-ion geochemistry for spring and well groundwater are used in calculating geothermometry for thermal waters (see Section 7). Geochemistry analyses were mainly performed by Turner Labs in Tucson. The University of Utah performed analyses for Rb and Cs with method detection limit at 0.00002 mg/l and 0.00003 mg/l, respectively, to meet the minimum detection limit required for geothermometry calculations.

Cations

The groundwater samples were analyzed for cations most often used in geothermometry calculations and ternary plots. A summary of analytical results for these metals are reported in Table 6.2. A summary of the analytical results are as follows:

- boron (B) was detected at concentrations ranging from 0.12-3.0 mg/l
- calcium (Ca) was detected at concentrations ranging from 7.2 – 870 mg/l
- iron (Fe) was detected at concentrations ranging from 2.0 mg/l
- lithium (Li) was detected at concentrations ranging from 0.32 – 6.1 mg/l
- magnesium (Mg) was detected at concentrations ranging from 4.7 – 20 mg/l
- potassium (K) was detected at concentrations ranging from 5.2 – 220 mg/l
- sodium (Na) was detected at concentrations ranging from 59 – 3,100 mg/l

- rubidium (Rb) was detected at concentrations ranging from 0.0013 – 1.31 mg/l)
- cesium (Cs) was detected at concentrations ranging from 0.0001 – .6828 mg/l

Relatively high boron values in a condensate may indicate high formation temperatures. Boron is considered a mobile component since it does not take part in rock forming reactions and its concentration in the geothermal fluids is controlled by the leaching rate from the reservoir rocks (Kanda, 2011).

Table 6.2 Summary of Results for Metals

Label	B	Ca	Fe	Li	Mg	K	Na	Rb	Cs
PQL:	0.1	4.0	0.3	0.2	3.0	5.0	5.0	0.00002	0.00003
Ts01	0.12	23	ND	0.34	ND	ND	140	0.0349	0.0098
Ts02	ND	ND	ND	ND	ND	ND	59	0.0040	0.0046
Ts25	ND	ND	ND	ND	ND	ND	59	0.0042	0.0045
Ts06	0.54	7.3	ND	0.87	ND	ND	310	0.0013	<0.00003
Ts03	0.37	7.2	ND	0.41	ND	ND	340	0.0161	0.0039
Tw07	ND	ND	ND	ND	ND	ND	63	0.0041	0.0028
Ts09	0.45	20	ND	0.89	ND	13	450	0.121	0.0524
Ts07	2.0	150	ND	3.1	9.5	13	2,900	0.0358	0.0029
Tw05	1.2	33	ND	1.4	4.7	11	1,200	0.0515	0.0130
Tw14	3.0	180	ND	0.43	5.9	11	680	0.0331	0.0032
Ts18	1.3	250	ND	0.59	11	13	620	0.0656	0.0054
Ts17	1.1	46	ND	0.33	15	7.8	200	0.0325	0.0051
Ts08	1.2	870	2.0	6.1	20	220	3,100	1.31	0.683
Ts05	0.63	74	ND	1.3	8.1	13	960	0.0586	0.0159
Tw22	0.72	6.0	ND	ND	ND	ND	110	0.0017	0.0001
Ts23	1.0	29	ND	0.33	ND	5.2	190	0.0258	0.0051
Ts24	1.1	18	ND	0.32	ND	7.9	230	0.0480	0.0093

The cations include those used in the empirical Na-K-Ca geothermometer (Fournier, 1981) which is found to be consistent with measured well temperatures. Geothermometers work because the relative equilibrium concentrations of chemical species change with respect to temperature. The rates at which different species react also vary, with cations like Na and K adjusting more slowly than silica. Cation geothermometry has a longer “memory” and typically reflects the temperature of a more distant or deeper source fluid. In contrast, the silica geothermometer reflects the temperature of a nearby aquifer. The representative ternary graphs (see Section 7) combine species with different sensitivity to temperature, mixing and other processes in order to resolve trends in geothermal reservoirs and their shallow manifestations (Powell and Cumming, 2010).

Anions Chloride, Fluoride, and Sulfate

General chemistry results for anions Cl, F, and SO_4 are summarized in Table 6.3.

- Chloride (Cl) was detected in all samples at concentrations ranging from 3.3 mg/l to 7,500 mg/l.
- Fluoride (F) concentrations ranged from 0.92 mg/l to 13 mg/l.
- Sulfate ($S0_4$) concentration ranged from 13 mg/l to 980 mg/l. Sulfate was not detected in two groundwater samples above the detection limit of 5 mg/l.

Very high Cl values in a steam condensate would represent a water dominated system, while extremely low values would be expected to originate from a vapor dominated system since chlorides are not known to partition into steam phase at any temperatures (Kanda 2011). A relatively high F content in a steam condensate may indicate deep crustal water circulation.

Table 6.3 Summary of Results for Anions Chloride, Fluoride, and Sulfate

Label	Cl	F	SO_4
PQL:	1	0.50	5
Ts01	26	5.5	170
Ts02	3.4	1.8	ND
Ts25	3.3	1.8	ND
Ts06	260	13	210
Ts03	190	9.1	280
Tw07	6.4	3.6	13
Ts09	470	8.7	160
Ts07	4,000	6.4	950
Tw05	1,200	7.8	510
Tw14	730	4.0	980
Ts18	1,100	2.2	600
Ts17	150	3.7	180
Ts08	7,500	0.92	69
Ts05	1,400	3.2	420
Tw22	51	8.8	70
Ts23	140	8.8	210
Ts24	65	8.0	95

Note: PQL – Practical Quantitation Limit

Dissolved Gases

Dissolved gases CO_2, CH_4, and hydrogen sulfide as S results are summarized in Table 6.4.

- Carbon dioxide (CO_2) was not detected above the method reporting limit of 1,000 µg/l in eight groundwater samples. In the remaining nine groundwater samples, concentrations ranged from 1,300 µg/l to 24,000 µg/l, with significantly higher concentrations detected in groundwater samples from 3 locations—Ts17 (Cofer) at 20,000 µg/l, Ts08 (Potter) at 24,000 µg/l, and Ts24 (Kaiser) at 23,000 µg/l.
- Methane (CH_4) was detected at low concentrations in groundwater samples from only 3 locations, Ts09 (Gillard) at 3.6 µg/l, Ts07 (Thatcher) at 22 µg/l, and Tw05 (Watson) at 2.1 µg/l. Methane was not detected in any of the other samples above the detection limit of 1.3 µg/l.
- Hydrogen sulfide as S was detected at low concentrations in 2 groundwater samples: Ts07 (Thatcher) at 48 µg/l and Ts18 (Ringbolt) at 100 µg/l. Hydrogen sulfide was not detected in any of the other groundwater samples.

Table 6.4 Summary of Results for Dissolved Gases (µg/l)

Label	CO_2	CH_4	Hydrogen Sulfide as S
MRL:	1000	1.3	0
Ts01	4,000	ND	ND
Ts02	ND	ND	ND
Ts25	ND	ND	ND
Ts06	ND	ND	ND
Ts03	ND	ND	ND
Tw07	ND	ND	ND
Ts09	5,400	3.6	ND
Ts07	ND	22	48
Tw05	3,400	2.1	ND
Tw14	2,100	ND	ND
Ts18	ND	ND	100
Ts17	20,000	ND	ND
Ts08	24,000	ND	ND
Ts05	2,500	ND	ND
Tw22	ND	ND	ND
Ts23	1,300	ND	ND
Ts24	23,000	ND	ND

Various different subcategories of mixed solutions can be found in and around geothermal areas. CO_2-rich waters can form where gas rich steam condenses in shallow aquifers. Similarly, CO_2-rich waters can form when unboiled (and undegassed) geothermal solutions mix with cold groundwater. Mixtures of boiled geothermal solutions and groundwaters result in mixtures with low gas content, but have temperatures and concentrations of non-volatile components that are intermediate between those of

the groundwater and the geothermal solutions. CO_2-rich waters are commonly found on the boundaries of active volcanic geothermal systems (Arnórsson et al., 2007) and around volcanoes (Aiuppa et al., 2003). Very high concentrations of CO_2 are sometimes observed in the reservoir fluids in old and cooling geothermal systems (i.e. Haedarendi and Leirá, Iceland). Other types of "mixed solutions" are found in and around geothermal areas where the groundwater table is high. The mixed solutions tend to be most common on the peripheries of geothermal systems where there are steep temperature and chemical gradients between the geothermal system and the adjacent groundwater systems (Fridriksson and Ármannsson, 2004).

Alkalinity

Total alkalinity ranged from 32 to 420 mg/l. Alkalinity results are summarized in Table 6.5. Alkalinity measures the ability of a solution to neutralize acids to the equivalence point of carbonate or bicarbonate.

Table 6.5 Summary of Results for Alkalinity

Label	Alkalinity, Bicarbonate as CaCO3	Alkalinity, Carbonate as CaCO3	Alkalinity, Hydroxide as CaCO3	Alkalinity, Total as CaCO3	Alkalinity, Bicarbonate as $HCO3^-$	Alkalinity, Carbonate as $CO3^-$
PQL:	2.0	2.0	2.0	2.0	1.22*Bicarbonate as CaCO3	0.6*Carbonate as CaCO3
Ts01	170	ND	ND	170	207.4	ND
Ts02	56	80	ND	140	68.32	48
Ts25	50	80	ND	140	61	48
Ts06	30	48	ND	78	36.6	28.8
Ts03	100	60	ND	160	122	36
Tw07	30	92	ND	120	36.6	55.2
Ts09	170	ND	ND	170	207.4	ND
Ts07	50	ND	ND	50	61	ND
Tw05	160	ND	ND	160	195.2	ND
Tw14	58	ND	ND	58	70.76	ND
Ts18	32	ND	ND	32	39.04	ND
Ts17	280	ND	ND	280	341.6	ND
Ts08	68	ND	ND	68	82.96	ND
Ts05	84	ND	ND	84	102.48	ND
Tw22	60	36	ND	96	73.2	21.6
Ts23	110	ND	ND	110	134.2	ND
Ts24	420	ND	ND	420	512.4	ND

In the natural environment carbonate alkalinity tends to make up most of the total alkalinity due to the common occurrence and dissolution of carbonate rocks, and presence of carbon dioxide in the atmosphere.

Sulfide and Silica

Sulfide (S_2) and silica as SiO_2 results are summarized in Table 6.6. Sulfide was not detected in 8 samples and was detected below the practical quantitative limit in 6 samples. Sulfide was detected in 3 samples at a low concentration of 1.0 mg/l. Silica was detected at concentrations ranging from 15 to 94 mg/l.

Table 6.6 Summary of Results for Sulfide and Silica

Label	Sulfide	Silica as SiO2
PQL:	0.5	10
Ts01	ND	50
Ts02	ND	40
Ts25	ND	39
Ts06	ND	20
Ts03	ND	57
Tw07	ND	41
Ts09	ND	94
Ts07	1	15
Tw05	<0.7	61
Tw14	1	41
Ts18	<0.8	36
Ts17	1	38
Ts08	<0.6	85
Ts05	<1.1 (Apparent 0.5)	38
Tw22	<1.0 (Apparent 0.4)	19
Ts23	<0.6	48
Ts24	ND	43

The silica geothermometer reflects the temperature of a nearby aquifer, as opposed to the cation geothermometer that reflects a more distant or deeper source fluid. Geothermometer temperatures can be calculated for amorphous silica, chalcedony, quartz via conductive cooling, and quartz via adiabatic cooling (see Section 7).

Stable Isotope Chemistry

Tritium

Tritium results ranged from an apparent 0.4 to 1.0 TU (Table 6.7). Groundwater age estimation using tritium only provides semi-quantitative estimates for a range of values. Tritium value ranges and interpretations are listed below (ranges given may vary slightly dependent on research reference).

- <0.8 to <1.2 TU indicates submodern water (prior to 1950s)
- 0.8 (1.2) to 4 TU indicates a mix of submodern and modern water
- 5 to 15 TU indicates modern water (<5 to 10 years)
- 15 to 30 TU indicates some bomb tritium
- >30 TU: recharge occurred in the 1960s to 1970s

Tritium results <1.2 TU indicate all groundwater were accumulated prior to 1950s (submodern). Submodern waters may be indicative of deep basin aquifers or waters derived from deep bedrock and transported through fractures and faults to basin aquifers or to the surface as thermal springs. As deep seated water migrates through fractures and along faults, it may mix with more recent water stored in aquifers as permeability permits.

Table 6.7 Summary of Results for Tritium in Thermal Springs and Wells

Label	Tritium TU	Error TU	Indicator
MDL:	0.6		
Ts01	<1.2 (apparent 0.6)	na	prior to 1950s
Ts02	0.7	0.33	prior to 1950s
Ts25	0.8	0.30	prior to 1950s
Ts06	<1.2 (apparent 0.6)	na	prior to 1950s
Ts03	0.9	0.35	prior to 1950s
Tw07	1.0	0.33	prior to 1950s
Ts09	0.9	0.34	prior to 1950s
Ts07	<1.0 (apparent 0.4)	na	prior to 1950s
Tw05	<1.0	na	prior to 1950s
Tw14	<0.7	na	prior to 1950s
Ts18	0.7	0.31	prior to 1950s
Ts17	<0.8	na	prior to 1950s
Ts08	0.9	0.31	prior to 1950s
Ts05	<0.6	na	prior to 1950s
Tw22	<1.1 (Apparent 0.5)	na	prior to 1950s
Ts23	<1.0 (Apparent 0.4)	na	prior to 1950s
Ts24	<0.6	na	prior to 1950s

14 Carbon

Results for ^{14}C in groundwater range from 2.8 to 40.4 percent modern carbon (pMC) (Table 6.8). 100 pMC is defined as the radiocarbon concentration of the atmosphere in 1950 AD (Stuiver and Polach, 1977). The radiometric age of a sample is calculated by assuming a time-independent atmospheric ^{14}C level in all past times. Using a Cambridge[1] half-life of 5,730, the conventional (uncorrected) radiocarbon age (t) of a sample before 1950 AD is given by

$$t = -8267 * \ln(F/100)$$

The uncorrected conventional radiocarbon age for the thermal spring and wells are calculated and represent the oldest possible date. Ages are rounded according to the convention of Stuiver & Polach (1977). The corrected radiocarbon age was calculated and provided as a comparison between the "conventional" and the "calculated" ages. The corrected radiocarbon age is given by

$$t = -8267 * \ln(fMC) = -8267 * \ln(fM/90)$$

where fM is the true fraction of modern ^{14}C (corrected) of the sample.

The corrected ages were based on dissolved inorganic carbonate (DIC) measured $\delta^{13}C$ values which were only readily available for the Tucson Basin (Ts01) and Safford Basin (Ts03, Ts05, Ts06, and Ts07). In both cases, the assumption was made that the C3:C4 ratio of organic matter contributing to soil gas is 3:1; and that infiltration occurs under alkaline conditions (Eastoe, 2014). Actual data for the $\delta^{13}C$ of rock carbonate was available for Agua Caliente in Tucson at -1 per mil based on caliche beds and for Safford at -4 per mil on the basis of measured carbonate in river sand (Eastoe, 2014). For comparison, the 'corrected' values differed from 10% to 48% lower than the 'uncorrected' dates. These results reflect the bulk ^{14}C for groundwater. Groundwater is usually a mixture of two or more genetically and chemically distinct groundwater components, often of different ages (Geyh et al., 2000).

The conventional (uncorrected) ^{14}C results show that these samples represent maximum groundwater ages originating at least several thousand to tens of thousands of years ago (Table 6.8). The maximum groundwater age dates to the Pleistocene glacial period (colder climate) transitioning into a Holocene interglacial period (warmer climate). The Wisconsin ice age lasted from 85,000-11,000 years ago with the Last Glacial Maximum (LGM) set at around 26,500 - 19,000 years ago. The Holocene marks the onset of the most recent interglacial period and warming trend (Table 6.8).

[1] This half-life was estimated by Libby. Later on (1960s) an improved value of the half-life came into use, the Cambridge half-life, $(T_{1/2})_C$=5730±40 years. Even though the Libby half-life is not correct, it is still often used to obtain radiocarbon age (which is further converted to calendar years: this process is called calibration). Moreover, neither may the Cambridge half-life be entirely correct (Chiu et al., 2007).

Table 6.8 Summary of Carbon 14 in Groundwater from Select Thermal Springs and Wells

Label	C14 pMC	Error pMC	δ13C ‰	Uncorrected Max Age	Corrected Age	Estimated glacial period
Ts01	40.4	0.3	-11.5	7,500	3,900	Holocene
Ts02	17.0	0.2	-13.1	14,600		Late Wisconsin-Holocene
Ts25	17.2	0.2	-12.4	14,500		Late Wisconsin-Holocene
Ts06	4.0	0.1	-10.0	26,600	23,700	Last Glacial Maximum
Ts03	3.4	0.1	-6.2	28,000	19,700	Last Glacial Maximum
Tw07	12.1	0.2	-9.6	17,500		Wisconsin
Ts09	8.0	0.2	-4.0	20,900		Wisconsin
Ts07	2.8	0.1	-7.4	30,000	23,400	Last Glacial Maximum
Tw05	4.1	0.1	-5.2	26,400		Last Glacial Maximum
Tw14	5.9	0.1	-7.7	23,400		Wisconsin
Ts18	19.1	0.2	-9.1	13,700		Late Wisconsin-Holocene
Ts17	29.0	0.2	-7.6	10,200		Holocene
Ts08	8.9	0.2	-6.2	20,000		Wisconsin
Ts05	15.3	0.2	-2.5	15,500	10,300	Holocene
Tw22	23.3	0.2	-11.9	12,000		Late Wisconsin-Holocene
Ts23	21.2	0.2	-9.0	12,800		Late Wisconsin-Holocene
Ts24	3.0	0.1	-5.8	29,000		Last Glacial Maximum

Notes: pMC – percent modern carbon
‰ – one per thousand

The $\delta^{13}C$ values reflect chemical interaction with the aquifer rock. The isotopic composition of carbon in the dissolved carbon constituents of groundwater is very variable. The sources of dissolved carbon are soil CO_2, CO_2 of geogenic origin or from magmatic CO_2 (from deep crustal or mantle sources) or in fluid inclusions, and living and dead organic matter in soils and rocks, methane and carbonate minerals, and vary with source type and elevation (Table 6.9).

Table 6. 9 Dissolved Inorganic Carbon Sources for δ13C in Groundwater

Carbon Origin	Range of δ13C ‰
Terrestrial Plants	-30 to -20
Soils CO_2	-22
Tropical Soils CO_2	-20 to -11
Magmatic	-6
Metamorphic Carbon (sedimentary / Marine Carbonate)	-4 to +4
Evaporate Carbonates (sedimentary basins)	+10

(Geyh et al., 2000)

Each of these sources has a different carbon isotopic composition and contributes to total dissolved carbon in various proportions; therefore, the isotopic composition of DIC compounds in groundwater has a wide range of $\delta^{13}C$ values (Geyh et al., 2000). Most southeast Arizona marine carbonate is mid-Cambrian to Permian.

Soil carbon dioxide usually has a value of about –22 ‰; in tropical soils it may be more positive to about –11 ‰. Carbon dioxide of a magmatic origin has $\delta^{13}C$ values of about –6 ‰. Metamorphic carbon from sedimentary rocks is usually close to zero (-4 to +4) if it is derived from marine carbonates. The organic carbon of terrestrial plants has $\delta^{13}C$ values between –30 and –20 ‰. The heaviest carbon-isotopic composition is found in evaporate carbonates with 10 ‰. Such carbonates occur in sedimentary basins where the $\delta^{13}C$ values of DIC of fresh groundwater might have elevated $\delta^{13}C$ values (Geyh et al., 2000).

The $\delta^{13}C$ results (Table 6.8) range from -13.1 to -2.5 ‰. The $\delta^{13}C$ values for groundwater samples Ts01 (Agua Caliente), Ts02 (Hooker), Ts06 (Dankworth), and Tw22 (Tonopah) range in value from -13.1 to -10.0 ‰ indicating CO_2 derived from tropical soils (warmer climate, lower elevation). The $\delta^{13}C$ values for groundwater samples from Ts03 (Dunes), Tw05 (Willcox), Tw07 (Watson), Ts07 (Thatcher), Ts08 (Potter), Tw14 (Radium), Ts17 (Cofer), Ts18 (Ringbolt), Ts23 (Castle), and (Ts24 (Kaiser) range from -9.6 to -5.3 ‰ and are likely associated with an endogenetic or magmatic source, and mixed interaction in carbonate rocks. Groundwater samples Ts08 (Potter), Ts17 (Cofer), and Ts24 (Kaiser) were also very high in CO_2 (20,000 to 24,000 µg/l) suggesting CO_2-rich waters that are commonly found on the boundaries of active volcanic geothermal systems and around volcanoes, or from reservoir fluids in old and cooling geothermal systems (Arnórsson et al., 2007) (Aiuppa et al., 2003). Groundwater $\delta^{13}C$ values for Ts05 (Indian), and Ts09 (Gillard) range from -2.5 to -4.0 ‰ and closely reflect that of sedimentary marine carbonates.

Light Stable Isotopes

Oxygen and Hydrogen Isotopes

Results for $\delta^{18}O$ and $\delta\ ^{2}H$ (D) are presented in Table 6.10 and plotted on Figure 6.1. The δD values range from -61 to -91 ‰. Results for $\delta^{18}O$ range from -8.4 to -12.2 ‰. Values are consistent with those reported for the same springs by Mariner et al. (1977). The concentrations of stable isotopes D and $^{18}0$ in water from different sources are used to characterize and indicate the origin and mixing patterns of individual waters. During passage through an aquifer, thermal and non-thermal groundwater retains the D composition characteristic of precipitation in the recharge area. Unlike oxygen, an isotope shift does not occur in hydrogen because rock minerals contain little hydrogen and because the water-to-rock ratios of geothermal systems are seldom so low that the hydrogen of rock minerals is a significant fraction of the total hydrogen (Truesdell and Hulston, 1980). The isotopic ^{18}O content in thermal water is usually enriched (becomes less negative) to varying degrees during circulation within the system, due to reaction with the more enriched isotopic $^{18}0$ of the confining rock.

Table 6.10 Summary of Results for δ ^{18}Oxygen and δ Deuterium Isotopes

Label	T^{o} C	δ ^{18}O ‰	δ D ‰
Analytical Precision:		0.08	0.9
Ts01	31.5	-10.1	-73
Ts02	47.8	-11.7	-84
Ts25	44.6	-11.7	-83
Ts06	35.5	-12.2	-91
Ts03	37.5	-11.3	-82
Tw07	40.3	-11.1	-79
Ts09	>60	-10.9	-83
Ts07	36.4	-11.5	-86
Tw05	31.4	-11.2	-85
Tw14	50.5	-8.4	-61
Ts18	48.7	-11.2	-89
Ts17	32.6	-10.1	-75
Ts08	46.6	-11.5	-86
Ts05	44.4	-11.3	-86
Tw22	30.1	-9.6	-70
Ts23	40	-11.2	-82
Ts24	33.9	-11.4	-85

Aquifers recharged by precipitation from lower altitudes have higher δ^{18}O and δD values, plot higher on the trend lines, and are more likely to have evaporative loss. Water that has evaporative loss (low humidity), plots to the right of the meteoric line. Aquifers recharged by precipitation from higher altitudes have lower δ^{18}O and δD values, plot low on the meteoric water line, and condensed at cooler temperatures—at a higher altitude or in a cooler climate long ago. Precipitation occurring under cooler conditions (higher latitudes and altitudes) is more negative in D values (Gat and Gonfiantini 1981). An increase over time in δ^{18}O and δD can be attributed to recharge from aquifers fed by precipitation from lower altitudes or by subsurface boiling and vapor separation.

A worldwide study of freshwater samples by Craig (1963) showed that the isotopic compositions of cold meteoric waters were related by the equation $\delta D=8*\delta^{18}O+10$ per mil. This straight line, commonly referred to as the Standard Meteoric Ocean Water (SMOW) line, is shown in figure 6.1. The slope of the trendline varies regionally. For this reason the Arizona (Flagstaff) Local Meteoric Water Line (LMWL) has been added; the primary reason for the relatively lower slope is the partial evaporation of falling droplets in Arizona's arid climate.

Figure 6.1 $\delta^{18}O$ and δD plotted against the SMOW and LMWL trend lines

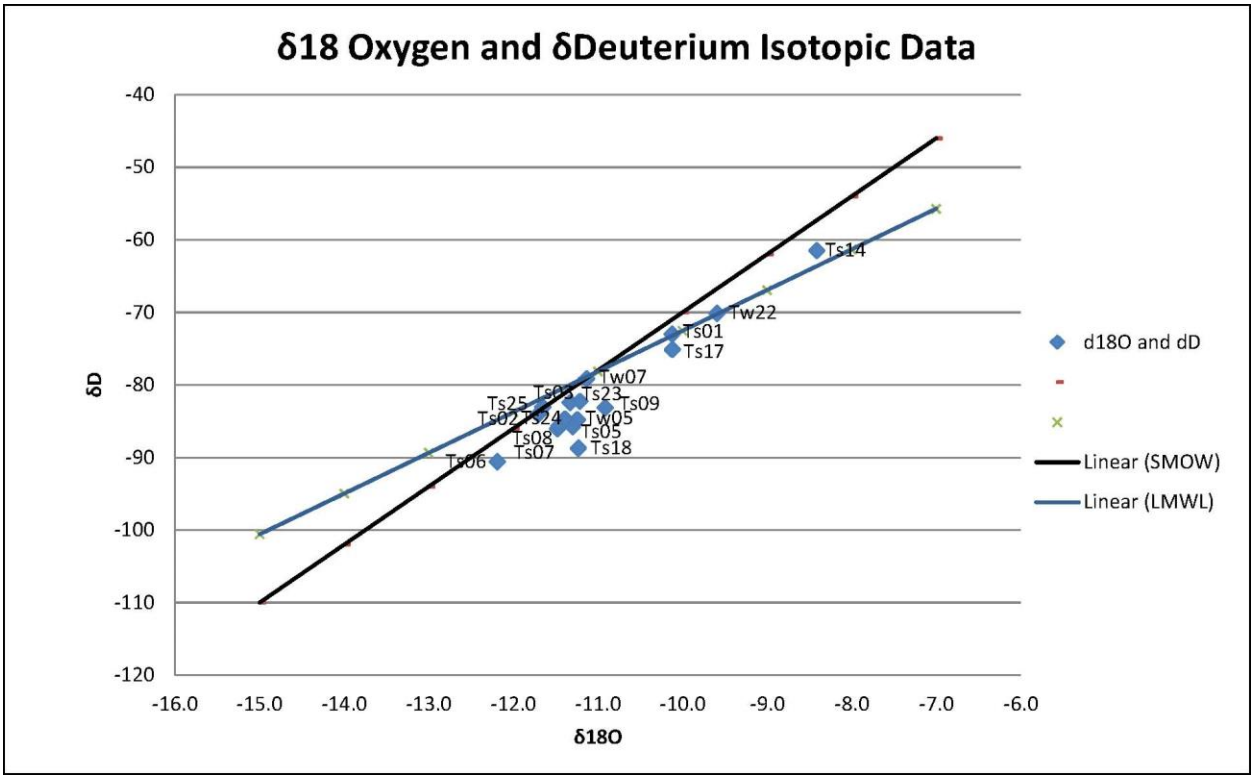

A plot of stable-isotope $\delta^{18}O$ and δD values, in standard δ values (‰) relative to the SMOW and LMWL, is shown in Figure 6-1. Most of the thermal spring water δD - $\delta^{18}O$ values fall adjacent to and to the right of the SMOW indicating groundwater that has had evaporative loss which is consistent with inland basins (Figure 6.1). The tightly clustered results low on the SMOW indicate accumulation at cooler temperatures and higher altitudes (or cooler climate) and more likely to be transported through bedrock to deep aquifers. The springs higher up the SMOW indicate surface evaporative loss before infiltration, more likely associated with summer precipitation events. The later results could also indicate precipitation during a warmer climate or lower altitude, or some mix of deeply circulated groundwater and shallow basin groundwater. Only the result from Ts14 (Radium) lies to the left of and higher up the trendline which indicates deeply circulated waters.

The plot of $\delta^{18}O$ versus ^{14}C age (uncorrected) (Figure 6.2) provides a first glance dating tool for maximum groundwater ages. If corrected ages had been used, the data plots would all shift right by varying number of years (an estimated 10-48% younger for corrected ^{14}C ages). The temperature dependence of the isotopic composition for precipitation is preserved in fossil groundwater of Pleistocene and Holocene age (Figure 6.2) recharged under different climatic conditions. During the Pleistocene glacial period, the precipitation was isotopically lighter because of a lower temperature of about 5°C (Stute,

Figure 6.2 Deviation of $\delta^{18}O$ values of Pleistocene and Holocene Groundwater in Arizona

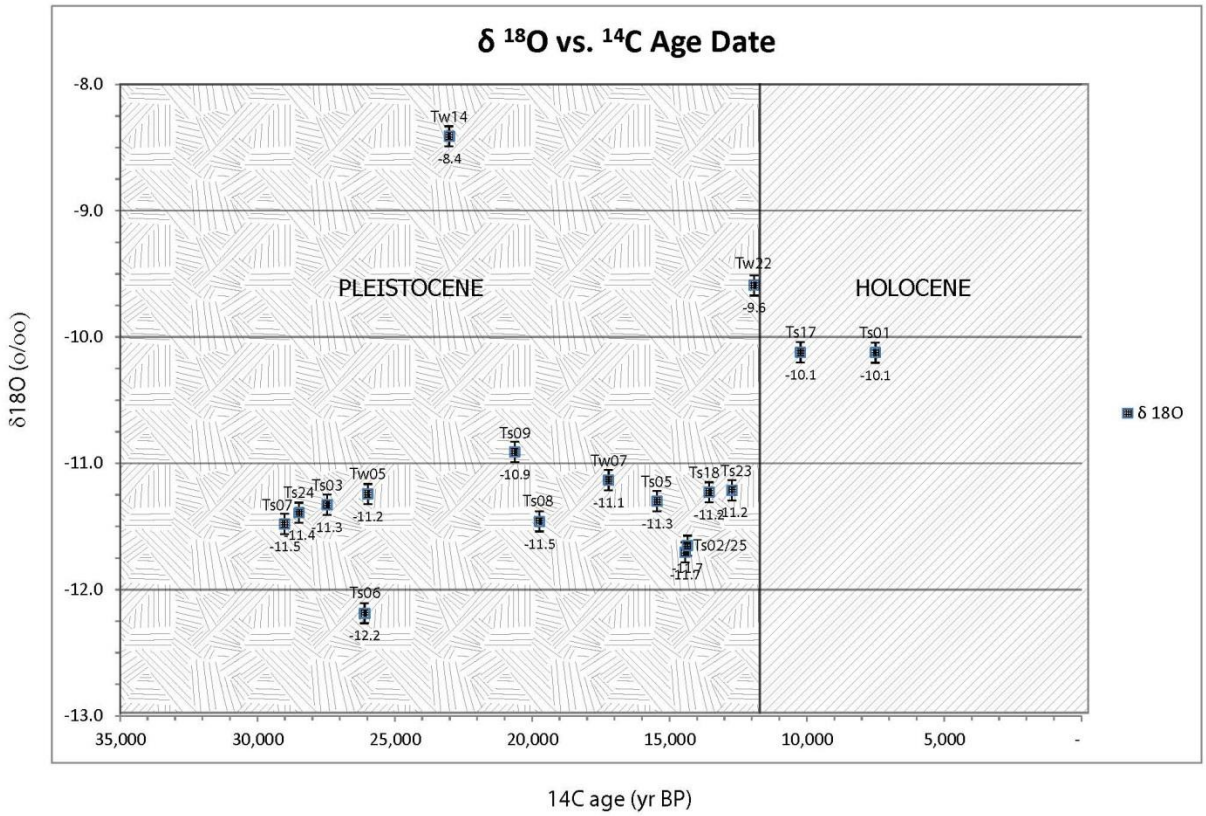

1989). In Europe the $\delta^{18}O$ values for groundwater of these two periods differ by 1.5 to 2.0 ‰ (Bath, Edmonds, and Andrews, 1978) which is consistent with plotted data in Figure 6.2. Sample Tw14 (Radium) is an anomaly with much higher than expected $\delta^{18}O$ value.

Strontium

The strontium concentrations measured in groundwater from thermal springs and wells range from 0.002 mg/l to 9.63 mg/l (Table 6.11). The $^{87}Sr/^{86}Sr$ ratios range from 0.70799 to 0.72558. The variations of strontium isotope ratios in bedrock result from original strontium isotopic variations and from differences in the amounts of radiogenic ^{87}Sr that have accumulated since rock genesis by sedimentary or igneous processes. The rate of ^{87}Sr accumulation varies greatly due to differences in rubidium concentration and in the geologic age of the rocks. Similar $^{87}Sr/^{86}Sr$ ratios suggest similar rock composition and age. All samples have relatively high $^{87}Sr/^{86}Sr$ ratios in a range that suggests groundwater circulation in continental crust origin rocks and some have accumulated significant amounts of ^{87}Sr due to their great age.

A summary of Sr and $^{87}Sr/^{86}Sr$ results is presented in Table 6.11.

Table 6.11 Summary of Results for Strontium and $^{87}Sr/^{86}Sr$ Isotopes

Label	Sr (mg/l)	$^{87}Sr/^{86}Sr$
Ts01	0.295	0.71942
Ts02	0.002	0.71175
Ts25	<0.002	0.71112
Ts06	0.138	0.71691
Ts03	0.046	0.71741
Tw07	0.004	0.71486
Ts09	0.429	0.72048
Ts07	9.424	0.71826
Tw05	0.607	0.71631
Tw14	1.634	0.71137
Ts18	2.836	0.71125
Ts17	0.52	0.71771
Ts08	9.63	0.72508
Ts05	0.57	0.71549
Tw22	0.012	0.70799
Ts23	0.288	0.71276
Ts24	0.171	0.72558

Strontium concentrations are plotted against $^{87}Sr/^{86}Sr$ (Figure 6.3). There appear to be three groups with potential similar age characteristics. Springs Ts07 (Thatcher) and Ts08 (Potter) have relatively high Sr concentrations at 9.424 mg/l and 9.63 mg/l, respectively, suggesting long duration circulation during which high strontium concentrations developed. Groundwater samples Ts18 (Ringbolt) and Tw14 (Radium) can be grouped as having higher than average Sr concentration (2.8 mg/l and 1.6 mg/l, respectively) and similar $^{87}Sr/^{86}Sr$ ratios close to surface water ratios (0.709). This suggests moderate duration circulation for the groundwater.

The remaining samples show relatively low Sr concentrations suggesting short-term circulation of groundwater, and a wide range of $^{87}Sr/^{86}Sr$ ratios, as expected, considering locations throughout the state with a large range of source rock compositions and origins.

Figure 6.3 Plot of Strontium versus $^{87}Sr/^{86}Sr$ for Thermal Groundwater in Arizona

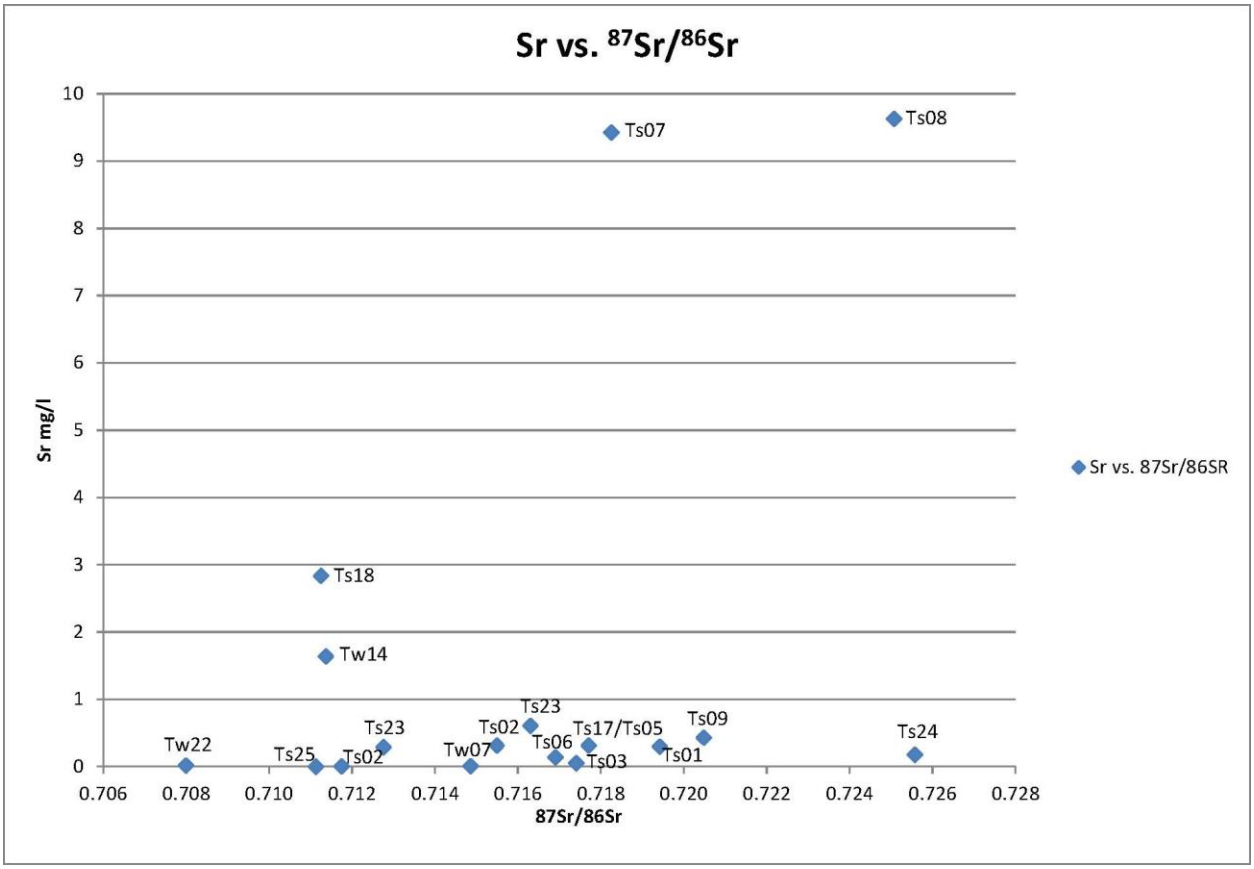

Noble Gases

Helium Dating

Helium concentrations were reported for each sample as ^{4}He and also as R/Ra, the ratio of sample $^{3}He/^{4}He$ to atmospheric $^{3}He/^{4}He$. Helium is measured in cubic centimeter of volume at standard temperature and pressure per gram of water ($cm^{3}STP/g$). He concentrations in the range of 10^{-7} to 10^{-4} represent a source of crustal fluids with long circulation times in deep rocks, with large accumulation of radiogenic ^{4}He (see Table 4.1). The common R/Ra value for crustal fluids range from 0.007 to 0.022, while the R/Ra for a source derived from surface water would reach approximately 1.0 (recent precipitation and infiltration).

All groundwater samples contained large amounts of excess ^{4}He indicating an enriched continental crust source (Table 4.1). The R/Ra values in Table 6.12 fall in between the two source indicators, suggesting the groundwater has components of both deeply circulated, long-resident time crustal fluids and more

recently accumulated (younger) groundwater. Mixing can occur when thermal deep groundwater seeps into basin aquifers through fractures or faults, and the mixed waters are circulated in the basin. Even in the case of a more direct transport mechanism, deep thermal groundwater could be diluted with basin meteoric groundwater as it migrates upward along faults.

Table 6.12 Summary of Results for Helium Isotopes

Label	He4 (ccSTP/g)	R/Ra	Notes
Ts01	3.25E-06	0.07	Large amount of excess ^{4}He
Ts02	1.67E-07	0.18	Large amount of excess ^{4}He
Ts25	-	-	Extraction failed - sample leaked (Ts02 Dup)
Ts06	5.41E-07	0.41	Large amount of excess ^{4}He
Ts03	-	-	Extraction failed - sample leaked
Tw07	1.85E-07	0.41	Large amount of excess ^{4}He
Ts09	3.57E-06	0.27	Large amount of excess ^{4}He
Ts07	2.43E-06	0.02	Large amount of excess ^{4}He
Tw05	1.85E-06	0.31	Large amount of excess ^{4}He
Tw14	1.35E-06	0.11	Large amount of excess ^{4}He
Ts18	4.41E-06	0.57	Large amount of excess ^{4}He
Ts17	1.86E-05	0.91	Large amount of excess ^{4}He
Ts08	7.22E-06	0.28	Large amount of excess ^{4}He
Ts05	3.36E-07	0.39	Large amount of excess ^{4}He
Tw22	1.77E-07	0.24	Large amount of excess ^{4}He
Ts23	1.95E-06	0.48	Large amount of excess ^{4}He
Ts24	3.75E-05	0.87	Large amount of excess ^{4}He

Both water samples Ts17 (Cofer) and Ts24 (Kaiser) show higher ^{4}He concentrations with R/Ra ratios closest to those for surface water, suggesting mixing of long term circulated waters (large amount of excess ^{4}He) with younger meteoric groundwater (high R/Ra) is likely.

Other Noble Gases

In addition to the Helium noble gas data, results for other noble gases including N_2, Ar, Ne, Kr, and Xe were reported for use in gas geothermometry interpretation, but not discussed further in this report. Noble gas results are summarized in Table 6.13.

Table 6.13 Summary of Results for Other Noble Gases

Label	N_2 total (ccSTP/g)	Ar total (ccSTP/g)	Ne total (ccSTP/g)	Kr total (ccSTP/g)	Xe total (ccSTP/g)
PQL:					
Ts01	1.56E-02	2.90E-04	1.84E-07	6.85E-08	9.21E-09
Ts02	7.48E-03	2.07E-04	1.11E-07	4.36E-08	7.77E-09
Ts25	-	-	-	-	-
Ts06	1.23E-02	4.04E-04	4.07E-07	7.06E-08	7.80E-09
Ts03	-	-	-	-	-
Tw07	1.12E-02	2.97E-04	2.66E-07	5.54E-08	7.01E-09
Ts09	2.33E-03	1.44E-04	1.05E-07	3.27E-08	4.77E-09
Ts07	2.98E-02	8.91E-04	1.32E-06	1.62E-07	1.75E-08
Tw05	4.77E-03	2.55E-04	1.77E-07	3.68E-08	5.23E-09
Tw14	6.15E-03	1.88E-04	1.64E-07	3.47E-08	5.22E-09
Ts18	7.08E-03	1.73E-04	1.50E-07	2.99E-08	3.84E-09
Ts17	1.78E-02	6.60E-04	9.14E-07	1.12E-07	1.16E-08
Ts08	2.24E-03	1.45E-04	9.56E-08	2.89E-08	4.13E-09
Ts05	1.35E-02	1.91E-04	2.97E-07	1.90E-08	1.85E-09
Tw22	7.97E-03	2.31E-04	1.59E-07	4.16E-08	6.14E-09
Ts23	6.56E-03	2.36E-04	1.67E-07	4.78E-08	6.06E-09
Ts24	5.28E-03	3.06E-04	1.81E-07	4.12E-08	6.06E-09

7. GEOTHERMOMETRY

Chemical geothermometers have been available since the 1960s. They are very useful as a prospecting tool to provide estimates of the temperature of a geothermal reservoir during exploration and development, and during on-going management of a resource. Careful consideration should be given to geothermometry data during interpretation and it is important to consider that the geothermal fluids are coming from a deep reservoir where the most important process is water-rock interaction, dependent mainly on temperature, and has a great influence on the chemical composition of the fluids. Geothermometers work because the relative equilibrium concentrations of chemical species change with respect to temperature. The rates at which different species react also vary, with cations like sodium and potassium adjusting more slowly than silica. Therefore, the cation geothermometry has a longer "memory" and typically reflects the temperature of a more distant or deeper source fluid. In contrast, the silica geothermometer reflects the temperature of a nearby aquifer. Deep-reaching groundwater circulation, separated from the shallow local flow system, is characterized by long residence times (e.g. thermal groundwater) (Geyh et al., 2000).

As geothermal fluids are transported to the surface, they can cool by conductive heat loss as they pass through cooler rocks or by adiabatic cooling which is boiling due to decreasing pressure. All of these processes produce changes in the composition of the rising fluids. Conductive cooling can cause some modifications in the chemical composition by mineral dissolution or precipitation, causing changes in the degree of saturation with respect to both primary and secondary minerals that can affect an estimated temperature. The boiling processes invariably cause change in the composition of rising geothermal fluid and affects the estimated temperature. The temperature decrease and saturation degree varies and mineral dissolution or precipitation can occur. Another very important process that occurs in the upper part of the geothermal system is mixing with groundwater, which causes dilution and cools the geothermal fluids.

Ternary Diagrams

The Powell and Cumming (2010) worksheets provide a way to quickly plot chemical analyses on many commonly used geothermal geochemistry plots. Most of these plots were developed in the 1980s–1990s by Werner Giggenbach, based on his work and the research of many others (Arnórsson, 2000; Fournier, 1989). Owing to Giggenbach, the graphics included in these worksheets generally remain state-of-the-art for the conceptual interpretation of geothermal geochemistry directed at the exploration of geothermal reservoirs (Powell and Cumming, 2010).The graphs combine species with different sensitivity to temperature, mixing and other processes in order to resolve trends in geothermal reservoirs and their shallow manifestations (Powell & Cumming, 2010). The interpretation for our data is more qualitative due to project constrictions and limited data collection. We did not attempt to incorporate previous research data, although that would make a more remarkable argument.

Geothermometry calculators and geoindicators used in the Powell and Cumming (2010) charts incorporate both silica and cation geothermometers derived through previous work by Giggenbach, Fournier, Fournier and Potter, and Arnorsson. We have attempted here to follow the Powell and Cumming (2010) geothermometry worksheets as appropriate to investigate potential thermal water sources for each of the springs investigated for this project. Thermal groundwater samples were analyzed for stable isotope analyses $\delta^{18}O$ and δD, ^{14}C, tritium, and $^{3}He/^{4}He$. Analytes used to plot the geothermometry ternary charts and diagrams include Na, K, Li, Cl, F, B, Rb, Cs, Mg, SO_4, HCO_3, and SiO_2. The various ternary diagrams using the Powell & Cumming geothermometry spreadsheets are presented and discussed below. The complete workbook is included as Appendix D.

Tcsh

The Cl-SO_4-HCO_3 ternary plot illustrates the proportions of the major anions present in geothermal water based on Giggenbach, (1991a). Labels (Peripheral Water, Mature Water, Volcanic Water, Steam Heated Water) indicate associations with either different parts or different types of geothermal systems. Figure 7.1 plots Cl-SO_4-HCO_3 for groundwater samples collected from the thermal springs and wells.

Figure 7.1 Tsch - SO_4-Cl-HCO_3 Ternary

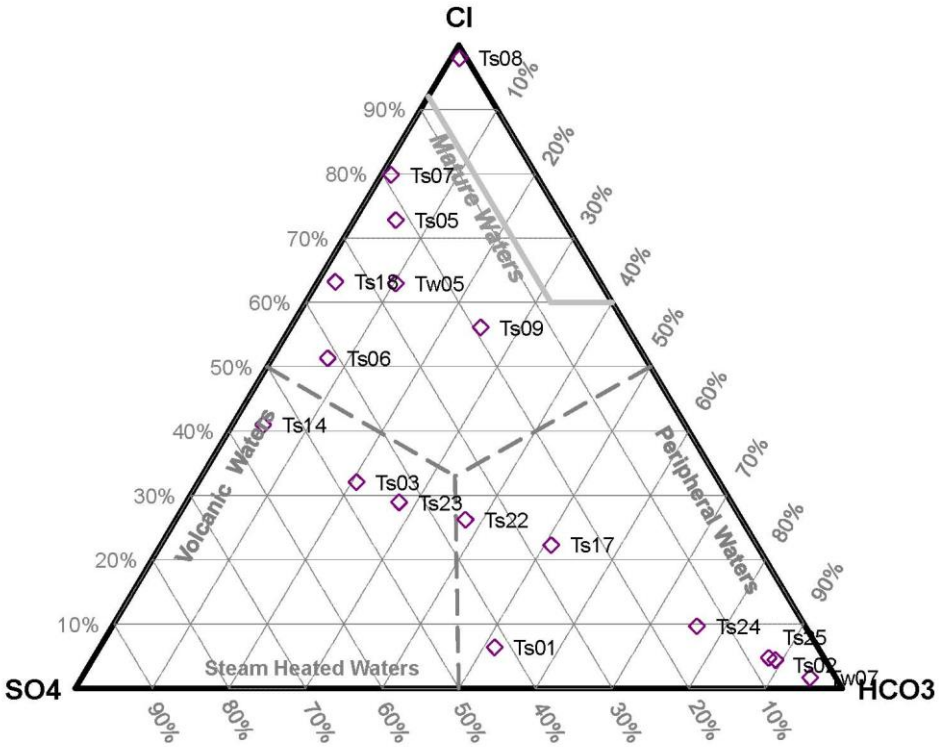

A hot spring with significant Cl, moderate HCO_3 and minimal SO_4 is consistent with outflow from a geothermal reservoir and is more likely to provide reliable cation geothermometry than a spring that is mainly bicarbonate or sulfate. Results related to this scenario fall within the upper sector of the ternary diagram. Based on this criteria, thermal water reflecting this balance include samples Ts07 (Thatcher), Ts05 (Indian), Tw05 (Watson), Ts08 (Potter), Ts09 (Gillard), Ts06 (Dankworth), and Ts18 (Ringbolt). The TS08 (Potter) groundwater has very high chloride with minimal sulfur and bicarbonate, and also falls within the criteria for mature waters. The source of the sodium chloride is not readily apparent because there is no evaporite deposit observed in the area; however, the salt may be from brines discharged from a high temperature reservoir (>150°C) (Witcher, 1979d). All the samples plotted in the upper sector of the ternary diagram, except Ts18 (Ringbolt), were collected in the Safford-Clifton area, which has been previously mapped as an area with high chemical geothermometry (Witcher, 1979d).

In a volcanic context, a bicarbonate hot spring with high HCO_3 and some SO_4 and no Cl is more likely related to groundwater heated by steam from a deeper reservoir. Samples Ts02 (Hooker), Ts01 (Agua Caliente), Tw07 (Watson), and Ts24 (Kaiser) meet the criteria as a bicarbonate hot spring having both very low Cl and some SO4. Other thermal water samples falling within this sector although with increasing Cl are Ts22 (Tonopah) and Ts17 (Cofer). Groundwater sample Ts02 (Hooker) and Tw07 (Watson) have Cl-HCO_3-SO_4 balances associated with peripheral waters.

A spring with high SO_4 is likely to be associated with a deeper boiling zone. Possible associations are more definitive when combined with analyses of other water and gas constituents and with other geoscience data sets, including geology and structure. Thermal water samples falling within the SO_4 sector, although not considered very high in SO_4, are Ts14 (Radium), Ts03 (Dunes), and Ts23 (Castle). Groundwater sample Ts14 (Radium) is more closely related to values associated with volcanic waters.

Tclb

The ternary of chloride, lithium and boron (Giggenbach, 1991a) is used to distinguish fluids from different sources, reveal fractionation associated with boiling or mixing with fluids that have boiled, or differentiate fluids generated by unique sources of high temperature steam (Powell and Cumming, 2010). The ternary Tclb (Figure 7.2) plots Cl-Li-B results for sampled thermal springs.

Chloride and boron concentrations in a geothermal field should have a linear relationship if very low-concentration cold water mixes with high-concentration hot water (Witcher, 1979d). Chloride and boron are not assumed to be involved in water-rock reactions after the hot water has left the reservoir. Due to the distance between most sample locations, you would not expect there to be a linear relationship between these sample results.

Figure 7.2 Tclb - Cloride-Lithium-Boron Ternary

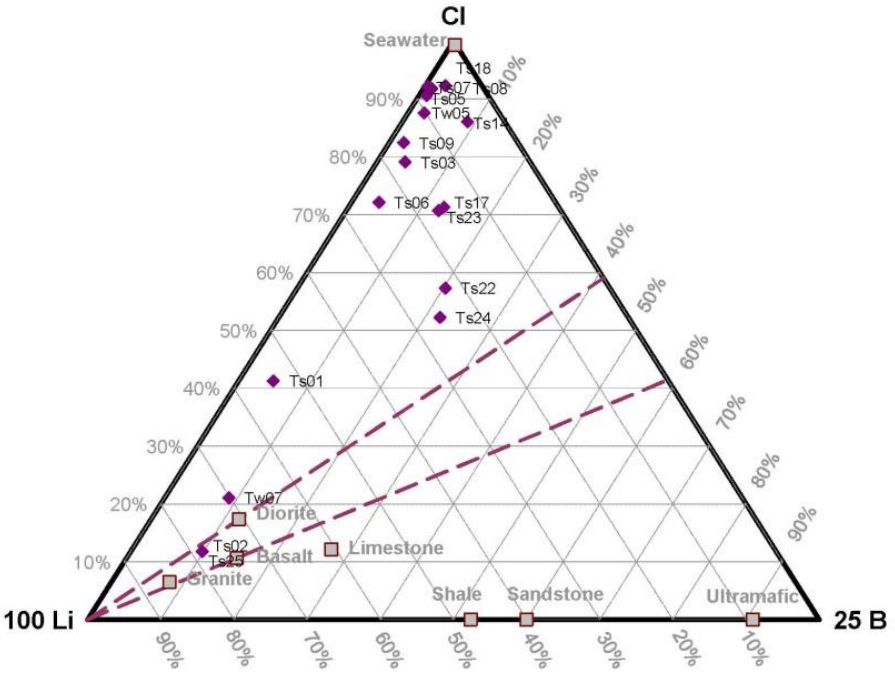

Results suggest spring water at Ts02 (Hooker) (dup Ts25) and Tw07 (Watson) likely circulate a diorite rock source. Ts01 (Agua Caliente) shows some association with granitic rock circulation, but being higher in chloride may indicate circulation in a basin with granitic detritus. Most of the other spring water samples appear to be more saline (higher chloride content) and possibly due to long term circulation of groundwater in deep source rocks and/or mixing with basin groundwater where gypsum and halite are deposits in basin fill and absorbed in solution.

Tcfb

This ternary of Cl-F-B is useful in tracing sources of water, because, in the absence of relatively rare fluorite with which to re-equilibrate, F can be expected to be conservative. The Tcfb ternary (Figure 7.3) was used to illustrate potential varying sources of thermal spring groundwater. Springs and wells were sampled throughout Arizona with only a few within close enough proximity to share source reservoirs; therefore, one would not expect the fluoride concentrations to be similar across the samples, and indeed they are not. All groundwater samples were low in B.

Figure 7.3 Tcfb - Chloride-Fluoride-Boron Ternary

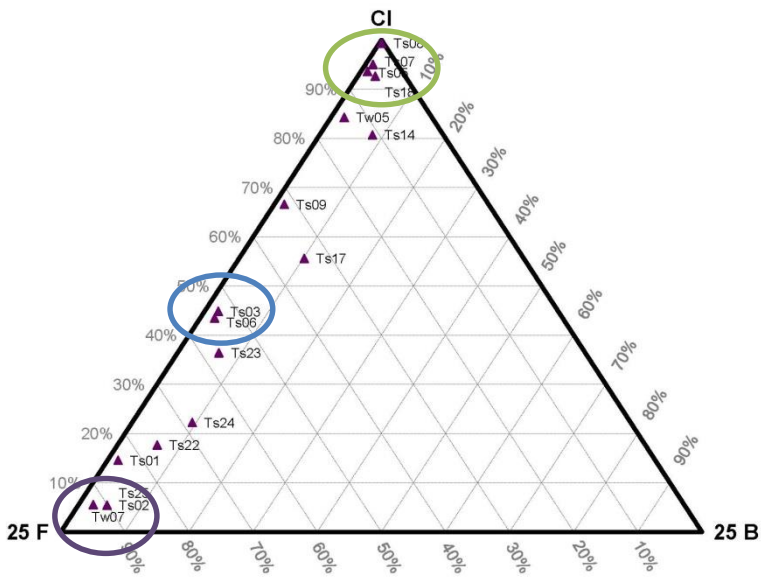

There were several springs along the transition zone from Safford and Clifton areas that plotted with high Cl and low F values, as circled in green, and may share similar source bedrock. The group with the lowest F and highest Cl concentrations are Ts08 (Potter), Ts07 (Thatcher), Ts05 (Indian), and Ts18 (Ringbolt). Thatcher and Indian thermal springs locations near Safford are along the base of the Gila Mountains and Transition zone, and may share the same source geothermal reservoir. Interestingly, Ts08 (Gillard) in Clifton and Ts18 (Ringbolt) collected in the Lake Mead Recreation Area in the NW portion of the state, share similar chemistry and are also at the base of the Transition zone.

The two samples Ts03 (Dunes) and Ts06 (Dankworth) circled in blue are from springs which are both in the Safford-San Simon Basin and share very similar F-Cl-B values suggesting a similar source reservoir.

Tw07 (Willcox) and Ts02 (Hooker) circled in purple plot with high F–low Cl-B values and are both in basins adjacent to the Winchester Mountain and have similar volcanic geology (See Section 8.3).

Tnkm

The Na-K-Mg graphic is probably the most widely used cation geothermometry plot, a ternary combining the sodium-potassium (Na-K) geothermometer with the potassium-magnesium (K-Mg) geothermometer. It is the most widely utilized version used of many effective cross-plots developed by Giggenbach, (1991a). This type of plot is known as a “geoindicator” because it organizes the plotted data

points in a manner that illustrates both the evidence that supports the interpretation of equilibrated water at high temperature and the influence of shallow processes, and possible equilibration at lower temperature (Powell and Cumming, 2010). Numerous case histories have illustrated the utility and limitations of this plot for interpreting the chemistry of neutral water from thermal springs and exploration wells. Barnett et al (2005), Mariner and Janik (1995) and Maturgo et al (2000) demonstrate that extrapolations of a geothermometer trend based on shallow samples can have excellent agreement with both geothermometers and measured temperatures from produced wells in the reservoir (Powell and Cumming, 2010).

On the ternary for Na-K-Mg (Figure 7.4), data plotted for several spring samples fall within the 'immature waters' sector. Since the cations for these samples are not in partial equilibrium, the waters are assumed to be from shallow sources or mixed, and temperatures likely are not accurate as plotted on this geothermometer grid. Several samples fall within this category: Ts17 (Cofer), Tw07 (Willcox), Ts22 (Tonopah), Ts02 (dup Ts25) (Hooker), Ts23 (Castle), and Ts01 (Agua Caliente).

Figure 7.4. Na-K-Mg Ternary

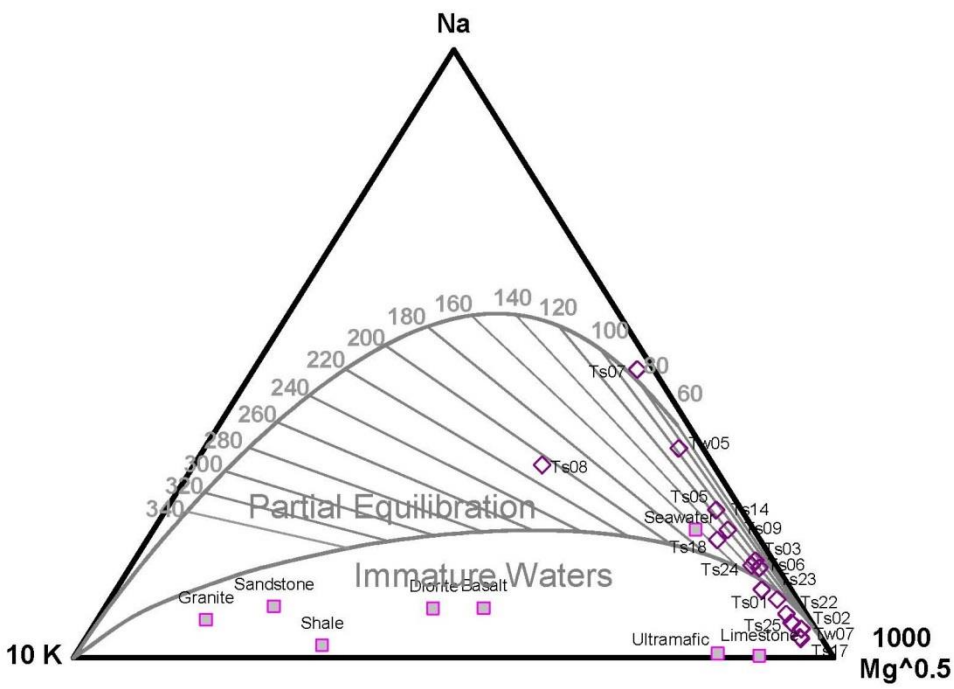

Waters that have been deeply circulated at high temperatures have cations in 'partial equilibrium' and plot on the geothermometer grid to estimate temperatures in the geothermal reservoir. The thermal water samples that plot in partial equilibrium and their approximate reservoir temperatures are: Ts06 (Dankworth, 120°C), Ts24 (Kaiser, 130°C), Ts18 (Ringbolt, 135°C), Ts03 (Dunes, 120°C), Ts09 (Gillard,

150°C), Ts14 (Radium, 120°C), Ts05 (Indian, 110°C), Tw05 (Watson, 95°C), and Ts08 (Potter, 205°C). Ts07 (Thatcher) plots in equilibrium suggesting that the geothermometer temperature of approximately 85°C may not be accurate as plotted on this grid and would likely be higher.

Piper

On the basis of water chemistry results, hot waters can be classified as Na-SO_4-HCO_3 type and cold waters Ca-HCO_3 type. In the Piper diagram (plotted in meq/kg; Powell and Cumming, 2010) (Figure 7.5), all samples have high Na+K and low Ca-Mg concentrations. Na+K are dominant cations plotting above 65% for all samples. Most samples [with the exception of Ts01 (Agua Caliente)] show Cl as the dominant anion. The Ts01 (Agua Caliente) artesian well groundwater is a sodium sulfate-bicarbonate type with low Cl. Results for two locations, Ts09 (Gillard) and Ts08 (Potter), show groundwater as a sodium bicarbonate-sulfate with equal parts SO_4 and HCO_3 with Cl as the dominant anion. Other groundwater types can be distinguished as being HCO_3 depleted and Cl-SO_4 enriched or, HCO_3 enriched and Cl-SO_4 depleted. Groundwater samples Ts02/25 (Hooker), Tw07 (Wilcox), Ts17 (Cofer), and Ts24 (Kaiser) plot as a sodium chloride-bicarbonate dominant groundwater type where $HCO_3 > SO_4$. Other groundwater from Ts03 (Dunes), TS05 (Indian) Ts06 (Dankworth), Ts07 (Thatcher), Tw05 (Watson), Tw14 (Radium), Ts18 (Ringbolt), Ts22 (Tonopah) and Ts23 (Castle) are of the sodium chloride-sulfate type where $SO_4 > HCO_3$.

Figure 7.5 Piper Trilinear (plotted in meq/kg)

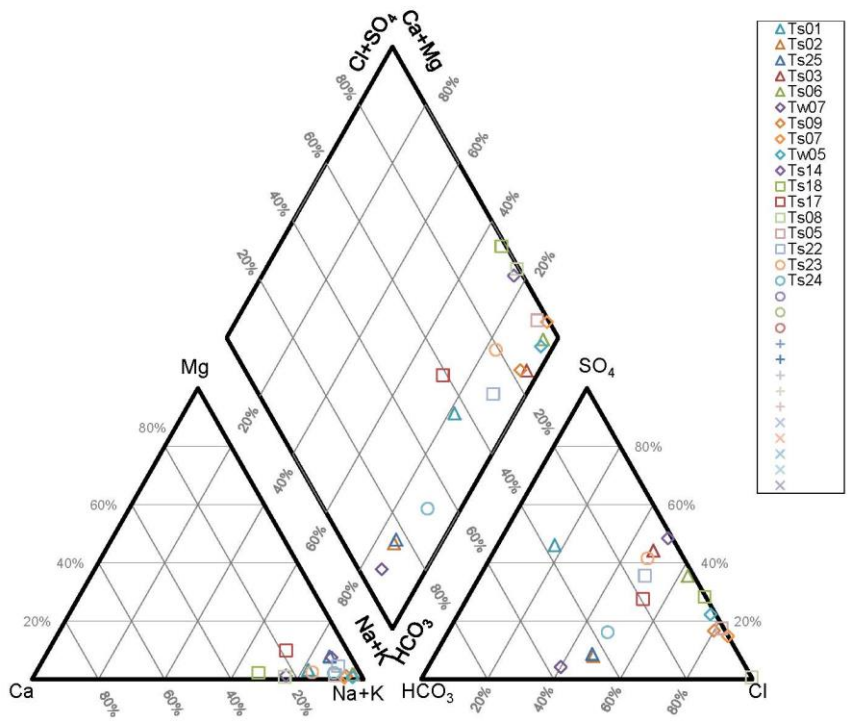

In this group Na^+ is the major cation and Cl^- is the major anion. The prevalence of sodium can be attributed to an increased potential of water to dissolve the aluminosilicate minerals of basement rocks due to increased CO_2 concentration (Ellis and Mahon, 1977). It is assumed that the high salt concentrations are the result of mixing between thermal fluids from greater depths and connate colder saline waters trapped in shallow sediments. Thermal Na-Cl waters generally have a higher mineralization (TDS > 1,000 mg/l) with concentrations sometimes exceeding 10,000 mg/l. TDS >1,000 mg/l was measured in 7 out of 17 groundwater samples. The origin of this fingerprint is two-fold. It could be due to the mixing of old, deep, strongly mineralized seawater and fresh water at different depths in the crystalline basement and Tertiary deposits, and by water-rock reactions with an increasing mineral dissolution due to the presence of CO_2 (Sonney, 2010). In more saline groundwater samples, the reduction of Ca^{2+}/Na^+ is typical of ion exchange, but a greater magnitude of Na+ enrichment compared to the Ca^{2+} decline suggests an additional source of Na+. In this case, the sources could be related to dissolution of basin evaporate minerals, such as halite (NaCl) (Al-Charodeh, 2013).

Thermal waters that have Na-SO_4 type water and a high TDS (> 1,000 mg/l) likely may circulate in crystalline rocks, their sulfate concentrations due to the dissolution of sulfide minerals or anhydrite veins and their sodium mainly from reactions with feldspars (Al-Charodeh, 2013). These include Ts07 (Thatcher), Tw05 (Watson), Tw14 (Radium), Ts18 (Ringbolt), and Ts05 (Indian). Spring waters with much higher mineralization and TDS such as Ts07 (Thatcher - 6,990 mg/l) and Ts08 (Potter - 9,740 mg/l) may be strongly influenced by the dissolution of formation evaporates. A decrease in HCO_3 is consistent with the loss of CO_2 during recycling (O´ Dochartaigh et al., 2010), and therefore, a tendency toward calcite precipitation.

Silica

Silica geothermometers are determined by experiment and temperature dependent variation in the solubility of silica in water. Geothermometer temperatures have been calculated for crystobalite, chalcedony, amorphous silica, and quartz via conductive cooling and via adiabatic cooling (boiling). The Fournier and Potter (1982) quartz geothermometer is used in the Powell and Cumming (2010) worksheets due to its accuracy in comparison to measured well temperatures. The quartz maximum steam loss geothermometer, based on the 1981 quartz formula, is more appropriate for boiling hot springs than the formula for conductive cooling. The amount of conductive heat loss of ascending geothermal waters is proportional to the distance travelled and inversely proportional to the flow rate. For vertical pipe flow, Truesdell et al., (1977) calculated that temperatures are reduced by half for waters flowing at 0.4 l/s from a 1 km deep reservoir. Conductive cooling can be expected to be important for isolated springs with flow of less than 1 l/s. In the case of closely spaced springs, trying to envisage the amount of conductive cooling in the upflow, the aggregate flow should be considered (Karingithi, 2009). When geothermometers are applied to estimate subsurface or aquifer temperatures, a basic assumption is made that temperature dependent chemical or isotopic equilibria prevail in the source aquifer—that chemical and isotopic reactions do not significantly modify the composition of the

fluid as it ascends from the source aquifer to the point of sampling, whether it is a thermal spring, vent, or wellhead.

The most important water geothermometers are silica (quartz and chalcedony) and K-Mg-Ca. In most geothermal systems, deep fluids at temperatures >180°C are in equilibrium with quartz; it is stable up to 870°C and has the lowest solubility compared to other silica polymorphs. Quartz is common as a primary and secondary (hydrothermal) rock-forming mineral. Silica polymorphs with a less ordered crystal structure (i.e. chalcedony, opal CT, cristobalite) have higher solubilities than quartz and form at cooler temperatures of < 180°C. The quartz geothermometer is best for reservoir conditions > 150°C.

If the quartz geothermometer or other geothermometers indicate temperatures of 120-180°C, it is possible that chalcedony may control silica solubility. If the chalcedony geothermometer gives temperatures of 100-120°C, it may represent the true deep temperature. However, if the calculated temperature is below 100°C, the amorphous silica may control the solubility (Karingithi, 2009).

Xkms

This cross-plot of the K-Mg geothermometer and the quartz (conductive) geothermometer is from Giggenbach and Goguel (1989). The plot uses the chalcedony geothermometer, which is often more appropriate to use than quartz for water from a lower temperature source. By comparing two low temperature geothermometers, it increases confidence in both if they agree. The quartz geothermometer calculations assume conductive cooling of the water after it leaves the reservoir. Disagreement between these two geothermometers might be due to dilution, equilibration with amorphous silica, or perhaps some residual effect of an acid zone that invalidates the geothermometry, even though the water has been neutralized (Powell and Cumming, 2010).

Figure 7.6 is a plot of silica versus temperature. Most groundwater samples give geothermometer temperatures ranging from 65°C to 79°C. Ts17 (Cofer) plots as a lower temperature at 57°C, whereas Ts09 (Gillard) gives a geothermometer at a slightly higher temperature of 88°C. An anomalous temperature is noted for Ts08 (Potter) which gives a geothermometer at 144°C. Both Gillard and Potter hot springs are located adjacent to the *Clifton Hot Springs Known Geothermal Resource Area* along the San Francisco River north of Clifton. Preliminary chemical geothermometer studies of the Clifton hot springs point toward a high temperature reservoir that is greater than 150°C (Witcher, 1979d).

Figure 7.6 SiO2-K/Mg Geothermometry

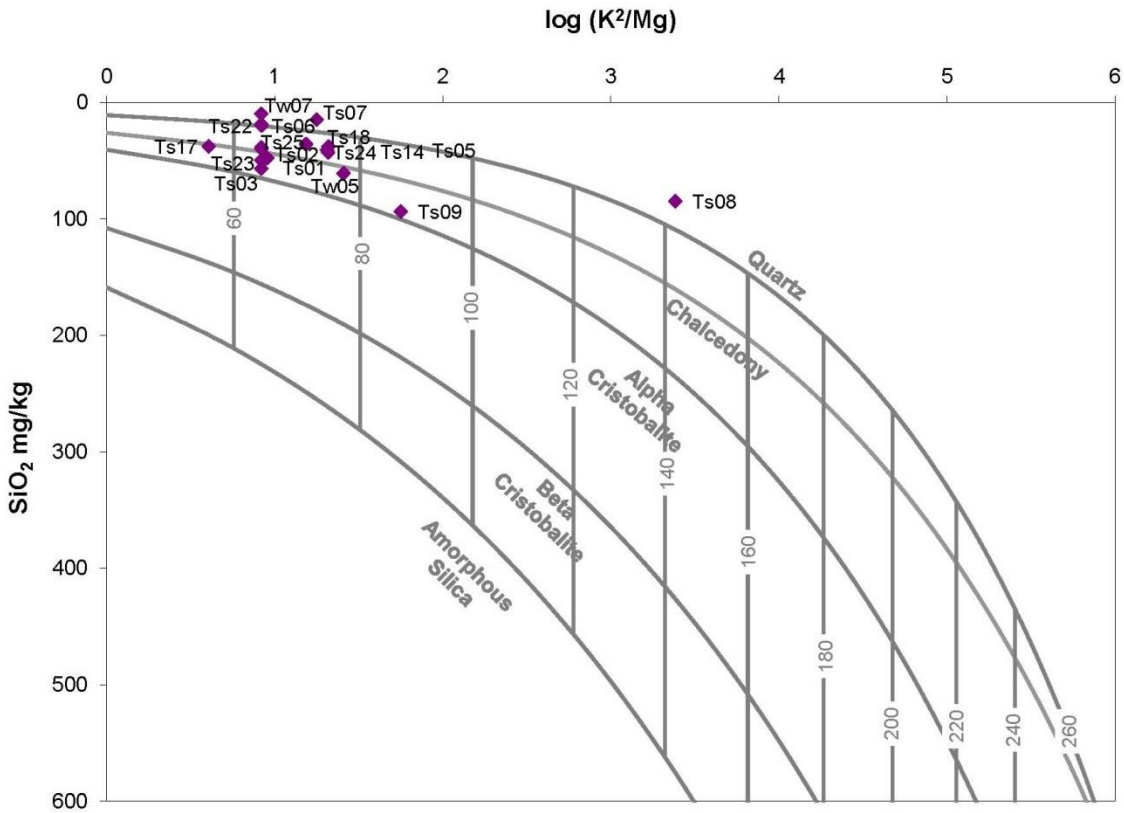

Xkmc

Giggenbach and Goguel (1989) refer to this cross-plot as a "geoindicator" rather than a geothermometer plot because it juxtaposes the potassium-magnesium geothermometer with a measure of the partial pressure of CO_2 based upon equilibrium between K-feldspar, calcite and K-mica on one side and dissolved Ca^{+2} and K^{+} on the other. The purpose of the cross-plot is to determine the partial pressure of CO_2 at the last temperature of the water equilibration with rock, as determined by the K-Mg geothermometer. In that values of the CO_2 partial pressure (P_{CO2}) assume equilibrium between calcite and the other mineral phases, P_{CO2} of analyses plotting outside the "calcite formation" envelope can only be interpreted qualitatively. This being the case, this plot is probably limited to assessments of whether the sampled fluid is likely to be in equilibrium with calcite in the subsurface (Powell and Cumming, 2010).

Figure 7.7 K-Mg-Ca Geothermometry

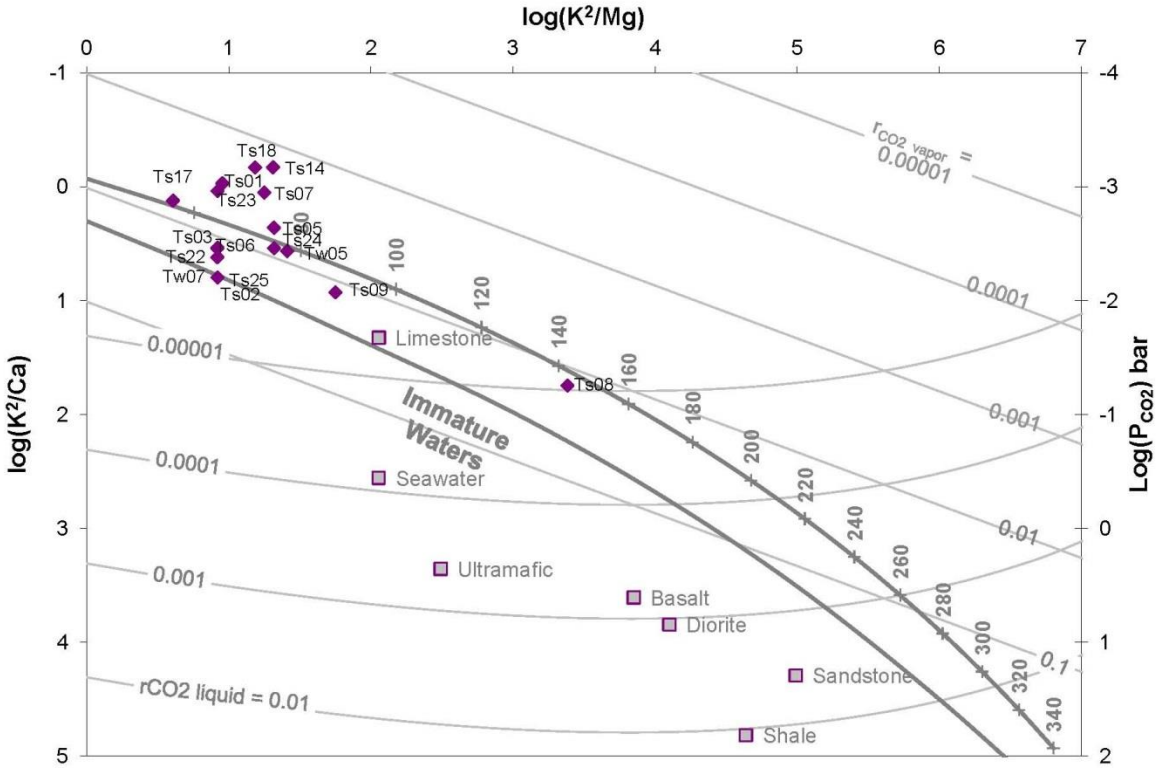

Sample results that plot on Figure 7.7 within the "calcite formation" envelope and likely in equilibrium with calcite in the subsurface are Ts03 (Dunes), Tw05 (Watson), Ts06 (Dankworth), Ts22 (Tonopah), and Ts24 (Kaiser) with geothermometer temperatures between 57°C and 79°C, Ts09 (Gillard) at 88°C, and Ts08 (Potter) at 144°C.

Liquid Geothermometers Report

The Liquid Geothermometry Report (Table 7.1) shows temperatures calculated using the common geothermometers discussed herein and by Powell and Cumming (2010). Fournier (1989) provides an excellent introduction to the models, derivations and assumptions used for the most widely used silica and cation liquid geothermometers. As a recap, the cation geothermometry has a longer "memory" and typically reflects the temperature of a more distant or deeper source fluid. In contrast, the silica geothermometer reflects the temperature of a nearby aquifer. The graphs (Figures 7.1–7.7) combine species with different sensitivity to temperature, mixing and other processes in order to resolve trends in geothermal reservoirs and their shallow manifestations. Table 7.1 lists the calculated temperatures in degrees C using the various geothermometers presented in this section and on the Powell and Cumming spreadsheets (Appendix D).

Table 7.1 Liquid Geothermometry Report (temperatures in degrees C)

						Not accurate below 150C and commonly greater than max temps in boreholes						
Sample Name	Chalcedony conductive	Quartz conductive	Quartz adiabatic	Na-K-Ca	Na-K-Ca Mg corr	Na/K Fournier 1979	Na/K Truesdell 1976	Na/K Giggenbach 1988	Na/K Tonani 1980	Na/K Nieva & Nieva 1987	Na/K Arnorsson 1983	K/Mg Giggenbach 1986
Ts01 Aqua Caliente	72	102	103	77	77	142	98	162	123	131	109	65
Ts02 Hooker	61	92	94	167	26	203	170	219	204	190	179	65
Ts25 (Dup Ts02)	60	91	93	167	26	203	170	219	204	190	179	65
Ts03 Dunes	79	108	108	111	50	94	45	115	65	84	57	65
Ts06 Dankworth	31	64	69	113	50	98	50	119	70	88	62	65
Tw07 Willcox	62	93	95	165	27	198	164	215	196	185	173	65
Ts09 Gillard	107	134	130	136	99	130	84	149	108	118	95	88
Ts07 Thatcher-S	21	53	60	76	76	44	-6	66	9	35	6	74
Tw05 Watson	82	112	111	99	96	73	22	94	40	63	35	79
Ts14 Radium	62	93	95	75	75	99	50	119	70	88	62	76
Ts18 Ringbolt	56	88	90	72	72	112	64	132	86	101	76	72
Ts17 Cofer	59	90	92	80	62	148	104	167	130	136	115	57
Ts08 Potter	101	128	125	180	176	189	153	206	185	177	162	144
Ts05 Indian	59	90	92	106	102	90	41	111	60	80	53	76
Ts22 Tohonopah	29	62	67	144	39	158	116	176	143	146	126	65
Ts23 Castle	70	100	101	76	76	126	80	146	104	115	92	66
Ts24 Kaiser	64	95	97	134	89	140	95	159	120	128	107	76

8. GEOLOGICAL MAPPING

8.1 Pinaleño Mountains-Safford Basin Geologic Investigation

By Brian Gootee and Joe Cook, Arizona Geological Survey, 2014

Geologic setting of the Cactus Flat, Buena Vista and Indian Hot Springs, Safford Basin

The Safford basin lies in a region of highly extended crust within the Basin and Range tectonic province. The Cactus Flat hot springs lie on the south-central margin of the Safford basin, bound by the Pinaleño Mountains to the south (Figure 8.1.1). The Buena Vista and Indian hot springs are found along the northeastern margin of the basin at the base of the Gila Mountains. The Pinaleño Mountains are composed of Precambrian metamorphic and plutonic granitoid rocks and Laramide-age granitoid plutonic rocks (Thorman et al., 1981; Long et al., 1995). The Gila Mountains are composed of mostly mid-Tertiary volcanic rocks with minor Laramide-age volcanic and intrusive rocks. In the Safford basin a thick accumulation of unconsolidated to semi-consolidated basin-fill sediment overlies the mid-Tertiary sequence. Overlying the basin-fill deposits are a relatively thin sequence of alluvial deposits related to the development of the through-flowing Gila River.

The Safford basin initially formed from crustal extension during the mid-Tertiary. Extension led to normal faulting, uplift and exposure of ranges, and tectonic subsidence of adjoining basins. Extension was accommodated primarily along low-angle detachment faults separated into an upper-plate hanging wall and a lower-plate footwall (Spencer and Reynolds, 1989). The Pinaleño Mountains represent the footwall, where exhumed crystalline basement is overprinted by a gently-dipping mylonitic fabric indicating a top-to-northeast sense of shear (Naruk, 1987; Long et al., 1995). Paleozoic, Mesozoic and early- to mid-Tertiary rocks generally form the upper plate or hanging wall of the detachment fault, and are present as faulted blocks in the Santa Teresa, Dos Cabezas and Chiricahua mountains to the west and south, and mid-Tertiary volcanic rocks in the Gila, Whitlock and northern Peloncillo Mountains to the north, northeast, and southwest (Figure 8.1.1). Initially, mid-Tertiary volcanic and sedimentary rocks were deposited during early Safford-basin formation, followed by non-volcaniclastic mid- to late-Miocene basin-fill sediment. Continued high-angle normal faulting on the southwest margin of the Safford basin during the Miocene and Pliocene allowed thick sequences of basin-fill sediments to accumulate in an asymmetric sedimentary half-graben (Kruger et al., 1995). Basin-fill strata consists of alluvial, playa and lacustrine sediments deposited in a closed basin, although fluvial deposits from the ancestral Gila River area are locally present in the Upper basin-fill (UBF) sequence.

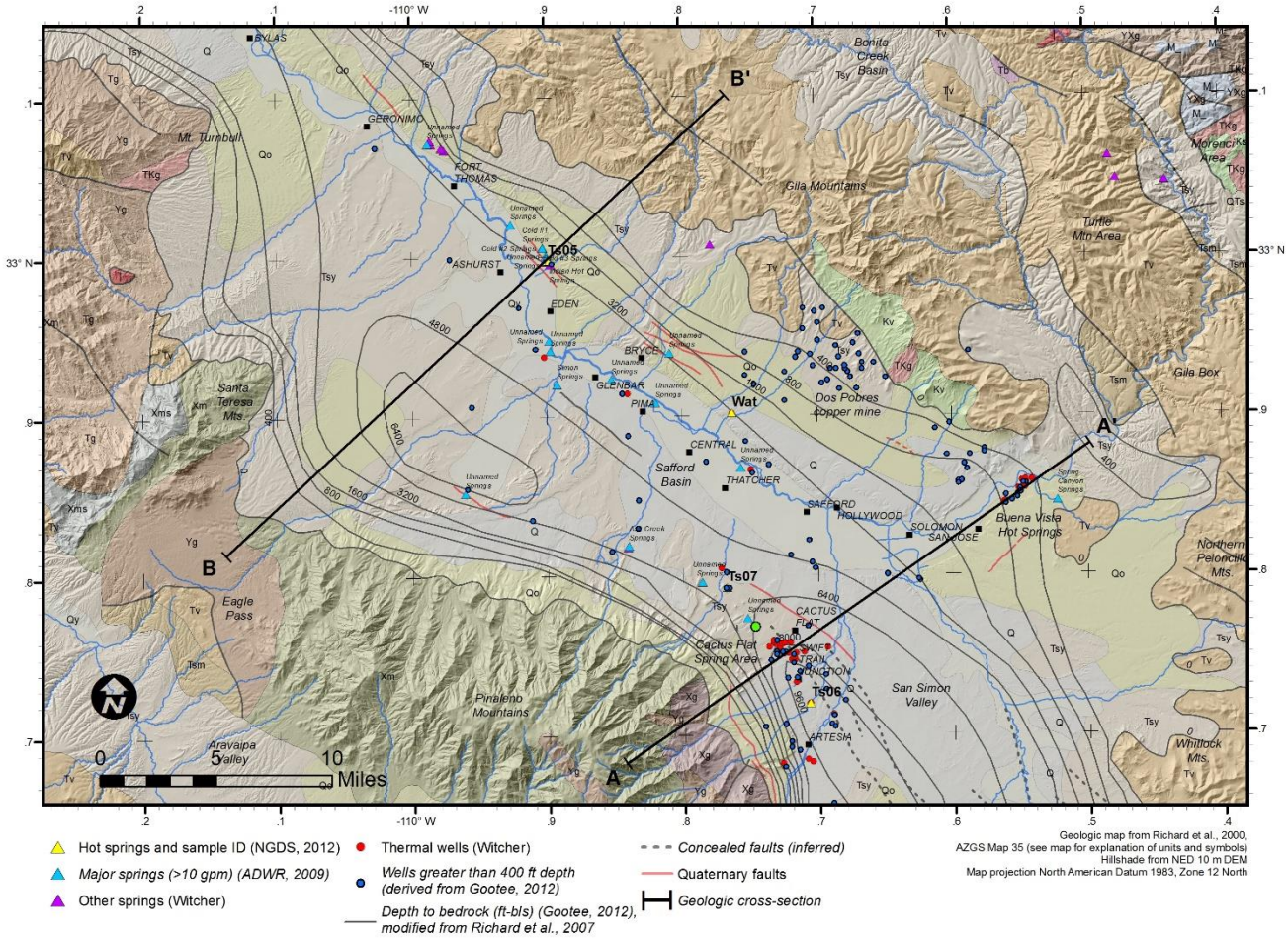

Figure 8.1.1 Geologic Map of the Pinaleño Mountains and Safford Basin including Cactus Flat, Buena Vista, and Indian Hot Springs

Structure

The Safford Basin is largely an asymmetric basin, bound on its southwest margin by a high-angle listric normal fault zone, referred to herein as the Pinaleño fault. The Pinaleño fault has been interpreted to represent a reactivated secondary-breakaway fault as part of a splay or continuation of the mid-Tertiary Pinaleño detachment fault (Spencer, 1984). The Pinaleño fault zone also coincides with the North and South Safford fault zones and Cactus Flat fault, most recently active during the late to latest Pleistocene (Houser et al., 2004). Several concealed faults in basin fill identified from seismic surveys lie between the Pinaleño fault and Gila and Whitlock Mountains to the northeast (Figure 8.1.1). Proximal fan deposits in basin-fill units appear to be restricted to within a few kilometers from basin margins, and mid- to distal-fan, playa and lacustrine facies lie toward basin centers.

The Pinaleño fault was active throughout basin-fill deposition between approximately 17 and 12 m.y., with the subsiding basin half-graben center located near the southwest margin of the Safford basin (Kruger et al., 1995). A southwest-dipping limb on the northeastern portion of the half-graben allowed the accumulation of proximal to distal alluvial fan facies to gradually thicken to the southwest in basin-fill units. However, basin-fill facies and depocenters interpreted from seismic profiles reveal both lateral and vertical changes throughout the basin-fill sequence. These changes are interpreted to be primarily driven by tectonism associated with the Pinaleño fault, more so than sedimentation rates, although the stratigraphy and structural history is not fully resolved (Kruger et al., 1995).

By ~12 m.y., low-magnitude, high-angle faulting associated with the Basin and Range disturbance became active in southern Arizona (Menges and Pearthree, 1989). Faults active during the mid-Tertiary event may have been reactivated during the Basin and Range event (Menges and Pearthree, 1989), with relatively minor offset, although faults may have had a significant effect on facies changes (Kruger et al., 1995). Faults may provide impermeable and/or permeable conditions. Fault-zone permeability would allow for mixing between downward-percolating meteoric/agriculture groundwater and upward endogenic magmatic groundwater flow. Basin-fill strata continued to thicken and aggrade towards the southern and western portions of Safford basin.

Quaternary faults are present along the southwest and northeast margins of the Safford basin (Houser et al., 2004) (Figure 8.1.1). Cactus Flat, Indian and possibly Buena Vista hot springs appear to be closely related to the trace of these faults, although exposures of the fault zones in these areas are concealed beneath Holocene alluvium. These faults offset upper basin-fill strata and Pleistocene alluvial fan pediments. Some of the faults on the northeast margin of the basin offset fluvial deposits associated with the ancestral Gila River, indicating the most recent activity was during the late to latest Pleistocene, prior to Holocene (Houser et al., 2004).

Stratigraphy

A sequence of mid-Tertiary volcanic and sedimentary rocks is present north and south of the Safford basin. The mid-Tertiary sequence which makes up a large part of the Gila Mountains projects

southwestward beneath basin-fill sediments in Safford basin towards the Pinaleño fault zone. Thickness of the mid-Tertiary sequence is unknown, although it is estimated from seismic reflection to be between 700 and 1,500 m (Kruger et al., 1995). The mid-Tertiary rocks are interpreted to be non-conformable with underlying Proterozoic basement, although older Mesozoic, Paleozoic, and/or Precambrian sedimentary and volcanic rocks found in nearby ranges may also be present beneath mid-Tertiary rocks.

Immediately overlying the mid-Tertiary sequence is a thick succession of basin-fill deposits, separated into the Lower basin-fill (LBF) and Upper basin-fill (UBF) sequences which formed in a closed-basin setting. A mid-Miocene erosional surface between mid-Tertiary and LBF sequences may be present along margins of the Safford basin, although sediments probably continued to aggrade in basin centers and may be conformable with mid-Tertiary strata. Younger basin-fill deposits are interpreted to on lap older basin-fill deposits and embayed piedmonts along basin margins (Kruger and Johnson, 1994). The LBF and UBF are distinguished primarily by differences in lithology and consolidation as revealed primarily by seismic-reflection profiling and scant well logs, although little is known about the LBF unit otherwise. The LBF generally consists of locally-sourced alluvial gravel, sand and clayey silt along basin margins, laterally grading into fine-grained distal alluvial sediments, evaporite sediments (gypsum and halite), and lacustrine deposits towards basin centers. Degree of consolidation and deformation (fractures, faults and folds) are more abundant in the LBF than the UBF. The UBF unit is unconsolidated to weakly consolidated, generally non-deformed, and consists of thicker and more extensive alluvial, playa and lacustrine deposits than interpreted in the LBF.

Cross Sections

Geologic cross-sections A-A' and B-B' were constructed in the vicinity of Cactus Flat-Buena Vista and Indian Hot spring areas, respectively (Figures 8.1.2 and 8.1.3), modified from Gootee (2012). Cross-sections are derived from existing well data, geologic mapping (Houser et al., 1985; Cook and Youberg, 2013; and Cook, 2013), seismic-reflection surveys (Kruger and Johnson, 1994; Kruger et al., 1995; and Kruger and Johnson, 2001), and modeled gravity data (Lysonski et al., 1981; Richard et al., 2007). Lithology and geophysical-log data for wells displayed in cross-sections are summarized and discussed further in Gootee (2012).

Cactus Flat Hot Springs

Information about stratigraphy and structural geology in the Cactus Flat hot springs area is derived largely from a cluster of five seismic lines, two deep oil and gas wells, and numerous shallow water wells and thermal wells. Basin-fill units are continuous across the Safford basin, and are interpreted to overlie mid-Tertiary volcanic and sedimentary rocks (Figure 8.1.2). The Safford basin is largely asymmetric, bound by the Pinaleño fault on the southern margin of the basin. Basin fill and possibly mid-Tertiary units along the southwest margin of the basin consist of predominantly coarse-grained sediments derived from the Pinaleño Mountains. These coarse-grained Pinaleño facies grade laterally into fine-

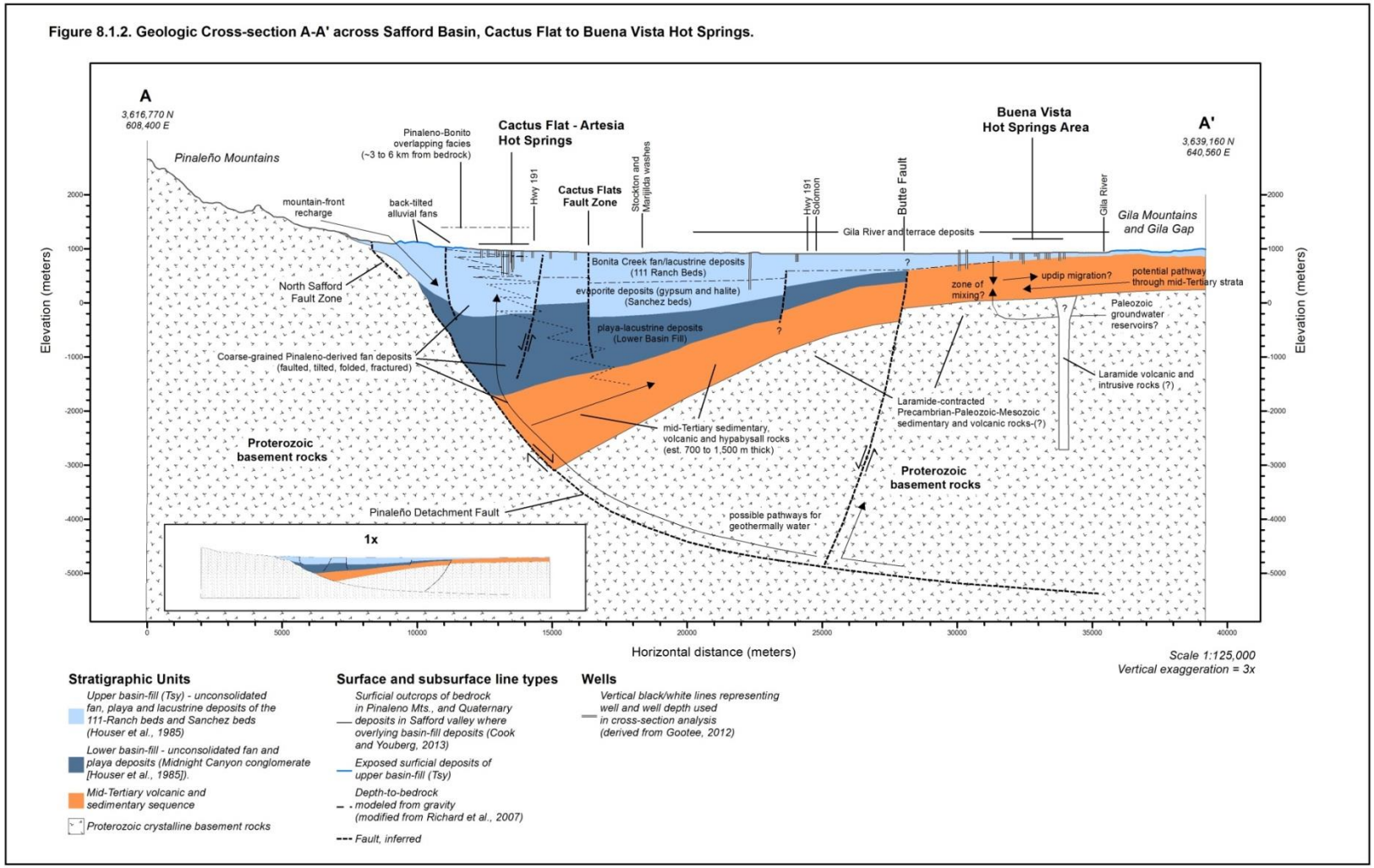

Figure 8.1.2 Geologic Cross Section A-A' Across Safford Basin, Cactus Flat to Buena Vista Hot Springs

grained sand, silt, clay and evaporite facies ~4 to 7 km from the mountain front in closed-basin distal-fan, playa and lacustrine environments.

Interbedded with the Pinaleño facies in the UBF is a bluish-reddish-brown facies derived from the Gila Mountains, part of the 111-Ranch beds (Houser et al., 1985). Proximal middle and distal fan, playa, and lacustrine facies are all present in the UBF. Across from the Gila Box between Buena Vista and Cactus Flat, a sequence of fluvio-lacustrine siliciclastic deposits derived from the ancestral Gila River makes up the upper part of the UBF. This distal fan sequence is also referred to as the Bonita Creek fan delta (Houser et al., 1985) (Figure 8.1.2). In the area of Cactus Flat, the Pinaleño facies consist of massive, light gray-green silty, micaceous sand with sparse lenses of poorly sorted pebble conglomerate. Grains consist of quartz, muscovite and biotite mica, mafic minerals, and alkali feldspars. The Bonita Creek fan facies contains generally well-sorted clasts, largely derived from volcanic rocks in the Gila Mountains, but also granite and sedimentary rocks from Precambrian and Paleozoic sources located outside the Safford basin. Sediment in these facies is noticeably more sorted than the Pinaleño facies and contains various well-formed sedimentary bedforms associated with a distal fan system. Quartz, mafic grains and feldspar grains are abundant in this facies. Basin-fill sediments in both facies are locally fractured and cemented with selenite gypsum, calcite and less commonly silica. Fractures are typically oriented N35W with near-vertical dips.

Alternating fine- and coarse-grained deposits from both facies likely create permeable and confining conditions for groundwater flow in the vicinity of the hot springs. Varying degrees of artesian flow are associated with the hot springs. Underlying the fluvio-lacustrine facies of the 111 Ranch beds are predominantly fine-grained siliciclastic and evaporite deposits formed in a more restricted deposition environment, referred to as the Sanchez beds (Houser et al., 1985) (Figure 8.1.2). Underlying the Sanchez beds the LBF sequence appears to be more coarse-grained with less abundant fine-grained basin deposits (Kruger et al., 1995). Much of the LBF is identified from few oil and gas wells and seismic reflection data. Data from these sources have been used to support a closed-basin model with coarse-grained fan facies grading laterally into fine-grained basin centers (Kruger et al., 1995). Facies and basin centers are largely asymmetric, hinged on the northeastern side of the basin, tilted toward the southwestern margin against the Pinaleño fault zone (Figure 8.1.2).

Basin-fill strata are gently tilted towards northeast - and southwest-dipping faults in the vicinity of Cactus Flat. The Cactus Flat hot springs lie between the North Safford and Cactus Flat fault zones, and may be associated with other concealed faults immediately beneath surficial Quaternary deposits (Figures 8.1.1 and 8.1.2). Basin-fill deposits are generally tilted west towards the Pinaleño fault zone, as much as 6 to 10 degrees, although northeast-tilts are present also. The North Safford and possibly Cactus Flat fault zones are interpreted to have been active during the late Miocene. Gently-folded LBF strata are also visible from a seismic-reflection profile ~10 km south of the Cactus Flat hot springs (Kruger and Johnson, 1995). Although relationships between tectonic uplift of the Pinaleño range, subsidence of the Safford basin, and on lap sedimentation are not fully resolved, folds and tilted bedding

are expressed in the Pliocene UBF, and at least as much in the LBF and mid-Tertiary strata (Kruger et al., 1995).

Deep-seated geothermal groundwater flow to the Cactus Flat hot springs is likely following major high-permeability fault zones, fractures, and conglomeratic strata along the Pinaleño fault zone. Low-permeability features such as fine-grained siliciclastic, evaporite and lacustrine deposits, fault gouge, and fold traps, are all present, and further complicate pathways for upward-migrating geothermal water. Downward-percolating meteoric groundwater derived from mountain-front recharge likely mixes with upward-migrating groundwater flow in mixing zones. Southwest-tilted permeable fanglomerate strata in the hanging wall could redirect upward-migrating geothermal groundwater towards impermeable fault zones, faults juxtaposing with permeable/impermeable strata, against abrupt facies changes, or a combination of these boundary conditions (Figure 8.1.2).

Buena Vista Hot Springs

The Buena Vista hot springs are located northeast of Safford near the town of San Jose in the Gila River floodplain where the Gila River exits the Gila Mountains (Figure 8.1.1). The Buena Vista hot springs were previously characterized by Witcher (1979, 1981, and 1982) and Witcher and Stone (1983).

Wells in the Buena Vista hot springs have thermal-artesian and saline groundwater conditions with temperatures ranging from 30° to 50° C. Geothermal groundwater in these wells is derived at various depths from modern Gila River floodplain deposits, basin-fill deposits, and mid-Tertiary and Laramide volcanic and intrusive rocks (Witcher, 1981). Thermal water is present in permeable gravels that are concealed beneath an aquiclude and are interpreted to be within basin-fill sediments. UBF facies associated with the formation of the 111-Ranch beds (Houser et al., 1985) are interpreted to truncate older basin-fill deposits and the upper part of mid-Tertiary (Miocene and Oligocene) volcanic rocks (Figure 8.1.2). LBF deposits beneath the hot springs may be present but are not shown. Basal conglomerate near the basin-fill/mid-Tertiary boundary may provide hydraulic connectivity to geothermal groundwater in basin-fill sediments further basinward (Witcher, 1981).

Geochemical analyses of thermal water suggest geothermal sources may be greater in extent and depth than the cluster of wells that define the spring area (Witcher, 1981). Geochemistry also indicates geothermal water has dissolved constituents derived from sulfur- and calcium-bearing rocks/sediment, which may suggest groundwater flow to wells has had contact with gypsum-bearing basin-fill sediment (Witcher, 1981a).

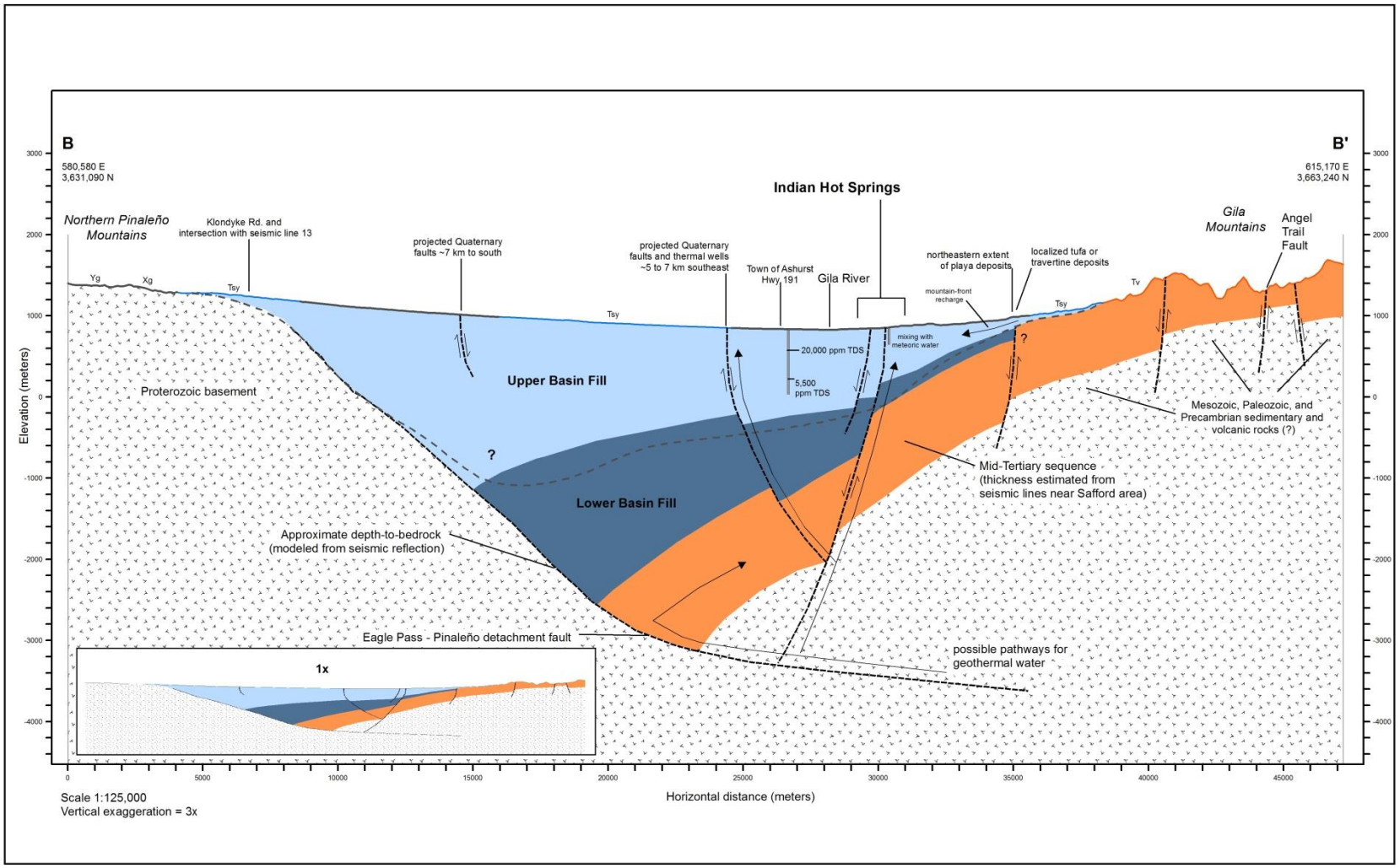

Figure 8.1.3 Geologic Cross-section B-B' across Safford Basin, Northern Pinaleño Mountains to Indian Hot Springs

The Buena Vista hot springs may be associated with geophysical lineaments, fracture and shear zones, and Laramide/mid-Tertiary intrusive and volcanic centers (Witcher, 1981; Lepley, 1978). Northwest of the Buena Vista springs, a major northwest-southeast trending fault, the Butte fault, offsets mid-Tertiary, Laramide volcanic stocks, and older rocks, and may project southeast in the vicinity of the Buena Vista hot springs (Figures 8.1.1 and 8.1.2). A combination of these structures may allow for geothermal groundwater to migrate upward into rocks and sediment to the spring area. High-angle normal block faults similar to the Butte fault with down-to-the-west displacement may be major antithetic faults to the main detachment fault (Kruger et al., 1995). If so, geothermal groundwater flow may migrate along such structures into overlying basin-fill deposits and ultimately to the hot spring area (Figure 8.1.2).

Indian Hot Springs Area

Indian Hot Spring is one of several springs located on the northeast margin of the Safford basin (Figure 8.1.1). Indian Hot Spring discharges from basin-fill deposits with temperatures ranging from 45°C to 50° C (Witcher, 1981). Calcium and sodium-bearing salts are deposited at the surface. Modern Gila River floodplain deposits that host the hot springs may also discharge thermal waters mixed with shallow groundwater.

The Pinaleño/Eagle Pass Detachment Fault system is considered to be the main basin-forming fault in the basin (Figure 8.1.3). Indian Hot Spring is associated with an alignment of Quaternary faults along the northeast side of the Gila River floodplain (Figure 8.1.1) (Davis and Hardy, 1981; Kruger et al., 1995). Basin-fill deposits are locally deformed, and offset with down-to-southwest displacement. Other hot springs and seeps in the area are associated with this lineament (Witcher, 1981). The steep slope in bedrock on the northeastern margin of the basin is interpreted to represent faults antithetic to the main detachment fault (Kruger et al., 1995), considered to be active during deposition of the LBF. However, dominant movement along the Pinaleño range-bounding fault produced a largely asymmetric basin-fill distribution in both the LBF and UBF. Basin-fill sediment at the surface consists of flat-lying, fine-grained gypsiferous sand, silt and clay deposited in a playa setting. Playa deposits extend northeast to within 2 to 3 km of bedrock, which may indicate the presence of a range-bounding fault that controlled basin subsidence and created abrupt facies changes on the northeast margin of the basin (Figure 8.1.3).

Basin-fill strata are relatively non-deformed with horizontal to gently-dipping strata, and are interpreted to unconformably overlie early Miocene volcanic and Precambrian crystalline bedrock along basin margins (Kruger and Johnson, 1994). Upper and Lower basin-fill units were deposited in a largely asymmetric basin with significant range-bounding faults on the northeastern and southwestern basin margins active throughout deposition of basin fill. The upper 300 m of the UBF is dominated by clay and silt across the width of the basin and is interpreted to be equivalent to the clay-rich 111-Ranch beds known to create confined conditions for artesian flow from deeper, saline-rich basin-fill sediments.

Stratigraphy and facies characteristics of the LBF were not discernible in this portion of the basin; however, seismic data suggest alluvial fan, playa and possibly lacustrine deposits were also deposited in an asymmetrically-closed basin. Basin-fill deposits near the gravity low closer to the Pinaleño Mountains remains untested, and may contain more extensive, thick evaporite and/or lacustrine deposits (Figures 8.1.1 and 8.1.3).

Geochemical analyses of the Indian Hot Spring during this study indicates geothermal water may be derived from deep-crustal sources. Geothermal groundwater flow may migrate upwards along the Eagle Pass-Pinaleño detachment fault primarily, through fractured crystalline bedrock along the fault contact, and subsequently into overlying mid-Tertiary and basin-fill units through tilted bedding, fracture zones, and secondary block-faults in the upper plate (Figure 8.1.3). Laramide volcanic and intrusive rocks, Mesozoic and Paleozoic sedimentary rocks, and Precambrian sedimentary and volcanic rocks may underlie the mid-Tertiary sequence, which if present, may provide reservoirs for geothermal groundwater and enough permeability for groundwater migration, although faults would likely provide conduits into overlying rocks. Upward-migrating geothermal water with high-temperatures and/or long-term residence in Paleozoic/Mesozoic bedrock, or flowing through saline-rich evaporite deposits in basin-fill units, particularly the UBF, can create high-saline groundwater conditions. Elevated salinity in the Safford basin has been identified as being derived from a combination of agricultural recharge and artesian leakage from underlying basin-fill sediments with elevated connate saline groundwater (Harris, 1999; Towne, 2009). In addition, fine-grained clay and evaporite deposits, limestone, fault traps, and gently-folded strata create confining conditions for groundwater, and artesian flow to the surface through permeable strata, Quaternary fault zones, and springs and wells, basinwards from Indian Hot Spring.

References - Pinaleño Mountains

Cook, J.P., 2013, Geologic Map of the Artesia 7 ½' Quadrangle and the Northeastern Corner of the Mount Graham 7 ½' Quadrangle, Graham County, Arizona. Arizona Geological Survey Digital Geologic Map, DGM-106, 1 map sheet, 1:24,000 map scale.

Cook, J.P. and Youberg, A., 2013, Geologic Map of Safford 7 1/2' Quadrangle, Graham County, Arizona. Arizona Geologic Survey Digital Geologic Map, DGM-104 v.1.0, one map plate, map scale 1:24,000.

Davis, G.H., and Hardy, J.J., Jr., 1981, The Eagle Pass detachment, southeastern Arizona; product of mid-Miocene listric(?) normal faulting in the southern Basin and Range: Geological Society of America Bulletin, v. 92, p. 749-762.

Gootee, B.F., 2012, Geologic Evaluation of the Safford Basin for Carbon Dioxide Sequestration Potential, Arizona Geological Survey Open-File Report OFR-12-01, 71 p., 1 plate.

Harris, R.C., 1999, Feasibility of using isotopes as tracers of the sources of dissolved solids in the upper Gila River, Arizona: Arizona Geological Survey Open-File Report 99-03, 89 p., 1 sheet, scale 1:250,000.

Houser, B.B., Richter, D.H. and Shafiqullah, M., 1985, Geologic map of the Safford Quadrangle, Graham County, Arizona, USGS IMAP 1617, 1 map 1:48,000.

Houser, B.B., Pearthree, P.A., Homburg, J.A. and Thrasher, L.C., 2004, Quaternary stratigraphy and tectonics, and late prehistoric agriculture of the Safford basin (Gila and San Simon River valleys), Graham County, Arizona, for the Friends of the Pleistocene, Rocky Mountain Cell 46th Field Conference and Arizona Geological Society fall field trip, 2002, USGS Open-File Report 2004-1062, 53 p.

Kruger, J.M. and Johnson, R.A., 1994, Raft model of crustal extension: Evidence from seismic reflection data in southeast Arizona, Geology, v.22, pp.351-354.

Kruger, J.M. and Johnson, R.A., 2001, From transition zone to core complex: deep reflection seismic imaging of the Basin and Range, Southeast Arizona, in Utah Geological Association Publication 30, Pacific Section American Association of Petroleum Geologists Publication GB78, pp. 313-335.

Kruger, J.M., Johnson, R.A. and Houser, B.B., 1995, Miocene-Pliocene half-graben evolution, detachment faulting and late-stage core complex uplift from reflection seismic data in south-east Arizona, Basin Research, v.7, p. 129-149.

Lepley, L.K., 1978, Skylab Lineament Map of Arizona with Tectonic Model and Exploration Guide for Geothermal Resources, State of Arizona Bureau of Geology and Mineral Technology Open-File Report 78-4, 1 map, 1:500,000, 31 p.

Long, K.B., Baldwin, S.L., and Gehrels, G.E., 1995, Tectonothermal evolution of the Pinaleño-Jackson Mountain core complex, southeast Arizona: Geological Society of America Bulletin, v. 107, n. 10, p. 1231-1240.

Lysonski, J.C., Aiken, C.L.V., and Sumner, J.S., 1981, Complete residual Bouguer gravity anomaly maps: Arizona Geological Survey Open-file Report 81-24, 2 p., 23 sheets, scale 1:250,000.

Menges, C.M., and Pearthree, P.A., 1989, Late Cenozoic tectonism in Arizona and its impact on regional landscape evolution, in Jenny, J.P. and Reynolds, S.J., eds., Geologic evolution of Arizona: Tucson, Arizona Geological Society Digest XVII, p. 649-680.

Naruk, S.J., 1987, Displacement calculations across a metamorphic core complex mylonite zone: Pinaleño Mountains, southeastern Arizona: Geology, v. 15, no. 7, p. 656-660.

Richard, S.M., Reynolds, S.J., Spencer, J.E. and Pearthree, Pa, P.A., 2000, Geologic map of Arizona: Arizona Geological Survey Map 35, scale 1:1,000,000.

Richard, S.M., Shipman, T.C., Greene, Lizbeth, Harris, R.C., 2007, Estimated Depth to Bedrock in Arizona: Tucson, Arizona Geological Survey Digital Geologic Map 52 (DGM-52), version 1.0, 1 Adobe Acrobat (PDF) file (8 p., 1 sheet), design scale 1:1,000,000.

Spencer, J.E., 1984, Role of tectonic denudation in warping and uplift of low-angle normal faults: Geology, v. 12, p. 95-98.

Spencer, J.E., and Reynolds, S.J., 1989, Middle Tertiary tectonics of Arizona and adjacent areas, in Jenney, J.P., and Reynolds, S.J., eds., Geologic evolution of Arizona: Tucson, Arizona Geological Society Digest XVII, p. 539-574.

Thorman, C. H., 1981, Geology of the Pinaleño Mountains, Arizona: A preliminary report: Tucson, Arizona Geological Society Digest, v. 13, p. 5-12.

Towne, D.C., 2009, Ambient groundwater quality of the Gila Valley sub-basin of the Safford basin: A 2004 baseline study: Arizona Department of Environmental Quality Open File Report OFR 09-12, 99 p.

Witcher, J.C., 1979, A preliminary report on the geothermal energy potential of the Safford basin southeastern Arizona: Arizona Geological Survey Open-File Report 79-02, 34p.

Witcher, J.C., 1981, Geothermal resource potential of the Safford-San Simon Basin, Arizona: Arizona Bureau of Geology and Mineral Technology Open-File Report 81-26, 131 p.

Witcher, J.C., 1982, Exploration for geothermal energy in Arizona Basin and Range - A summary of results and interpretation of heat flow and geochemistry studies in Safford basin, Arizona: Arizona Bureau of Geology and Mineral Technology Open-File Report 82-05, 51 p.

Witcher, J.J. and Stone, C., 1983, A CO2-Silica Geothermometer for Low Temperature Geothermal Resource Assessment, with application to resources in the Safford basin, Arizona, for the Arizona Solar Energy Commission and the U.S. Department of Energy, November 1983, 69p.

8.2 Geohydrology of Agua Caliente Regional Park Vicinity, Northeastern Tucson Basin, Arizona

By Jon Spencer and Diane Love, Arizona Geological Survey, 2014

Introduction

The Roy P. Drachman-Agua Caliente Regional Park, located in northeastern Tucson Basin at approximately 841meter (m) elevation (2760 feet), is ~150 m (~450 feet) west of exposed bedrock at the foot of the southeastern Santa Catalina Mountains (Figure 8.2.1). The Santa Catalina Mountains include Agua Caliente Hill, a massif with a summit at 1,636 m elevation (5,369 feet) elevation that is only ~6 km (~4 miles) east-northeast of Agua Caliente Regional Park. Other springs in Tucson Basin are similarly located at the foot of the Santa Catalina Mountains, but these are not warm springs. This brief report is intended to outline the geologic setting of Agua Caliente Regional Park vicinity and identify geologic features that are possibly responsible for discharge of geothermal waters at the spring.

Geologic setting

The Santa Catalina and Rincon Mountains, which form the northern and eastern margins, respectively, of Tucson Basin, comprise a large metamorphic core complex (Davis, 1980; Keith et al., 1980; Spencer and Reynolds, 1989; Dickinson, 1991; Force, 1997; Fornash et al., 2013). Granitic and gneissic rocks that make up the southern side of the Santa Catalina Mountains and the western and southern side of the Rincon Mountains are characterized by mylonitic foliation that dips gently to moderately beneath Tucson Basin. Crystal-plastic deformation that produced the mylonitic foliation occurred during Oligocene to early Miocene shearing down-dip from the Catalina detachment fault (e.g., Davis, 1983; Davis et al., 1986; Spencer, 2006). Slip on the normal fault and its down-dip, mid-crustal continuation as a ductile shear zone, caused tectonic uplift (exhumation) and tilting of the ranges, as well as subsidence of Tucson Basin. Displacement on the detachment fault is estimated at 30 +/- 10 km.

The Catalina detachment fault was last active at ~10–15 m.y., and has since been partially buried by younger sediments. In areas where it is exposed, especially around the western Rincon Mountains, it is located at the foot of the mountain range (Drewes, 1977; Pain, 1985; Davis, 1987; Dickinson, 1999; Richard et al., 2004). In areas where it is buried, as at Agua Caliente Regional Park, the buried trace of the fault is probably within a few hundred meters of exposed bedrock and could be present only a few meters or tens of meters directly below the spring.

Hydrology

Groundwater generally occurs in Tucson Basin in rocks of all principal types: intrusive, metamorphic, and volcanic rocks; pre-Basin and Range sedimentary rocks of Tertiary age; and basin-fill sediments. The water-bearing properties of these rocks, however, vary widely. Well yields range from a few gal/min to more than 6,000 gal/min. The water-bearing characteristics of the intrusive, metamorphic, and volcanic

rocks are dependent on localized joint fractures and weathering characteristics. In general, well yields from intrusive and metamorphic rocks are limited to a few gallons per minute. Volcanic rocks, which can be more porous and fractured, may yield more water and serve as local sources, but, like intrusive rocks, their water-yielding properties are generally limited. Depth to the water table in Arizona's basins varies widely, but is greater near the mountain fronts where ground elevation is higher. Velocities generally are greater near the mountain fronts, where gradients are steeper and permeability higher than those in the interior of the basins (Robertson, 1991).

Olson (1982) and Morbacher (1984) used chemical and isotopic data in groundwater in the foothills of the Santa Catalina Mountains to distinguish two mechanisms of mountain-front recharge. These studies identified two isotopically and chemically distinct classes of groundwater. Both studies suggested that one class receives recharge from the infiltration of mountain streams at the basin margin, and the other class received recharge directly from fractures in the crystalline mountain mass (Olson, 1982; Mohrbacher, 1984).

Agua Caliente Warm Spring and Well

Agua Caliente Regional Park is located in Quaternary alluvium. All older rocks and structures are buried at the spring, and there are no local geomorphic, structural, or lithologic indications of the geologic factors responsible for the presence of the only warm-water spring in Tucson basin, although numerous warm wells (>30) are reported in the Tucson basin several miles southwest of the park (Witcher and Stone, 1983). Inferences about the origin of spring water and geologic factors affecting spring water location and temperature must be derived from groundwater geochemistry and knowledge of regional geology and hydrogeology. A temperature of 31.5°C in was measured in October 2012 at the Agua Caliente artesian well within the park. Water quality sampling of the Agua Caliente warm spring and on-site well strongly suggests the waters are from the same source (Pima County Regional Flood Control District, 2014). The well is drilled to a total depth of 799 ft below ground surface (bgs) and is screened in [decomposed] granite from 659 to 699 ft bgs and from 739 to 799 ft bgs with a pea gravel pack from 550 to total depth (ADWR, 2014). Groundwater was first encountered during drilling at 675 ft bgs. The Pima County Natural Resources Parks and Recreation reported that the flow has diminished in the past several years and the pools are not maintaining their previous levels.

Analysis of tritium in water from Agua Caliente warm spring in the 1990's determined that water derived from precipitation in the previous 30 years had not mixed with the spring water (Eastoe et al., 2004). Analytical results from artesian well water collected in October 2012 (Table 6.7) show tritium apparent concentration at less than 0.6 TU, confirming Eastoe's (2004) results and indicating that the water accumulated at least prior to the 1950s.

Analysis of carbon-14 indicates that the water has not interacted with the atmosphere or with plants for probably thousands of years (Eastoe et al., 2004), which is consistent with its inferred long residence time and heating deep underground. The corrected ^{14}C results for the artesian well water samples

collected in October 2012 (Table 6.8) provides an age at ~3,900 years (BP 1950), again confirming Eastoe's (2004) estimate that the water accumulated thousands of years ago.

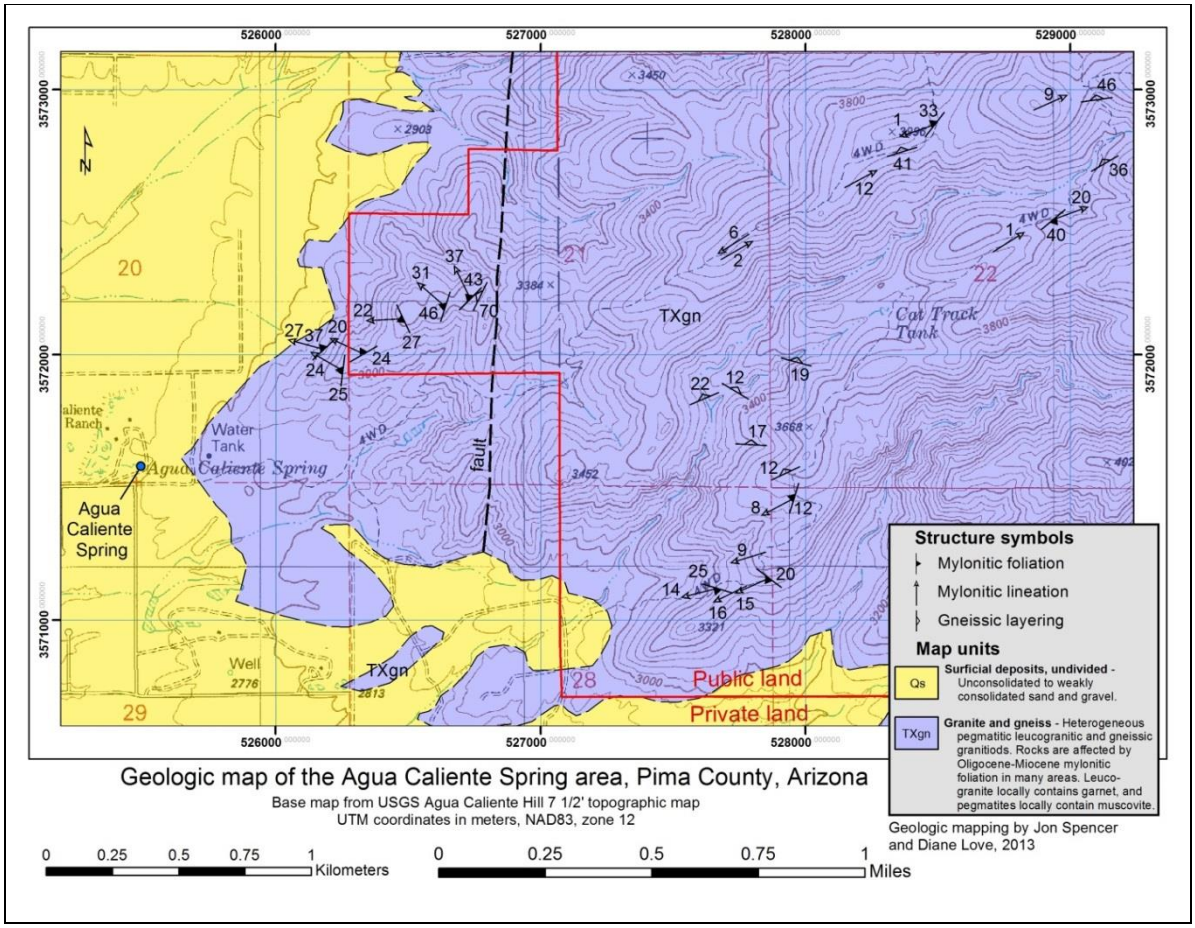

Figure 8.2.1. Geologic map of the southwestern flank of Agua Caliente Hill.

Low concentrations of deuterium and oxygen-18 in Agua Caliente artesian well groundwater indicate that the water was ultimately derived from precipitation at higher elevations, where rainwater is more depleted in heavy isotopes of oxygen and hydrogen (Cunningham et al., 1998).

Structural Geology of Agua Caliente Hill

Bedrock at Agua Caliente Hill near Agua Caliente Regional Park was mapped in the field and examined with aerial imagery in order to determine if it contained fault zones or other features with possibly elevated permeability (Figure 8.2.2). A single north-south striking fault was identified based on the presence of a linear zone where rocks are less resistant to erosion, presumably because of fault-zone crushing. Minor iron staining also characterizes some rocks along the fault zone, as would be expected for a zone of enhanced permeability, although no evidence of hydrothermal activity was identified. A mylonitic fabric is common in the area depicted on Figure 8.2.1, as shown by foliation measurements,

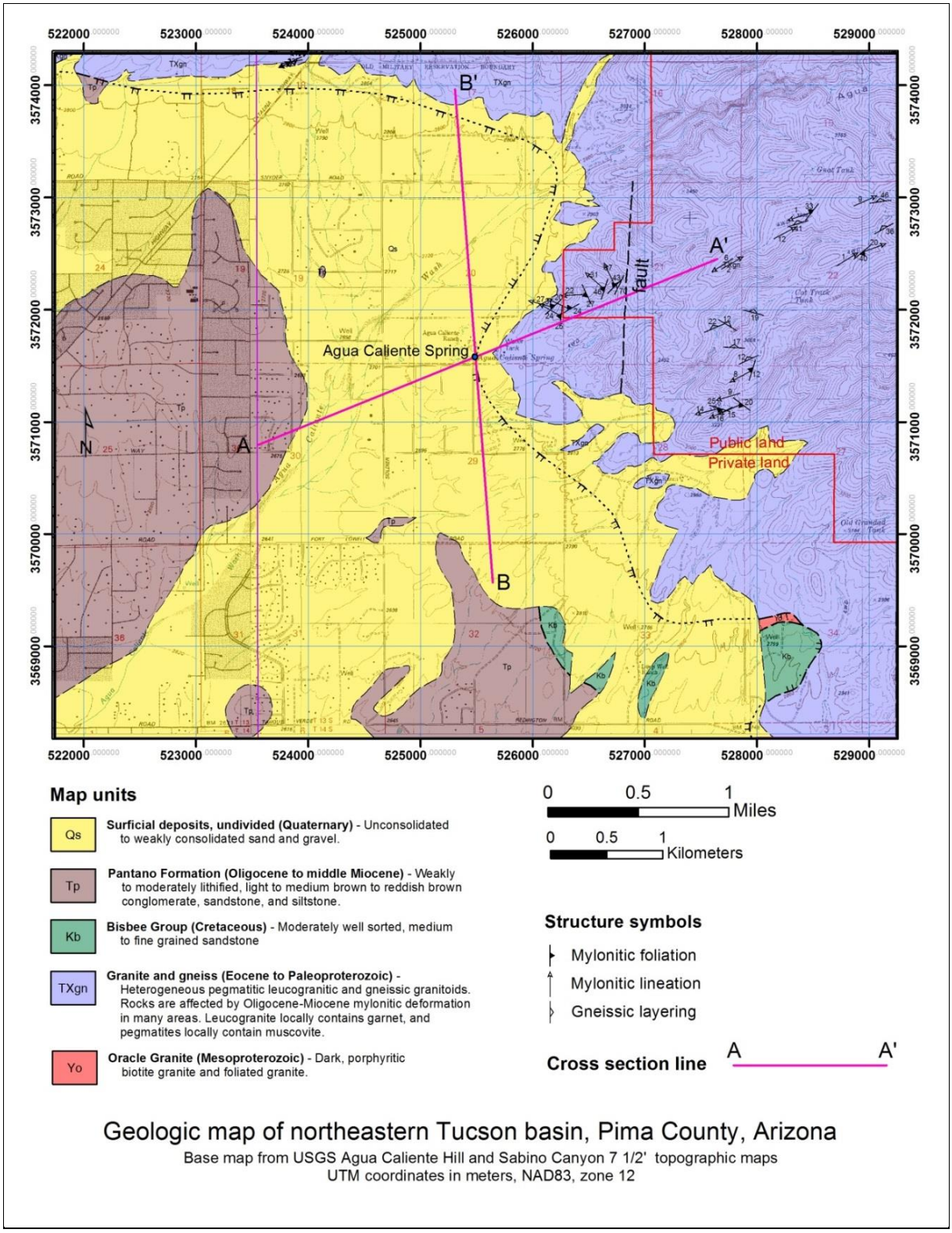

Figure 8.2.2 Geologic map of the northeastern corner of Tucson Basin

but this high-temperature deformation fabric did not obviously influence fracturing or other features that would elevate permeability. Force (2002) mapped a fault extending southwestward along the approximate bottom of the canyon containing “Cat Track Tank” (Fig. 8.2.1). We examined rocks downstream from Cat Track Tank, but found no evidence of faulting in extensive outcrops of bedrock. In summary, field mapping revealed no features in the granitic and gneissic rocks of Agua Caliente Hill that would provide a permeable pathway for flow of groundwater to Agua Caliente Warm Spring.

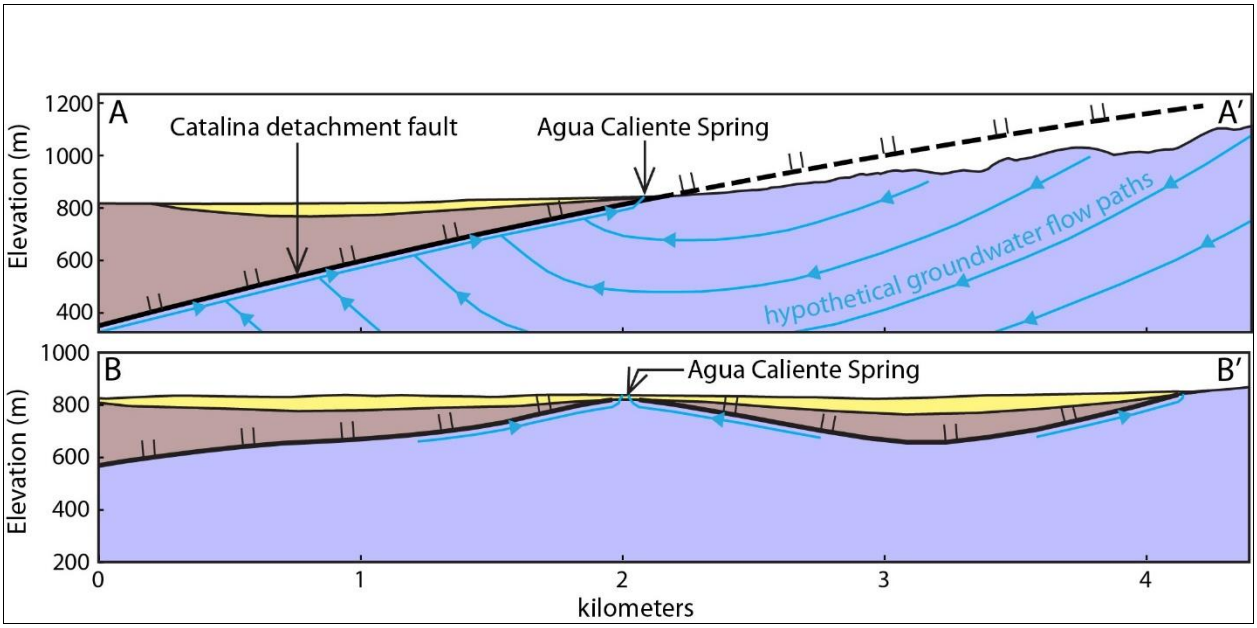

Figure 8.2.3. Cross sections of the northeastern corner of Tucson basin

Catalina detachment fault

The fracture permeability of granitic and gneissic rocks that make up the Santa Catalina and Rincon Mountains is not well characterized and is assumed to be low. Similarly, the Pantano Formation in Tucson Basin is not a particularly productive aquifer, unlike younger, unconsolidated to poorly consolidated basin-filling sand and gravel. The granitic and gneissic rocks that form the mountains and the Pantano Formation in Tucson Basin are juxtaposed by the Catalina detachment fault in the basin subsurface (Figures 8.2.2 and 8.2.3). The fault zone is known to contain crushed rocks that are the source of water for at least two water wells located north of the Tortolita Mountains (Spencer et al., 2002).

Where permeable rock overlies rock of much lower permeability, a contact spring may result. Faulting may also create a geological control favoring spring formation. In addition, joint or fracture springs may occur from the existence of joints or permeable fault zones in low-permeability rocks. It is difficult to determine the origin of the Agua Caliente spring due to buried subsurface geology. Discharge at springs along the foot of the Santa Catalina and Rincon Mountains is inferred to be derived from water in

fractures at higher elevations in the mountains. Springs discharge along the trace of the Catalina detachment fault at the northern edge of the Tucson Basin where it abuts the Catalina Mountains.

The force potential is the driving impetus behind groundwater flow and is the product of the hydraulic head and gravity. The hydraulic head (force per unit weight) drives water downward from the recharge surface, increasing pressure head as elevation decreases, and flows through pore space toward lower elevation aquifers where the water pressure in pore space is now higher. Although generally under hydrologically unconfined conditions, silts and clays are interlayered in the basin units creating localized semi-confined conditions. Change in size of pore space from one rock type to another changes permeability rates and also affects the pressure at lower elevations. Where water reaches sufficient bedrock depths it is warmed by ambient heat.

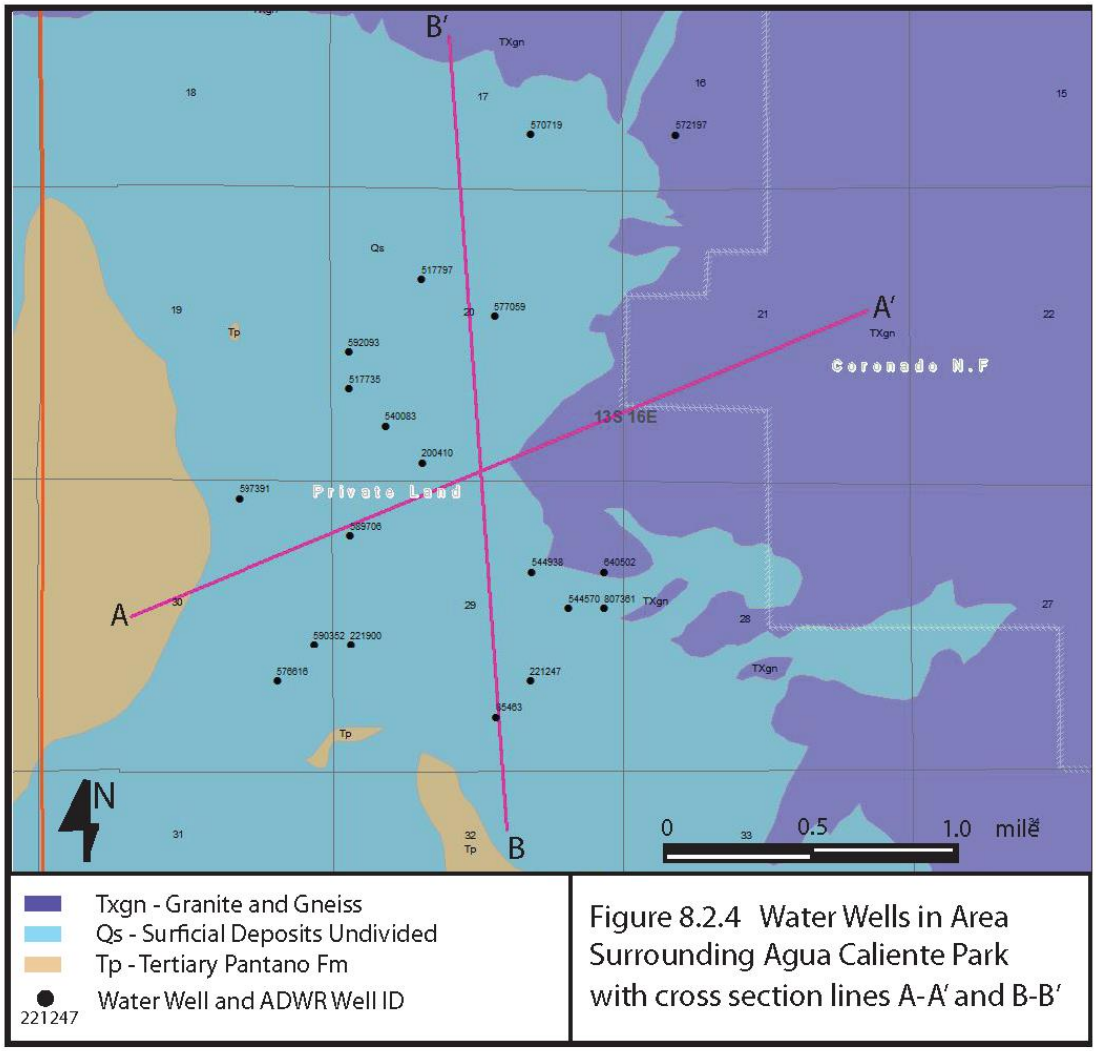

Figure 8.2.4 Water Wells in the Area Surrounding Agua Caliente Park

At least 30 wells are reported to produce thermal (>30°C) water in the Tucson basin. Thermal wells in the basin range from 64 to 959 m in depth. The deeper thermal wells pump up to 6,100 L/min of 57°C groundwater. A notable concentration of thermal wells exist in T15 S, R14 E (about 12 miles southwest of Agua Caliente) where the highest temperature thermal water known in the basin occurs. Chemical quality of the water is good except for high fluoride concentrations (Witcher and Stone, 1983).

Flow of warm water laterally and upward into Tucson basin will likely be affected by the buried Catalina detachment fault. If the fault channels groundwater flow because of higher permeability in crushed fault zone rocks, then ascending groundwater could reach the surface at springs that are above the buried trace of the fault, possibly including the Agua Caliente warm spring. In this context, warm water at Agua Caliente warm spring would be the result of a deep flow path or paths moving groundwater quickly with little heat loss during ascent to the surface, maintaining its elevated temperature (Fig. 8.2.3 A-A'). Furthermore, upward flow along the broadly corrugated Catalina detachment fault (Fig. 8.2.2) would converge along the axes of these gently plunging corrugations (Fig. 8.2.3 B-B'). We suggest that the warm water at Agua Caliente warm spring results from such flow paths.

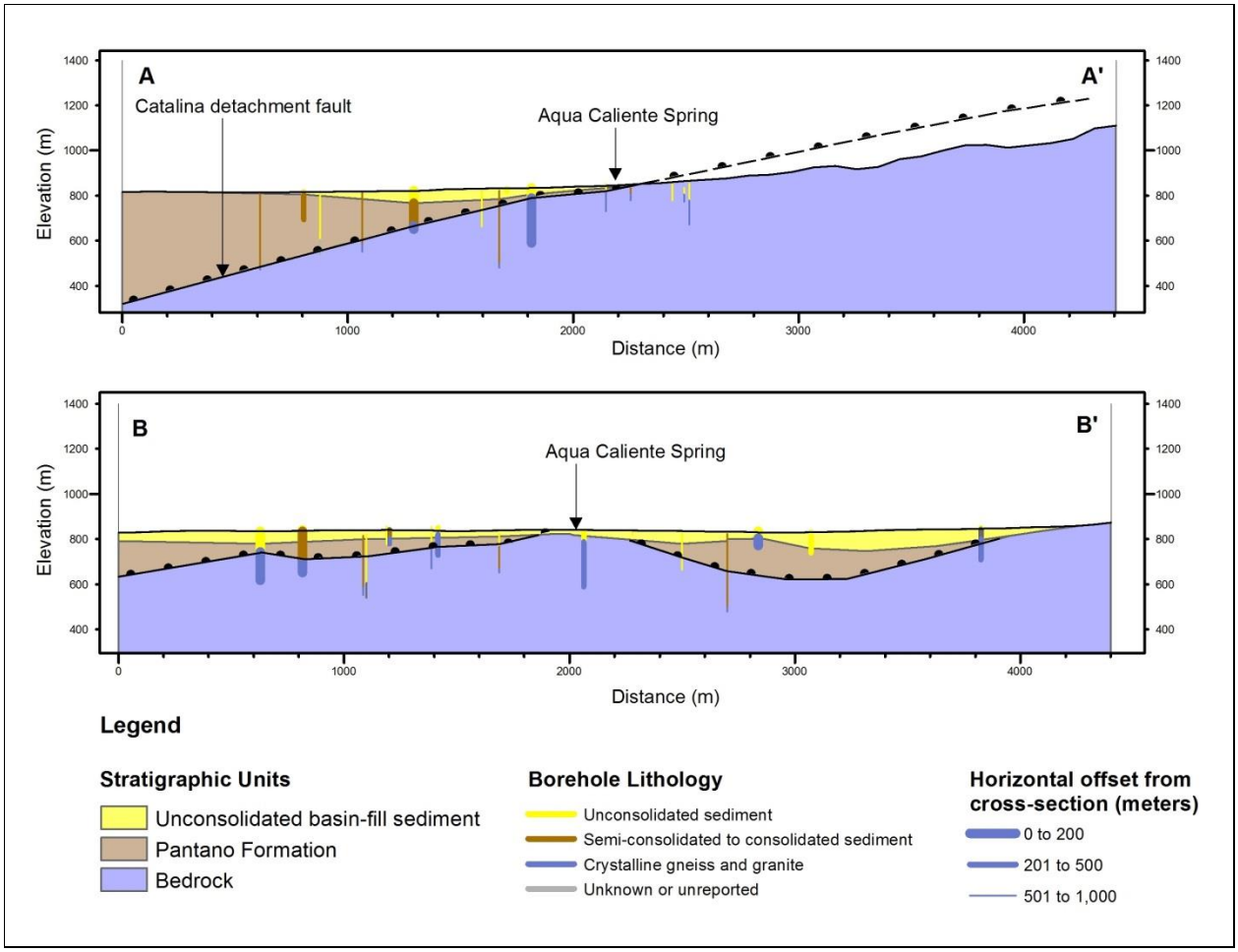

Figure 8.2.5. Cross Sections A-A' and B-B' located on Figure 8.2.4 showing geologic structure

Numerous water wells have been drilled in the populated areas surrounding the Agua Caliente Warm Spring (Figure 8.2.4). Driller's logs were obtained from Arizona Department of Water Resources. Although driller's logs report rock types that are often ambiguous, they can provide insight as to the formation unit encountered during well emplacement. Driller's logs reporting borehole lithology were reviewed (Table 8.2.1) and modeled using Aquaveo software. Cross sections A-A' and B-B' were generated and formation tops defined (Figures 8.2.4 and 8.2.5). Cross section lines closely overlay those in Figure 8.2.2. A comparison of the mapped geology cross section structure in Figure 8.2.3 and the cross sections from well lithology reported in driller's logs and modeled using Aquaveo (Figure 8.2.5), suggests a close correlation between structure configurations, confirming the corrugation effect in cross section B-B' and potential thermal upwelling potential culminating at the Agua Caliente warm spring. Note that the bedrock annotated for the well between Agua Caliente Spring and B' location is granite from the upper plate, not the granitic and gneissic rocks of the lower plate.

Conclusion

The Agua Caliente warm spring is located adjacent to bedrock at the foot of Agua Caliente Hill. Geologic mapping of granitic and gneissic rocks near the spring revealed no faults or other structures that could be linked to groundwater discharge. The Catalina detachment fault is the dominant structural feature in the northeastern Tucson basin. It separates granitic and gneissic rocks in its footwall block from moderately lithified clastic strata of the Oligocene to middle Miocene Pantano Formation. The fault is largely buried by younger, post-faulting alluvial deposits at the foot of the Santa Catalina Mountains, but the buried trace is suspected to be located below Agua Caliente warm spring. Groundwater flowing through fractures in the Santa Catalina Mountains and Rincon Mountains likely migrates downward, in some cases to depths where ambient geothermal temperatures are significantly elevated (many hundreds of meters to perhaps 1-2 km). We suggest that these geothermal waters flow into the buried Catalina detachment fault and ascend within the fracture zone along the fault to enter alluvial deposits just below Agua Caliente warm spring. The Agua Caliente warm spring is conspicuously located above the plunging crest of a corrugation in the Catalina detachment fault (Fig. 8.2.2), as would be expected if the spring is associated with converging hot groundwater migrating up along the detachment fault contact toward the axis of the corrugation (Fig. 8.2.3).

Table 8.2.1 Agua Caliente Warm Spring Surrounding Wells and Lithology

Table 8.2.1 Wells Surrounding Agua Calinte Hot Springs

Well Label	Elev. (ft)	Elev. (m)	From Depth (ft)	To Depth (ft)	From Depth (m)	To Depth (m)	Top Elev. (m)	Bottom Elev. (m)	Thick-ness (ft)	Description	HGU ID	HGU Code
221247	2760	841	0	17	0	5	841	836	17	loose broken rock clay and sand	1	BF
221247	2760	841	17	480	5	146	836	695	463	Pantano	2	Pantano
221247	2760	841	480	622	146	190	695	652	142	Granite	3	Bedrock
85463	2740	835	0	2	0	1	835	835	2	top soil	1	BF
85463	2740	835	2	15	1	5	835	831	13	sand	1	BF
85463	2740	835	15	300	5	91	831	744	285	clay	1	BF
85463	2740	835	300	640	91	195	744	640	340	Granite	3	Bedrock
85463	2740	835	640	710	195	216	640	619	70	broken granite with water	3	Bedrock
200410	2735	834	0	30	0	9	834	824	30	gray sandy clay	1	BF
200410	2735	834	30	145	9	44	824	789	115	brown clay	1	BF
200410	2735	834	145	799	44	244	789	590	654	decomposed granite	3	Bedrock
221900	2690	820	0	15	0	5	820	815	15	loose sandy soil	1	BF
221900	2690	820	15	500	5	152	815	668	485	Pantano	2	Pantano
221900	2690	820	500	770	152	235	668	585	270	black rock layers throughout Pantano	2	Pantano
221900	2690	820	770	880	235	268	585	552	110	semi-consolidated rock green white	3	Bedrock
517735	2710	826	0	18	0	5	826	821	18	sand and gravel	1	BF
517735	2710	826	18	530	5	162	821	664	512	clay and sandstone	1	BF
517797	2730	832	0	35	0	11	832	821	35	decomposed granite and silts	1	BF
517797	2730	832	35	305	11	93	821	739	270	clay and sandstone	1	BF
540083	2722	830	0	3	0	1	830	829	3	clayey sand	1	BF
540083	2722	830	3	35	1	11	829	819	32	silty sand with some cobbles and auger refrusal at 35 ft	1	BF
544938	2795	852	0	60	0	18	852	834	60	clay	1	BF
544938	2795	852	60	100	18	30	834	821	40	clay	1	BF
544938	2795	852	100	160	30	49	821	803	60	rock water	3	Bedrock
544938	2795	852	160	220	49	67	803	785	60	rock water	3	Bedrock
544938	2795	852	220	240	67	73	785	779	20	white rock	3	Bedrock
544938	2795	852	240	260	73	79	779	773	20	pink rock fractured	3	Bedrock
544938	2795	852	260	280	79	85	773	767	20	white rock	3	Bedrock
544938	2795	852	280	300	85	91	767	760	20	black and shite granite	3	Bedrock
544938	2795	852	300	320	91	98	760	754	20	white rock	3	Bedrock
544938	2795	852	320	340	98	104	754	748	20	white rock	3	Bedrock
544938	2795	852	340	360	104	110	748	742	20	pink rock	3	Bedrock
544938	2795	852	360	380	110	116	742	736	20	black rock	3	Bedrock
544938	2795	852	380	400	116	122	736	730	20	white rock	3	Bedrock
544570	2770	844	0	10	0	3	844	841	10	clay and cobble	1	BF
544570	2770	844	10	35	3	11	841	834	25	ecelitile or unknown	4	Unknown
544570	2770	844	35	125	11	38	834	806	90	dark brown rock	2	Pantano
544570	2770	844	125	212	38	65	806	780	87	granite fractured	3	Bedrock
570719	2790	850	0	20	0	6	850	844	20	dirt and rock	1	BF
570719	2790	850	20	160	6	49	844	802	140	broken limestone	4	Unknown
570719	2790	850	160	460	49	140	802	710	300	granite first water at 190 ft	3	Bedrock
572197	2820	860	0	1	0	0	860	859	1	sand	1	BF
572197	2820	860	1	350	0	107	859	753	349	granites	3	Bedrock
576616	2675	815	0	28	0	9	815	807	28	loose sand and rock	1	BF
576616	2675	815	28	1085	9	331	807	485	1057	Pantano shale	2	Pantano
576616	2675	815	1085	1125	331	343	485	472	40	white gray and green quartz and flowing 56 gpm	3	Bedrock
577059	2740	835	0	30	0	9	835	826	30	sand and gravel	1	BF
577059	2740	835	30	100	9	30	826	805	70	very clayey	1	BF
577059	2740	835	100	205	30	62	805	773	105	bedrock green first water at 130 ft	3	Bedrock
589706	2700	823	0	20	0	6	823	817	20	dirt and clay	1	BF
589706	2700	823	20	180	6	55	817	768	160	clay	1	BF
589706	2700	823	180	515	55	157	768	666	335	Pantano Formation	2	Pantano
589706	2700	823	515	560	157	171	666	652	45	granite first water at 520 ft	3	Bedrock
590352	2690	820	0	15	0	5	820	815	15	weathered granite	1	BF
590352	2690	820	15	705	5	215	815	605	690	brown clay	1	BF
590352	2690	820	705	910	215	277	605	543	205	brown andesite	4	Unknown
590352	2690	820	910	920	277	280	543	540	10	decomposed granite	4	Unknown
592093	2715	828	0	14	0	4	828	823	14	loose sand and gravel	1	BF
592093	2715	828	14	1085	4	331	823	497	1071	Pantano shale ie clay	2	Pantano
592093	2715	828	1085	1140	331	347	497	480	55	white gray and green rock water indicated	3	Bedrock
597391	2680	817	0	10	0	3	817	814	10	top soil sandy	1	BF
597391	2680	817	10	40	3	12	814	805	30	sandy gravel with thin clay layers	1	BF
597391	2680	817	40	404	12	123	805	694	364	consolidated sandy clay with minor cobbles	2	Pantano
640502	2805	855	0	40	0	12	855	843	40	clay and sand	1	BF
640502	2805	855	40	250	12	76	843	779	210	decomposed granite	1	BF
640502	2805	855	250	605	76	184	779	671	355	cataline gneiss banded soft streaks and fractures 410 to 414 and 577 to 582	3	Bedrock
807361	2805	855	0	40	0	12	855	843	40	clay and sand	1	BF

References - Agua Caliente

Arizona Department of Water Resources (ADWR), 2014. Water Resource Data, Interactive online Well Registry (Wells 55).

Cunningham, E.E.B., Long, A., Eastoe, C., and Bassett, R.L., 1998, Migration of recharge waters downgradient from the Santa Catalina Mountains into the Tucson basin aquifer, Arizona, USA: Hydrogeology Journal, v. 6, p. 94-103.

Davis, G.A., Lister, G. S., and Reynolds, S. J., 1986, Structural evolution of the Whipple and South Mountains shear zones, southwestern United States: Geology, v. 14, p. 7-10.

Davis, G.H., 1980, Structural characteristics of metamorphic core complexes, southern Arizona, *in* Crittenden, M.D., Jr., Coney, P.J., and Davis, G.H., eds., Cordilleran metamorphic core complexes: Geological Society of America Memoir 153, p. 35-77.

Davis, G.H., 1983, Shear-zone model for the origin of metamorphic core complexes: Geology, v. 11, p. 342-347.

Davis, G.H., 1987, Saguaro National Monument, Arizona: Outstanding display of the structural characteristics of metamorphic core complexes, *in* Hill, M.L., ed., Cordilleran Section of the Geological Society of America: Geological Society of America Centennial Field Guide, v. 1, p. 35-40.

Dickinson, W.R., 1991, Tectonic setting of faulted Tertiary strata associated with the Catalina core complex in southern Arizona: Geological Society of America, Special Paper 264, 106 p., with map, scale 1:125,000.

Dickinson, W.R., 1999, Geologic framework of the Catalina foothills, outskirts of Tucson (Pima County, Arizona): Arizona Geological Survey Contributed Map CM-99-B, scale 1:24,000, 31 p.

Drewes, H., 1977, Geologic map and sections of the Rincon Valley Quadrangle, Pima County, Arizona: U.S. Geological Survey Miscellaneous Investigations Series Map I-997, scale 1:48,000.

Eastoe, C.J., Gu, A., and Long, A., 2004, The origins, ages, and flow paths of groundwater in Tucson basin: Results of a study of multiple isotope systems, in Hogan, J.F., Phillips, F.M., and Scanlon, B.R., eds., Groundwater recharge in a desert environment: The southwestern United States: American Geophysical Union, Water Science and Application, v. 9, p. 217-234; DOI: 10.1029/WS009

Force, E.R., 1997, Geology and mineral resources of the Santa Catalina Mountains, southeastern Arizona: Tucson, Arizona, Center for Mineral Resources, Monographs in Mineral Resource Science, n. 1, 134 p.

Force, E.R., 2002, Structural reconnaissance of lower-plate rocks along the Catalina-Rincon range front, Pima County, Arizona: Arizona Geological Survey Contributed Map CM-02-A, 2 sheets, scale 1:24,000 and 1:48, with 11 p. text.

Fornash, K.F., Patchett, P.J., Gehrels, G.E., and Spencer, J.E., 2013, Evolution of granitoids in the Catalina metamorphic core complex, southeastern Arizona: U-Pb, Nd, and Hf isotopic constraints: Contributions to Mineralogy and Petrology, v. 165, p. 1295-1310; DOI 10.1007/s00410-013-0859-4

Keith, S.B., Reynolds, S.J., Damon, P.E., Shafiqullah, M., Livingston, D.E., and Pushkar, P.D., 1980, Evidence for multiple intrusion and deformation within the Santa Catalina-Rincon-Tortolita

crystalline complex, southeastern Arizona, *in* Crittenden, M.D., Jr., Coney, P.J., and Davis, G.H., eds., Cordilleran metamorphic core complexes: Geological Society of America Memoir 153, p. 217-267.

Mohrbacher C.J., 1984. Mountain-front recharge to the Tucson basin from the Santa Catalina Mountains, Arizona. M.S. thesis, University of Arizona, 87 pp.

Olson, M.C., 1982. Mountain-front recharge to the Tucson basin from Tanque Verde Canyon, Arizona. M.S. thesis, University of Arizona, 124 pp.

Pain, C.F., 1985, Cordilleran metamorphic core complexes in Arizona: A contribution from geomorphology: Geology, v. 13, p. 871-874.

Pima County Regional Flood Control District, 2014. Personal communication with Frank Postillion, Chief Hydrologist, July 16.

Richard, S.M., Spencer, J.E., Youberg, A., and Ferguson, C.A., 2004, Geologic map of the Rincon Valley area, Pima County, Arizona: Arizona Geological Survey Digital Geologic Map 44 (DGM-44), scale 1:24,000.

Robertson, Frederick N., 1991,Geochemistry of groundwater in alluvial basins of Arizona and adjacent parts of Nevada, New Mexico, and California. U.S. Geological Survey professional paper; 1406-C. 102 pg.

Spencer, J.E., 2006, A geologist's guide to the core complex geology along the Catalina Highway, Tucson area, Arizona: Arizona Geological Survey Open File Report 06-01, ver. 1.1, 38 p.

Spencer, J.E., and Reynolds, S.J., 1989, Middle Tertiary tectonics of Arizona and the Southwest, *in* Jenney, J.P., and Reynolds, S.J., eds., Geologic evolution of Arizona: Arizona Geological Society Digest, v. 17, p. 539-574.

Spencer, J.E., Richard, S.M., Youberg, A., Ferguson, C.A., and Orr, T.R., 2002, Geologic map of the Chief Butte 7 ½' Quadrangle, southeastern Pinal County, Arizona: Arizona Geological Survey Digital Geologic Map 22, version 1.1, scale 1:24,000.

8.3 Geology of Hooker's Hot Spring, Galiuro Mountains, southeastern Arizona

By Jon E. Spencer and Bradford J. Johnson, Arizona Geological Survey, 2014

Introduction

Hooker's Hot Spring is located approximately 70 km (40 miles) east of Tucson, Arizona, and is within the Hooker's Hot Spring 7.5' Quadrangle in the southern Galiuro Mountains. The hot spring itself is on the southwest flank of the wide wash in Hot Springs Canyon, east of the San Pedro River. Water temperature is reported at 52°C. Hooker's Hot Spring and surrounding land are part of the Nature Conservancy's Mule Shoe Ranch Preserve. Arizona Geological Survey geologists were granted permission to access the area in 2014. Jon E. Spencer and Bradford J. Johnson of the Arizona Geological Survey mapped the geology of approximately 18 km^2 (7 mi^2) to identify geologic features that potentially influence groundwater hydrology. Specifically, it was hoped that geologic features could be identified that are responsible for the hot water emanating from the spring. Ultimately, this geologic study was intended to provide better understanding of the geothermal resources in the area.

Regional geology

The largest and possibly most important structure with bearing on the subsurface geology is the Pinaleño metamorphic core complex. Metamorphic core complexes occur in a belt from Idaho through western Nevada and across central Arizona (Crittenden and others, 1980; Davis, 1980; Davis and Coney, 1979; and Dickinson, 1991). Core complexes were accompanied by intense thin-skinned extension prior to Basin and Range rifting. Extension occurs along a low-angle "detachment" fault that is overlain by relatively closed-spaced planar and listric normal faults that rotate progressively downward as extension proceeds (Spencer and Reynolds, 1989). The overall thinning of the crust results in tectonic denudation and erosional unroofing of much deeper crustal rocks below the detachment fault through isostatic compensation and uplift (Spencer and Reynolds, 1989). The important feature for geothermal in the northern Willcox basin is the potential for fracture permeability in the upper plate rocks and syntectonic sediments above the detachment. The breakaway fault for the Pinaleño metamorphic core complex is probably at the base of the Winchester and Galiuro Mountains (Witcher, 2008). Mount Graham in the northern Willcox Basin represents the tectonically denuded and uplifted block of deeper crust beneath the detachment (Witcher, 2008). Upper plate faulted and rotated volcanics and syntectonic core complex alluvial fill packages with possible fracture permeability would be found below undeformed Neogene Basin and Range basin fill in the subsurface (Witcher, 2008). Significant vertical uplift and erosion during and post Mesozoic has removed any potential reservoir rocks in the Paleozoic and Mesozoic section in the Willcox Basin (Sulfur Springs Valley). Highly-fractured Precambrian fault zones involved in Mesozoic deformation have potential for reservoirs where Neogene tectonism might have created permeability in older fractures zones (Witcher, 2008).

Volcanic rocks in the range are older than ~20 m.y.—consequently, there has been no geologically recent magmatic activity that would provide heat to a thermal reservoir and thus produce hot springs, and no young igneous rocks were identified in this study. Few geochronologic analyses have been done in the southern Galiuro Mountains, however, so it is not known for certain that the area lacks young volcanic rocks.

Geology of the Hooker's Hot Spring area

Hooker's Hot Spring is within the basin west of the southern end of the Galiuro Mountains, a ~100 km long, north-northwest trending mountain range that consists primarily of 20-30 million-year-old volcanic rocks (Dickinson and Shafiqullah, 1989; Dickinson, 1991; Richard et al., 2000). The range itself resembles a typical Basin and Range fault block (horst), with flanking normal faults dipping outward from the range. Many of the bounding normal faults, however, dip gently rather than steeply away from the range (Davis and Hardy, 1981; Dickinson et al., 1987; Goodlin and Mark, 1987; Dickinson, 1991).

The Galiuro Mountains bifurcate southward into two narrow ranges separated by an intramontane basin that includes Allen Flat and upper Hot Springs Canyon (Allen Flat basin of Burtell, 1989). The western range includes the Johnny Lyon Hills, while the Winchester Mountains form the eastern range. Hot Springs Canyon drains much of the area in this intramontane basin, crosses the western side of the Galiuro Mountains, and empties into the San Pedro River. Hooker's Hot Spring is located about a half kilometer upstream from the point where Hot Springs Canyon Wash flows from the intramontane basin to cut across bedrock of the southwestern Galiuro Mountains. The boundary between these two geographic features is a steeply east-dipping, east-side-down normal fault located ~600m downstream from Hooker's Hot Spring (Figure 8.3.1). The basin sediments incised by upper Hot Springs Canyon and its tributaries consist of poorly to moderately lithified, poorly sorted, sandy pebble and cobble conglomerate with generally crudely defined bedding (map unit Tcg on Figure 8.3.1). Beds in the conglomerate are generally gently dipping, but near the basin-bounding normal fault west and south of Hooker's Hot Spring, bedding steepens to approximately 30° to the west-southwest and projects down-dip into the normal fault with a bedding-fault intersection angle of ~90° (Figure 8.3.2B). Clasts in the conglomerate are derived from the older volcanic units eroded from the nearby Winchester Mountains.

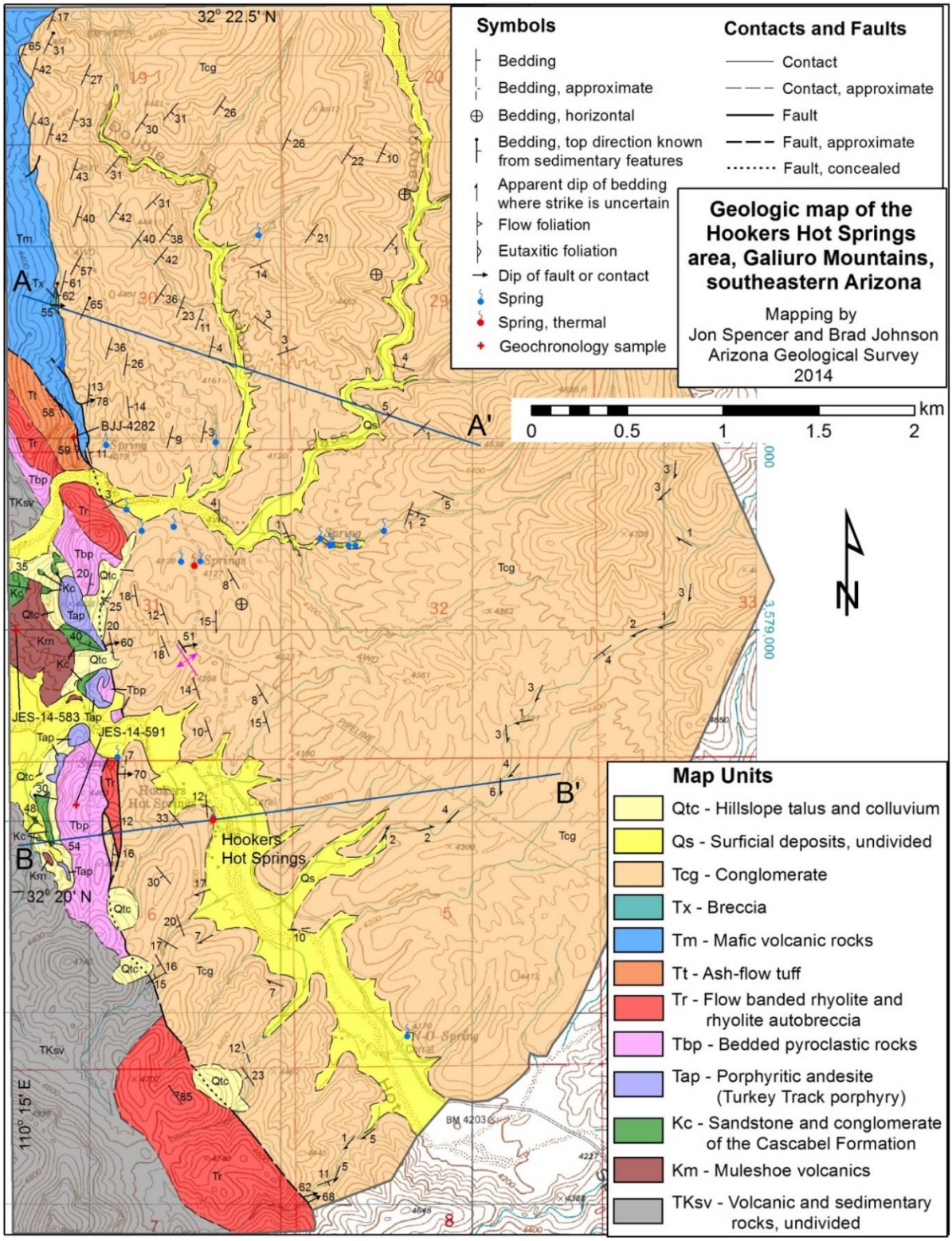

Figure 8.3.1. Geologic map of the Hooker's Hot Spring area

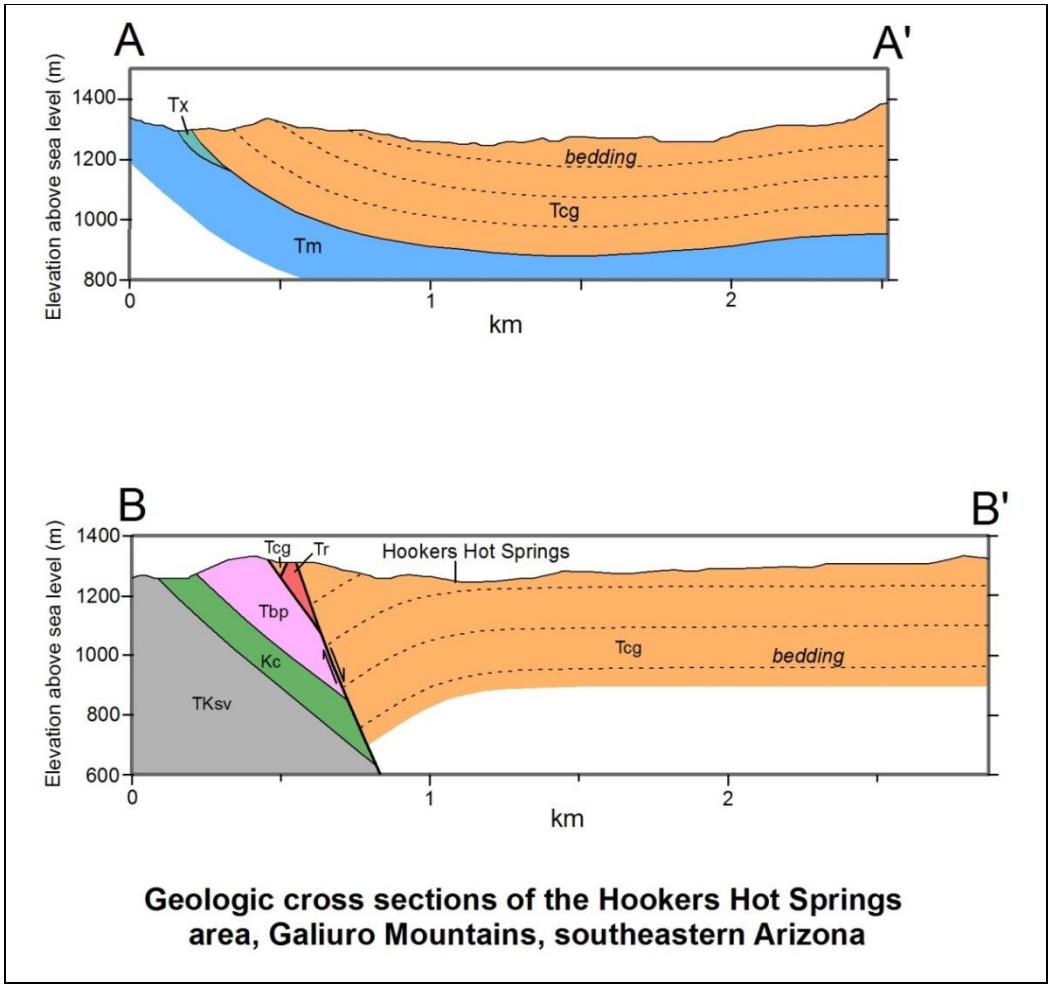

Figure 8.3.2. Geologic cross sections of the Hooker's Hot Spring area (See Fig. 1 for location.)

North of Hot Springs Wash the steep normal fault dies out into a steeply east-dipping depositional contact. Beds in the basin-filling conglomerate unit dip moderately to steeply eastward near the depositional contact, with bedding dips decreasing up section to the east so that more than ~1km away beds are gently dipping (Figures 8.3.1, 8.3.2A). Based on cross section A (Fig. 8.3.2A) we estimate that the preserved thickness of the conglomerate unit is ~400m. The northward transition from a normal fault with adjacent west dipping beds to a depositional contact with adjacent east dipping beds is unusual, and we are not aware of a similar structure anywhere. Conglomerate beds in northern exposures are folded, reflecting horizontal shorting, whereas to the south, a normal fault offsets conglomerate beds, reflecting horizontal extension. The implication of this structural contrast is that fault blocks on opposite sides of the fault were rotated relative to each other about a pivot point ~1km north of Hooker's Hot Spring, with shortening to the north and extension to the south. The fact that the areal extent of east-tilted beds increases northward is consistent with this interpretation, and suggests that a reverse fault in the subsurface accommodates shortening in basement rocks.

The Tertiary conglomerate is presumed to be underlain by Tertiary mafic volcanics (Figure 8.3.2). The conglomerate, on the flanks of the Winchester Mountain, includes clasts derived from erosion of Winchester Mountain volcanic rocks. Where the normal fault trends north along the western edge of the basin, west-side up, the conglomerate unit is offset against the underlying Tertiary rocks, exposing east-dipping beds of mafic volcanics, bedded tuff, banded rhyolite, and bedded pyroclastic volcanics (Figures 8.3.1 and 8.3.2). No wells have been drilled deep enough in this basin to confirm the formation sequence underlying the conglomerate; however, similar stratigraphy can be found to the east of Winchester Mountain, where the Wilcox Greenhouse geothermal well was drilled to 4,004 feet depth (Witcher, 2008). Upper basin fill was encountered in the first 2,230 feet followed by lower basin fill consisting of gravely, coarse sand and coarse sand with rounded basalt, andesite, and rhyolite clasts (clasts provenance from the west) to 2,770 feet depth. Below the basin fill, Tertiary rhyolite encountered from 2,770 feet to 3,750 feet depth was reported to be fractured and water producing, and is the reservoir for the geothermal water. This fractured zone is underlain by rhyolitic welded ash-flow tuff to total depth which is likely impermeable. It would appear that the same rhyolitic fractured zone also underlies the conglomerate at Hooker's Hot Spring area at depth.

Geohydrology of the Hooker's Hot Spring area

As a consequence of its poor cementation and coarse grain size, the conglomerate unit in the Hooker's Hot Spring area is porous and permeable. The unit hosts approximately 20 springs in the study area (Figure 8.3.1). The simplest explanation for the abundance of springs in basin-filling sediments near and north of Hooker's Hot Spring is that the conglomerate unit contains much groundwater, and this groundwater is driven to the surface by elevated hydrostatic head resulting from recharge in the eastern, elevated side of the basin on the flank of the Winchester Mountains. Basically, the basin is like a tilted bowl of sand, with water flowing to the surface at the lowest part of the bowl (and spilling out to the west across bedrock in Hot Springs Canyon).

Most of the springs, and the highest density of springs, are near lower Bass Canyon, in the area where bed dips change along strike. Only one spring is noted as thermal (warm) and the others are cold springs. We suggest that enhanced permeability and high spring density in this area is due to structural disruption associated with the along-strike twisting deformation of beds. Small faults and crushed rocks in this zone, expected as a consequence of deformation where bedding dips reverse direction along strike, is not apparent but may be concealed by abundant disaggregated conglomerate and derivative soil.

Hooker's Hot Spring area discharges one hot and one cold spring, with the two only ~10m apart. The only other thermal spring is ~1km due north of Hooker's Hot Spring, and it is only a warm seep. Thus, of ~20 springs in the area, only one is a significant hot spring. The most obvious potential source of thermal water in the area is the fault along the west side of the basin, which should provide a pathway for water flow to great depths (~1-3 km) where temperatures are naturally elevated; however, the four springs

that are on or near the fault are not thermal springs. Heating due to magma intrusion in the past 1-2 million years is another potential source of heat. Although we did not identify any obviously young igneous rocks, three samples of nearby volcanic rocks were collected and submitted for $^{40}Ar/^{39}Ar$ geochronologic analysis in order to evaluate the age of past igneous activity. The cold springs are likely originating from shallow basin aquifers. Possibly another buried fault intercepts the normal fault creating a preferred conduit at the confluence and is supplying thermal water from a deeper source, such as the fractured rhyolitic reservoir. In conclusion, we were not able to definitively determine, on the basis of the surficial geology of the area, why Hooker's Hot Spring and one other are thermal springs, whereas others in the same area are not.

References Cited

Burchell, A., 1992, Mid-Tertiary volcanic stratigraphy and petrogenesis; Galiuro Mountains, southeastern Arizona – A field based geochemical reconnaissance: Tucson, University of Arizona, M.S. thesis, 156 p.

Burtell, R.T., 1989, Geochemistry and occurrence of groundwater in the Allen Flat basin, Arizona: Tucson, University of Arizona M.S. thesis, 163 p.

Creasey, S.C., Jinks, J.E., Williams, F.E., and Meeves, H.C., 1981, Mineral resources of the Galiuro Wilderness and contiguous Further Planning Areas, Arizona: U.S. Geological Survey Bulletin 1490, 94 p., 2 sheets, scale 1:62,500.

Cunningham, E.E.B., Long, A., Eastoe, C., and Bassett, R.L., 1998, Migration of recharge waters downgradient from the Santa Catalina Mountains into the Tucson basin aquifer, Arizona, USA: Hydrogeology Journal, v. 6, p. 94-103.

Davis, G.H., and Hardy, J.J., Jr., 1981, The Eagle Pass detachment, southeastern Arizona; product of mid-Miocene listric(?) normal faulting in the southern Basin and Range: Geological Society of America Bulletin, v. 92, p. 749-762.

Dickinson, W.R., 1991, Tectonic setting of faulted Tertiary strata associated with the Catalina core complex in southern Arizona: Geological Society of America, Special Paper 264, 106 p., with map, scale 1:125,000.

Dickinson, W.R., and Shafiqullah, M., 1989, K-Ar and F-T ages for syntectonic mid-Tertiary volcano-sedimentary sequences associated with the Catalina core complex and San Pedro trough in southern Arizona: Isochron/West, n. 52, p. 15-27.

Dickinson, W.R., Goodlin, T. C., Grover, J. A., Mark, R. A., and Shafiqullah, M., 1987, Low-angle normal-fault system along the range front of the southwestern Galiuro Mountains in southeastern Arizona: Geology, v. 15, p. 727-730.

Eastoe, C.J., Gu, A., and Long, A., 2004, The origins, ages, and flow paths of groundwater in Tucson basin: Results of a study of multiple isotope systems, *in* Hogan, J.F., Phillips, F.M., and Scanlon, B.R., eds., Groundwater recharge in a desert environment: The southwestern United States: American Geophysical Union, Water Science and Application, v. 9, p. 217-234; DOI: 10.1029/WS009

Goodlin, T.C., and Mark, R.A., 1987, Tectonic implications of stratigraphy and structure of Cretaceous rocks and overlying mid-Tertiary cover in Hot Springs Canyon, Galiuro Mountains, southeastern Arizona, *in* Dickinson, W.R., and Klute, M.A., eds., Mesozoic rocks of southern Arizona and adjacent areas, p.177-188.

Richard, S.M., Reynolds, S.J., Spencer, J.E., and Pearthree, P.A., 2000, Geologic map of Arizona: Arizona Geological Survey Map 35, scale 1:1,000,000.

Spencer, J.E., and Reynolds, S.J., 1989, Middle Tertiary tectonics of Arizona and the Southwest, *in* Jenney, J.P., and Reynolds, S.J., eds., Geologic evolution of Arizona: Arizona Geological Society Digest, v. 17, p. 539-574.

Appendix. Hooker's Hot Spring map unit descriptions

Qs – Surficial deposits, undivided (Quaternary) – Unlithified streambed sediments and incised soil and alluvial deposits on the flanks of streambeds.

Qtc – Hillslope talus and colluvium – Talus on steep slopes, and unsorted hillside deposits that have not been sorted by alluvial processes and have not been displaced significantly from bedrock sources.

Tcg – Conglomerate and conglomeratic sandstone (Oligocene to lower Miocene) – Conglomerate and pebbly lithic sandstone containing pebbles, cobbles, and locally boulders of mafic, intermediate, and felsic volcanic rocks in poorly sorted, medium- to coarse-grained, lithic sandstone matrix. The unit is thick-bedded, weathers light tan, and forms resistant ledges although some conglomerate intervals high in the section are poorly indurated and form recessive slopes. Conglomerate near the base of the section contains clasts apparently derived from underlying volcanic units, including cobbles and sparse boulders of altered-pyroxene basalt and cobbles of phenocryst-rich and flow-laminated rhyolites. Within the lower 70 to 150 m, basal conglomerate grades upward to an interval of medium- to fine-grained sandstone and pebbly sandstone that is medium-bedded with local cross bedding. This grades upward into conglomerate and pebbly sandstone in which most of the pebbles and cobbles are of mafic to intermediate volcanic rocks. Felsic volcanic cobbles reappear higher in the section. Generally, pebbles and cobbles in the lower part of the section range from well-rounded to subangular, with subrounded being the mode. Cobbles in the upper part of the exposed section in the northern part of the map area are well-rounded.

Tx – Sedimentary breccia (Oligocene to lower Miocene) – Breccia composed of subangular to subrounded (some rounded) cobbles, pebbles, and boulders of altered-pyroxene basalt, evidently derived from the underlying volcanic unit Tm. The breccia is a local unit, up to 30 m thick. It is massive, showing no internal stratification. It overlies basalt of unit Tm in depositional contact and is overlain depositionally by thick-bedded conglomerate of unit Tcg, which contains mainly basalt cobbles and pebbles but other clast types as well. The breccia and conglomerate both have medium-grained sandy matrix, light tan in color.

Tm – Mafic volcanic rocks (Oligocene to lower Miocene) – Undivided mafic lavas including aphyric basalt or andesite, pyroxene basalt, and olivine basalt. Most of the unit in this map area consists of pyroxene basalt, containing 2-4% light-green-altered phenocrysts, 2-4 mm across, that apparently are pseudomorphs of pyroxene replaced by epidote or uralite. Aphyric, vesicular, mafic lava apparently underlies the pyroxene basalt in the southwestern most part of the unit and is in fault contact with ash-flow tuff of unit Tt. Olivine basalt, containing Iddingsite pseudomorphs after olivine phenocrysts, is present in the extreme north.

Tt – Rhyolite ash-flow tuff (Oligocene to lower Miocene) – Phenocryst-rich rhyolite ash-flow tuff, containing 20-30% sanidine phenocrysts (1-4 mm), 1-2% biotite phenocrysts (<1 to 2 mm, rarely 3-4 mm), and 5-10% flattened pumice and volcanic-lithic fragments, in a light-orange-brown groundmass.

Tr - Flow-banded rhyolite and rhyolite autobreccia (Oligocene to lower Miocene) - Flow-banded rhyolite and rhyolite autobreccia with 2-3%, <1mm quartz, <1%, <1mm biotite, and 1-2%, <1mm sanidine. Locally includes vitrophyre. In some areas autobreccia contains flow-banded and flattened rhyolite clasts. Subvertical flow banding and irregular outcrop areas in southern exposures suggest that this unit is partly intrusive.

Tbp - Bedded pyroclastic rocks (Oligocene to lower Miocene) – This unit consists primarily of pale gray, bedded tuff containing 6-10%, <1mm, generally fresh biotite, ~15%, <1mm quartz, and 2-5%, <1mm hornblende. Layering in this unit is defined by minor variations in resistance to weathering and by aligned pits that are not flattened and so can't be interpreted as flattened pumice fragments (hence, no eutaxitic foliation, but rather bedding). Locally the unit is interlayered with volcanic-lithic conglomerate in which clasts contain much less biotite and hornblende.

Tap - Porphyritic andesite (Turkey-Track porphyry) (Oligocene to lower Miocene) – Rocks of this unit commonly contain 40-60%, <25 mm plagioclase in dark gray matrix. Some rocks of this unit lack megacrysts but are otherwise similar.

Kc - Sandstone and conglomerate of the Cascabel Formation (upper Cretaceous) - Dark reddish brown, interbedded sandstone and siltstone, and dark reddish brown, matrix supported conglomerate with high silt content. Subrounded to subangular cobbles in conglomerate consist at least locally of primarily volcanic rocks. Some sandstone is quartz rich.

Km - Muleshoe volcanics (upper Cretaceous) – Gray to tan to brown volcanic rocks with up to 4%, <1mm biotite, up to 8%, <2mm sanidine, and up to 15%, <2mm plagioclase (mostly acicular and generally altered).

TKsv - Volcanic and sedimentary rocks, undivided (upper Cretaceous to lower Miocene) – Rocks of the Muleshoe volcanics, Cascabel Formation, and porphyritic andesite, undivided.

9. DISCUSSION

Summary

The AZGS collected thermal spring water samples from 16 springs and wells throughout Arizona's Basin and Range Province and Transition Zone. The samples were analyzed for analytical suites incorporated into the Powell and Cumming (2010) geothermometry workbook to better understand heat sources for these thermal waters in relation to the geology of the region. The study of hot springs and discharge temperatures is important as they represent the surface leakage of thermal water from a subsurface geothermal reservoir. As geothermal waters percolate to the surface, various forms of cooling and precipitation of some minerals can occur. Thermal waters can cool by mixing with meteoric water near the surface or by conductive or convective cooling methods. Geothermometers and geoindicators can be used to predict such things as the likely source of thermal waters, if mixing occurs, or if conductive cooling has occurred. Geothermometry models, when used in combination, can also provide indicators of the thermal water temperatures at depth. This report presents the data and our interpretation to the extent of our limited understanding of geochemistry and complex factors that contribute to the geothermometry. It is meant to provide data for geothermal experts and others interested in pursuing additional interpretation.

Geological mapping was conducted at three locations in southeast Arizona. At two locations, Agua Caliente and Hooker's Hot Spring, thermal springs are suspected to be associated with subsurface fractures and faults, but lack mapped geological detail. The third location is the Safford basin between the Gila Mountains and the Pinaleño Mountains, where lineations and faulting are believed to be major structural factors controlling geothermal groundwater movement. Structural disturbances resulting in faulting, flexing, erosion, deposition of sediments, and volcanic activity have taken place intermittently and with variable intensity throughout the geologic history of the Basin and Range Province (Wilson and Moore, 1959). On a regional scale, Arizona thermal springs are controlled by ambiguous crustal inhomogeneity and structure. Springs occur where topographic relief is greatest, and most often in areas with relatively large exposures of crystalline basement rocks. Over 75 percent of Arizona thermal springs lie in a 120-km wide, NW-trending belt that coincides with the Transition Zone, a region that has some characteristics of both the Colorado Plateau and the Basin and Range province (Stone and Witcher, 1983). In Arizona, thermal waters are closely associated with major fault zones (Hahman, 1978; Waring, 1965). Thermal water moving vertically from deep-heated crustal rock along faults into Tertiary, Quaternary, and Recent sediments and then moving outward horizontally in these sediments from fault zones, appears to be the most probable transport mechanism (Giardina and Conley, 1978).

Mapping

Geological mapping was conducted at Safford Basin situated between the Pinaleño Mountains and the Gila Mountains (Figure 8.1.1). The Safford Basin is largely an asymmetric basin, bound on its southwest

margin by the Pinaleño fault. The Pinaleño fault zone coincides with the North and South Safford fault zones and Cactus Flat fault. Thermal groundwater likely transported along faults is believed to migrate into fractured or permeable basin sediments and mix with older meteoric basin groundwater before surfacing as springs and through artesian wells. Deep-seated geothermal groundwater flowing to Indian hot spring and Cactus Flat hot springs are likely following major high-permeability fault zones, fractures, and conglomeratic strata along the Pinaleño fault zone. Low-permeability features such as fine-grained siliciclastic, evaporite and lacustrine deposits, fault gouge, and fold traps are all present, and further complicate pathways for upward-migrating geothermal water.

Agua Caliente Warm Spring is located along the northeastern edge of the Tucson Basin adjacent to bedrock at the foot of Agua Caliente Hill (Figure 8.2.1). The Catalina detachment fault, the dominant structural feature in the northeastern Tucson Basin, separates granitic and gneissic rocks in the footwall block from moderately lithified clastic, Oligocene to middle Miocene Pantano Formation in the upper block (Figure 8.2.2). The Catalina detachment fault is largely buried by younger, post-faulting alluvial deposits at the foot of the Santa Catalina Mountains, but the fault trace is buried although suspected to be located below Agua Caliente Warm Spring. Corrugated grooves in the footwall are a common feature of low-angle detachment faults (Figure 8.2.3). Groundwater flowing through fractures in the Santa Catalina Mountains and Rincon Mountains likely migrates downward, in some cases to depths where ambient geothermal temperatures are significantly elevated (many hundreds of meters to perhaps 1-2 km). Agua Caliente Warm Spring is located above the structural plunging crest of a groove in the Catalina detachment fault (Fig. 8.2.2). Potentially, geothermal groundwater flows into the buried Catalina detachment fault at depth and ascends along the detachment fault within the fracture zone to enter alluvial deposits just below Agua Caliente Warm Spring. The spring may be associated with hot groundwater migrating up along detachment fault grooves and converging toward the crest of the corrugation (Fig. 8.2.3).

Hooker's Hot Spring is west of the southern Galiuro Mountains (Figure 8.3.1) which consists primarily of 20-30 million-year-old volcanic rocks (Figure 8.3.1) (Dickinson and Shafiqullah, 1989; Dickinson, 1991; Richard et al., 2000). The range itself resembles a typical Basin and Range fault block (horst), with flanking normal faults dipping outward from the range. Many of the bounding normal faults, however, dip gently rather than steeply away from the range (Davis and Hardy, 1981; Dickinson et al., 1987; Goodlin and Mark, 1987; Dickinson, 1991). Volcanic rocks in the range are older than ~20 m.y.—consequently, there has been no geologically recent magmatic activity that would provide heat for hot-spring activity, and no young igneous rocks were identified in this study. Few geochronologic analyses have been done in the southern Galiuro Mountains, however, so it is not known for certain that the area lacks young volcanic rocks. Samples were submitted to the University of Arizona for geochemistry analysis, but results have not been received before publication.

Of numerous springs in the Hooker's Hot Spring area, only one is a significant hot spring. The most obvious potential source of thermal water here is the fault along the west side of the basin, which could

provide a conduit for water flow to great depths (~1-3 km) where temperatures are naturally elevated; however, the four springs that are on or near the fault are not thermal springs. The cold springs are likely originated from basin groundwater aquifers. Potentially, another fracture or preferred pathway is supplying the thermal waters from a deeper source. Magma intrusion in the past 1-2 million years is another potential source of heat, although no obvious young igneous rocks were identified.

Characterization of Thermal Springs

Tritium values ranged from an apparent 0.4 TU to 1.0 TU and indicate submodern water for all springs (Table 6.7). Tritium results <0.8 TU indicate all sampled groundwater was accumulated prior to 1950s (submodern), indicative of deep basin aquifers or waters derived from deep bedrock.

The uncorrected ^{14}C age dates were calculated for the thermal springs groundwater (Table 6.8). The range of uncorrected ages indicates maximum ages from 7,501 years old at Ts01 Agua Caliente to as old as 29,010 years at Ts07 (Thatcher) (corrected dates are expected to be younger by 10% to 48%). Results indicate that groundwater has been stored for at least several thousand years to over 20,000 years, whether in deep basin aquifers or bedrock reservoirs. Groundwater younger than 11,700 years accumulated during the interglacial Holocene epoch and warmer climate. Older groundwater accumulated during the Wisconsin glaciation period spanning from 80,000 years ago to 12,000 years ago. Mixed groundwater may have source components older or younger than the ages given.

The δD / $\delta^{18}O$ values are consistent with those reported for the same springs by Mariner et al. (1977) (Table 6.10). Most of the thermal groundwater δD - $\delta^{18}O$ values plot adjacent to or to the right of the SMOW and LMWL indicating groundwater that has had evaporative loss consistent with inland basins (Figure 6.1). The tightly clustered results low on the LMWL indicate accumulation at cooler temperatures or higher altitudes. The springs higher up the SMOW indicate surface evaporative loss before infiltration, more likely associated with precipitation during a past warmer climate or lower altitude and include Ts01 (Agua Caliente), Ts11 (Cofer), and Ts22 (Tonopah) which were also interpreted using ^{14}C dating to be Holocene (post glacial and warmer climate) groundwater (Figure 6.2). All other groundwaters dated to the late Pleistocene glacial period (colder climate) and clustered lower on the LMWL. The results are consistent with the ^{14}C age dates (even as uncorrected) relating groundwater with older ages to a colder climate and younger ages to a warmer climate.

All samples have relatively high $^{87}Sr/^{86}Sr$ ratios in a range that suggests groundwater circulation in rock with continental crust origins (Table 6.10). Springs Ts07 (Thatcher) and Ts08 (Potter) have high Sr concentrations suggesting long duration circulation (Figure 6.3). Samples Ts18 (Ringbolt) and Tw14 (Radium) can be grouped as having higher than the average Sr concentration and similar $^{87}Sr/^{86}Sr$ ratios closer to surface water ratio (0.709) which suggests deeply circulated meteoric groundwater. The remaining samples show relatively low Sr concentrations suggesting younger groundwater, and a wide range of $^{87}Sr/^{86}Sr$ ratios, as expected considering locations throughout the state with a large range of source rock compositions and origins.

All groundwater samples contained large amounts of excess ^{4}He indicating groundwater circulation in a He enriched continent crust material (Table 6.12). The R/Ra values fall in between two source indicators (Figure 4.1), suggesting the groundwater has components of both deeply circulated, long-resident time crustal fluids and younger groundwater. Both groundwater samples Ts17 (Cofer) and Ts24 (Kaiser) show highest ^{4}He concentrations (10^{-5}) and the R/Ra ratio closest to that of surface water, indicating mixing of long term circulated waters (large amount of excess ^{4}He) with younger meteoric groundwater (high R/Ra).

Clifton Area

Geothermal studies show a complex structure and distribution of temperatures in the shallow crust, which are favorable for geothermal resources in the Clifton area. The lower San Francisco River area lies in the transition zone on the southern margin of the Colorado Plateau and extensive Quaternary basaltic volcanism associated with high regional conductive heat flow (Witcher, J.C., 1981b). Thermal springs in this area probably originate from predominantly forced convection, which circulates water through fractured Precambrian granite and Paleozoic rocks that have been displaced by Cenozoic volcano-tectonic processes and faulting. Thick sequences of volcanic flows and clastic sediment cap these aquifers. With groundwater transverse along the fault zone to regional ground-water flow, this hot water leaks to the surface with flow rates as high as 200 gpm (Mann, 1980). It is reported that a magmatic heat source is not indicated for this area; rather, above-normal mantle heat flow or radiogenic crustal heat production provides heat to hydrothermal systems in the Clifton-Morenci region (Stone and Witcher, 1983). Potential exists for geothermal resources between 90°C and 140°C (Stone and Witcher, 1983). Both Potter and Gillard Hot Springs are located in the Clifton area. Measured temperatures and geothermometers indicate these springs potentially have the highest reservoir temperatures in Arizona.

At Potter Hot Spring (Ts08), the uncorrected age of groundwater using isotopic $\delta^{14}C$ (19,741 years) correlates to accumulation during the Pleistocene. The isotopic $\delta^{13}C$ value (-6.2) indicates a potential endogenetic or magmatic source (Table 4.1). Both the $^{87}Sr/^{86}Sr$ and $^{3}He/^{4}He$ ratios indicate long duration circulation. The strontium result for Ts08 (Potter) was the highest measured at 9.6 mg/l, an indication of a deep bedrock fluid source. High Na and TDS (9,740 mg/l) values may be associated with mixing of old, deep, strongly mineralized sea water and fresh water at different depths in the crystalline basement and Tertiary deposits, and by water-rock reactions with an increasing mineral dissolution due to the high dissolved CO_2 content (24,000 mg/l). Ts08 (Potter) is a sodium-chloride sulfate water consistent with outflow from a geothermal reservoir. The Cl-SO_4-HCO_3 ternary shows Ts08 as mature water and more likely to provide reliable cation geothermometry. The Na-K-Ca (cation) geothermometer indicates a deeper source temperature calculated at 180°C. The Quartz conductive (silica) geothermometer (temperatures >150°C) gives 128°C for a near reservoir temperature.

At Gillard Hot Spring (Ts09), the $\delta^{14}C$ data gives an uncorrected age of 20,634 years and accumulation during the Pleistocene glacial period and colder climate. The $^{3}He/^{4}He$ ratio indicates long term circulation of groundwater, while the $^{87}Sr/^{86}Sr$ ratio (0.718) indicates younger groundwater or a bulk mix of older deep groundwater and young groundwater. This groundwater has moderate concentrations of CO_2 (5,400 µg/L) and TDS (1,520 mg/l). Ts09 (Gillard) is a sodium-chloride sulfate water with significant Cl and minimal SO_4 consistent with outflow from a geothermal reservoir. The Cl-SO_4-HCO_3 ternary shows Ts09 as matured water and should provide reliable cation geothermometry. The Na-K-Ca (cation) geothermometer indicates a deep source temperature calculated at 136°C. The Chalcedony conductive (silica) geothermometer (temperatures >100°C) gives 107°C for a near reservoir temperature.

Safford Area

A summary of the geochemistry data for Safford-San Simon Basin springs shows that those springs in close proximity of each other had similar data results and mineral equilibrium: Ts05 (Indian), Ts07 (Thatcher), and Tw05 (Watson); Ts03 (Dunes) and Ts06 (Dankworth); and Ts02 (Hooker) and Tw07 (Willcox). Surface temperatures measured for these springs ranged from 31.4°C to 44.6 °C.

Tw05 (Watson) and Ts05 (Indian) are located in the upper Safford basin and show similar geochemical characteristics. The uncorrected ^{14}C age dates the groundwater at 26,400 and 29,600 years, respectively. The $^{87}Sr/^{86}Sr$ ratios (0.715-0.716) are similar and indicate similar rock source and age. The low Sr concentration (0.607 and 0.57 mg/l) can be attributed to short-duration circulation or a source rock depleted in strontium. Moderate concentrations of dissolved CO_2 were detected in both Ts05 (Indian) (2,500 µg/l) and Tw05 (Watson) (3,400 µg/l). Moderate TDS (2,680 and 2,960 mg/l) and Cl (1,200 and 1,400 mg/l) and increased Na (1,200 and 960 mg/l) for Tw05 and Ts05, respectively, infer dissolution of basin evaporate minerals, such as halite (NaCl) or water-rock reactions with an increasing mineral dissolution due to moderate concentrations of dissolved CO_2. The Cl-SO_4-HCO_3 ternary shows Tw05 (Watson) and Ts05 (Indian) as matured water and should provide reliable cation geothermometry. The Na-K-Ca (cation) geothermometer indicating deep source temperatures gives 99°C for Tw05 (Watson) and 106°C for Ts05 (Indian). The Chalcedony conductive (silica) geothermometer (temperatures >100°C) at Ts05 (Indian) gives 59°C for a near reservoir temperature. The Chalcedony conductive (silica) geothermometer at Tw05 (Watson) gives 82°C for near reservoir temperature.

Ts03 (Dunes) and Ts06 (Dankworth) are located in the Cactus Flats area of the Safford basin and show geochemistry characteristics similar to Tw05 (Watson) and Ts05 (Indian). The uncorrected ^{14}C age dates the groundwater at 26,600 and 28,000 years old, respectively. The $^{87}Sr/^{86}Sr$ ratios (0.715-0.716) indicate rock source and age similar to Tw05 (Watson and Ts05 (Indian). The Sr concentrations (0.046 and 0.138 mg/l) are very low and indicate short-duration circulation or a source rock depleted in strontium. Unlike dissolved CO_2 at Tw05 (Watson) and Ts05 (Indian), dissolved CO_2 was not detected in either Ts03 (Dunes) or Ts06 (Dankworth). Moderate TDS (900-970 mg/l), and low Cl (190 and 260 mg/l) and Na (310 and 340 mg/l) content infer low water-rock reactions perhaps due to lack of dissolved CO_2. The Cl-SO_4-

HCO_3 ternary shows the Ts03 (Dunes) reservoir associated with volcanic waters and Ts06 (Dankworth) with mature waters. The Na-K-Ca (cation) geothermometer gives 111°C for Ts03 (Dunes) and 113°C for Ts06 (Dankworth) for a deep source temperature. The Chalcedony conductive (silica) geothermometer (for temperatures >100°C) gives 71°C and 31°C for near reservoir temperatures.

For Ts07 (Thatcher), the data varies from that of nearby Tw05 (Watson), Ts05 (Indian), Ts03 (Dunes) and Ts06 (Dankworth) on several levels. The uncorrected ^{14}C age of groundwater at Ts07 (Thatcher) is 15,200 years (10,300 yrs. corrected), much younger than given for the other nearby springs. Similar to Ts05 and Tw05, Ts07 (Thatcher) shows somewhat higher $^{87}Sr/^{86}Sr$ ratios (0.718) and a Sr concentration (9.424 mg/l) indicating long-duration circulation. No dissolved CO_2 was detected in Ts07 (Thatcher) groundwater. Ts07 (Thatcher) plots as "matured water" on the Cl-SO_4-HCO_3 ternary and should provide reliable cation geothermometry. The Na-K-Ca (cation) geothermometer for Ts07 (Thatcher) for deep source temperatures gives only 76°C and the Chalcedony conductive (silica) geothermometer (temperatures <100°C) for a near reservoir temperature gives 21°C. By all indications, it appears that Thatcher groundwater is derived from a separate reservoir or has much more mixing with colder groundwater than the other nearby hot springs, given the age, geochemistry, and temperature differences.

Willcox Area

The Hooker's Hot Spring is located to the west and the Willcox Greenhouse is located to the east of the Winchester Mountain range in the southern Galiuro Mountains. Winchester Mountain area stratigraphy comprises Tertiary conglomerate and conglomerate sandstone underlain by Tertiary mafic volcanics, ashflow tuff, flow-banded rhyolite and rhyolite autobreccia (fractured and water-bearing), bedded pyroclastic rocks, and porphyritic andesite. Although faulted and tectonically disrupted, the geology near the Winchester Mountain is generally similar on the west and east flanks. The Hooker's Hot Spring and Willcox thermal well are located in two separate unconnected basins, but the geochemistry of the spring groundwater is remarkably similar.

Geologic mapping at the Hooker's Hot Spring area (See Section 8.3) shows approximately 400 feet of Tertiary conglomerate underlain by mafic volcanics (Figure 8.3.2) in the basin to the west of Winchester Mountain. The conglomerate has volcanic clasts presumably eroded from the Winchester Mountain volcanics. A normal fault, west side up, trends north along the western edge of the basin, offsetting the conglomerate section against the underlying Tertiary rocks, exposing east-dipping beds of mafic, rhyolite, and bedded pyroclastic volcanics (Figures 8.3.1 and 8.3.2). No wells have been drilled deep enough in this basin to confirm the formation sequence underlying the conglomerate; however, similar stratigraphy can be found to the east of Winchester Mountain, at the Willcox Greenhouse geothermal well drilled to 4,004 feet depth. Upper basin fill was encountered in the first 2,230 feet followed by lower basin fill to 2,770 feet depth. Below the basin fill, Tertiary rhyolite encountered from 2,770 feet to

3,750 feet depth was reported to be fractured and water producing, and is the reservoir for the geothermal water. This fractured zone is underlain by rhyolitic welded ash-flow tuff to total depth.

Since the geochemistry and isotopic data of the two groundwater samples, Ts02 (Hooker) and Tw07 (Willcox), are so similar, we might assume that the geothermal reservoir for the thermal water surfacing at Hooker's Hot Spring is the same fractured and water producing banded rhyolite unit as logged at the Willcox well. We might also assume that the Hooker spring water is being transported through deep fractures, and flows to the surface from a focused conduit along the normal fault on the west side of the basin. The cold springs in the area are likely the results of the shallower aquifer within the conglomerate and artesian seeps due to elevated hydrostatic head resulting from recharge in the eastern-elevated side of the basin on the flank of the Winchester Mountains.

The uncorrected ^{14}C ages of groundwater at Ts02 (Hooker) and Tw07 (Willcox) are 14,600 years and 17,500 years, respectively. The $^{87}Sr/^{86}Sr$ ratios (0.711 and 0.714) indicate continental crust rock sources and similar age. The Sr concentrations (0.002 and 0.004 mg/l) are of the same low magnitude and indicate short-duration circulation or source rock depleted in strontium. Dissolved CO_2 was not detected in either Ts02 (Hooker) or Tw07 (Willcox). Low TDS (250 and 230 mg/l), very low Cl (3.4 and 6.4 mg/l), F (1.8 and 3.6 mg/l), and very low Na (59 and 63 mg/l) also indicate similar groundwater source conditions. The Cl-SO_4-HCO_3 ternary plots both Ts02 (Hooker) and Tw07 (Willcox) chemistry as balanced in reservoirs associated with (volcanic) peripheral waters. Groundwater at Hooker and Willcox well are of the sodium chloride-bicarbonate type. The Na-K-Ca (cation) geothermometer for Ts02 (Hooker) gives 167°C for a deep source temperature and the Quartz conductive geothermometer gives 92°C for a near reservoir temperature. The Na-K-Ca (cation) geothermometer for Tw07 (Willcox) gives 165°C for a deep source temperature and the Quartz conductive geothermometer gives 93°C for a near reservoir temperature. With the similarity in geology, geochemistry and isotoptic data, as well as deep source temperatures, the thermal reservoirs for Ts02 (Hooker) and Tw05 (Willcox) could well be within the same rhyolite formation.

Yuma

The Yuma area is a favorable target for geothermal exploration. The area is proximate to and probably actively involved in the Gulf of California-Salton Trough tectonic regime, which has numerous associated geothermal anomalies in neighboring California and Mexico. It seems likely that as a result of the nearby, active rifting in the Salton-Trough-Gulf of California, the pre-Tertiary basement rocks in the Yuma area may have a high degree of fracture permeability, making them potential geothermal reservoirs (Stone, 1981). Zones of anomalously warm water and a geothermal-gradient anomaly along northwest-trending faults suggest the occurrence of hydrothermal systems (Stone, 1981).

The geochemistry results show the uncorrected ^{14}C age of groundwater at Tw14 (Radium) is 23,400 years. The $^{87}Sr/^{86}Sr$ ratio (0.711) and the Sr concentration (1.634 mg/l) indicate source rock depleted in strontium. Dissolved CO_2 for Tw14 (Radium) was detected at a moderate concentration of 2,100 µg/l.

Moderate TDS (2,350 mg/l), Cl (730 mg/l), and Na (680 mg/l) were also detected. The Cl-SO_4-HCO_3 ternary plots Tw14 (Radium) as a reservoir associated with volcanic waters. The Na-K-Ca (cation) geothermometer for Tw14 (Radium) gives 75°C for a deep source temperature and the Chalcedony conductive geothermometer gives 62°C for a near reservoir temperature.

Kaiser and Cofer Hot Springs

Kaiser Hot Spring, Cofer Hot Spring discharge thermal water in the Big Sandy River drainage area. Kaiser Hot Spring discharges thermal water at 37°C from a 25m-wide breccia zone striking N 45° W. The breccia zone is in Precambrian granitic rocks underlying the silicic flows and flow breccias of the Kaiser Spring-Elephant Head volcanic field (Goff, 1979; Moyer, 1982).

Geochemistry data for Ts24 (Kaiser) gives an uncorrected ^{14}C age of groundwater at 29,000 years. The plotted $\delta^{18}O$-δD indicates inland accumulation at lower altitude or during a warmer climate. The $^{87}Sr/^{86}Sr$ ratios (0.726) and the Sr concentration (0.171mg/l) indicate source rock depleted in strontium. The dissolved CO_2 was detected at a very high concentration of 23,000 µg/l. Kaiser Hot Spring discharges as a sodium chloride-bicarbonate water with high fluoride (8.0 mg/l) and relatively low TDS (660 mg/l). The Cl-SO_4-HCO_3 ternary plots Ts24 (Kaiser) as associated with peripheral waters. The Na-K-Ca (cation) geothermometer for Ts24 (Kaiser) gives a deep source temperature of 134°C and the Chalcedony conductive geothermometer gives a near reservoir temperature of 95°C.

Ts17 (Cofer) discharges at temperatures about 32.6°C from clastic sediments in the Big Sandy Valley southeast of Wikieup. Results for Ts24 (Kaiser) gives an uncorrected ^{14}C age of groundwater at 10,200 years. The plotted $\delta^{18}O$-δD indicates inland accumulation at lower altitude or during a warmer climate. The $^{87}Sr/^{86}Sr$ ratios (0.718) and the Sr concentration (0.310mg/l) indicate source rock of continental crust origin and short duration circulation and depleted in strontium. The dissolved CO_2 was detected at a very high concentration of 20,000 µg/l. Cofer Hot Spring has a sodium chloride-bicarbonate water with low TDS (790 mg/l), Cl (150 mg/l), and Na (200 mg/l). The Cl-SO_4-HCO_3 ternary plots Ts24 (Kaiser) as associated with peripheral waters. The Na-K-Ca geothermometer gives a temperature of 80 °C for Ts17 (Cofer), while the Chalcedony geothermometer gives a temperature of 59°C.

Studies by Los Alamos scientists indicated that no high temperature convection systems exist in the Mohave region; rather, several widely scattered low to intermediate temperature systems (120°C) occur. The systems are probably the result of forced convective flows of meteoric water to sufficient depth to be heated by the regional geothermal gradient (Witcher and Stone, 1983). The chemical quality of these thermal waters is good, making them suitable for direct-heat applications.

Ringbolt

Ringbolt Hot Spring discharges from faults and fractures in mid-Tertiary volcanic rocks below the Hoover Dam area within the Lake Mead Recreation Area.

The uncorrected ^{14}C age for Ts18 (Ringbolt) groundwater is 13,700 years. The plotted $\delta^{18}O$-δD indicates inland accumulation at a higher altitude or during a colder climate. The $^{87}Sr/^{86}Sr$ ratio (0.711) indicates continent crust rock origins and relatively high Sr concentration (2.836 mg/l) can be attributed to long-duration circulation or a source rock rich in strontium. No dissolved CO_2 was detected. Ts18 (Ringbolt) groundwater is a sodium chloride-sulfate with high fluoride (8.8 mg/l), and moderate TDS (2,430 mg/l). Mg was detected at high concentration of 11 mg/l. The Cl-SO_4-HCO_3 ternary plots Ts18 (Ringbolt) as mature waters. The Na-K-Ca Mg corrected (cation) geothermometer for Ts18 (Ringbolt) gives a deep source temperature of 72°C. The Chalcedony conductive geothermometer gives a near reservoir temperature of 56°C.

Castle Hot Spring

Castle Hot Spring is located in the transition zone at the southeastern flank of the Bradshaw Mountains. The spring issues water at a rate of about 1,300 L/min (Witcher and Stone, 1982).

The uncorrected ^{14}C age for Ts23 (Castle) groundwater is 12,800 years. The plotted $\delta^{18}O$-δD indicates inland accumulation at higher altitude or during a colder climate. The $^{87}Sr/^{86}Sr$ ratio (0.713) indicates a continental crust rock source and the low Sr concentration (0.288 mg/l) can be attributed to short-duration circulation or a source rock depleted in strontium. Moderate concentrations of dissolved CO_2 were detected at 1,300 µg/l. Ts23 (Castle) groundwater is a sodium chloride-sulfate with high fluoride (8.8 mg/l), and relatively low TDS (630 mg/l). Mg was not detected above the reporting limit. This coincides to previously identified "Group I" thermal water emanating from the related fault system (Sheridan et al., 1980). The Cl-SO_4-HCO_3 ternary plots Ts23 (Castle) as associated with volcanic or steam heated waters. The Na-K-Ca geothermometer for Ts23 (Castle) gives a deep source temperature of 76°C. The Chalcedony conductive geothermometer gives a near reservoir temperature of 70°C.

The heat source for the low-temperature spring at Castle Hot Spring is most likely heating by deep circulation along normal faults. The thermal water rises along the fault where it cools conductively and mixes with colder groundwater from shallow aquifers, emerging at a temperature around 40°C.

Tonopah

Tonopah thermal well is in the western Phoenix Basin in Maricopa County. The uncorrected ^{14}C age for Tw22 (Tonopah) groundwater is 12,000 years. The plotted $\delta^{18}O$-δD indicates inland accumulation at lower altitude or during a warmer climate. The $^{87}Sr/^{86}Sr$ ratio (0.708) and low Sr concentration (0.012 mg/l) can be attributed to continental crust rock origin and short-duration circulation or a source rock depleted in strontium. No dissolved CO_2 was detected. Tw22 (Tonopah) groundwater is a sodium chloride-sulfate with high fluoride (8.8 mg/l), and low TDS (320 mg/l). Mg was not detected. The Cl-SO_4-HCO_3 ternary plots Tw22 (Tonopah) as associated with peripheral waters. The Na-K-Ca cation geothermometry for Tw22 (Tonopah) gives a deep source temperature of 144°C and a Quartz

conductive geothermometry (>150°C) gives a near reservoir temperature of 62°C, while the Chalcedony conductive geothermometer (100°C - 120°C) gives a near reservoir temperature of 29°C.

Agua Caliente Tucson

The Agua Caliente Park well is one of over 30 wells that produce thermal water >30°C in Tucson Basin. Agua Caliente discharges water at 30 to 32°C.

The uncorrected ^{14}C age dates Ts01 (Agua Caliente) groundwater at 7,493 years; the corrected ^{14}C age at 3,900 years. The plotted $\delta^{18}O$-δD indicates inland accumulation at lower altitude or during a warmer climate. The $^{87}Sr/^{86}Sr$ ratio (0.719) and low Sr concentration (0.295 mg/l) can be attributed to short-duration circulation or a source rock depleted in strontium. Moderate concentrations of dissolved CO_2 were detected at 4,000 µg/l. Ts01 (Agua Caliente) groundwater is a sodium-sulfate-bicarbonate with moderately high fluoride (5.8 mg/l), and low TDS (560 mg/l). Mg was not detected. The Cl-SO_4-HCO_3 ternary plots Ts01 (Agua Caliente) as associated with peripheral waters. The Na-K-Ca cation geothermometer for Ts01 (Agua Caliente) gives a deep source temperature of 77°C and a Chalcedony conductive geothermometer for a near reservoir temperature of 72°C.

Conclusion

The geochemistry and isotopic data were input into the Powell and Cummings (2010) geothermometry worksheets to investigate potential sources of geothermal waters and related geology for thermal springs throughout Arizona. The Powell and Cummings (2010) report calculates temperatures using various geochemical reactions and balance equilibrations. The report is included as Figure 7.1. The difference between the deep source and near reservoir temperatures most likely reflects cooling due to convection during upward movement to the near reservoir where mixing with cold meteoric water occurs.

Confirming results of numerous previous works by Witcher, Stone, and others, the Clifton geothermal reservoir shows the most promise for geothermal energy production, pointing toward a high temperature reservoir ranging from 128°C to 180°C. Wilcox well and Hooker's Hot Springs thermal water also reflect high temperatures for near reservoir geothermal water. The thermal waters in these areas are presumed to be fault controlled, allowing deep heated water to be transported to near source reservoirs and discharged from springs.

The Safford area has moderately-high temperature, deep source water, but cooler reservoir temperatures due to mixing with meteoric cold water, recharged through fractures in the surrounding mountains and from the Gila River.

Kaiser Hot Spring in the Transition zone shows high, deep source temperatures. Both Kaiser Hor Spring and Castle Hot Spring have thermal waters controlled by fault contact between basement rock and

volcanic rocks. The volcanic rock is fractured and serves as a near source reservoir. This is also reported to be the case for some of the other springs in or near the Transition zone.

Further study of some of the less sensitive (conservation or private) properties is warranted. Development of geothermal resources may provide hot water for electricity where temperatures exceed 100°C, while space heating and cooling, and industrial applications, including mining operations, are appropriate for temperatures less than 100°C. The inflow of saline water discharged into rivers from large volumes of high TDS thermal seeps could be reduced during power production, thereby improving water quality downstream and providing improved quality water supplies.

10. REFERENCES

Aiuppa A., Bellamo S., Brusca L., D'Alessandro W., and Federico C., 2003. Natural and anthropogenic factors affecting groundwater quality of an active volcano (Mt. Etna, Italy). Applied Geochemistry, v. 18, 863-882.

Anderson, T.A., and Silver, L.T., 1979. The role of the Mojave-Sonora Megashear in the tectonic evolution of northern Sonora: Geol. Soc. of America Guidebook-Field Trip No. 27, Geology of Northern Sonora, p. 59-68.

Anderson, T.W., 1995. Summary of the Southwest Alluvial Basins, Regional; Aquifer System Analysis, South-Central Arizona and Parts of Adjacent States. USGS Professional Paper 1406-a

Arizona Geothermal Commercialization Team, 1979. Geothermal development plan: Graham and Greenlee Counties: Arizona Bureau of Geology and Mineral Technology Open-File Report 79-10, 31 p.

Arizona Geothermal Commercialization Team, 1979. Geothermal development plan: Graham and Greenlee Counties: Arizona Bureau of Geology and Mineral Technology Open-File Report 79-10, 31 p.

Arnórsson, S. 2000. Isotopic and chemical techniques in geothermal exploration, development, and use: sampling methods, data handling, and interpretation. International Atomic Energy Agency, Vienna, Austria.

Arnórsson S., Stefánsson A., and Bjarnason J.Ö., 2007. Fluid-Fluid Interactions in Geothermal Systems. Reviews in Mineralogy and Geochemistry, v. 65, 259-312.

Barnett, P., Clotworthy, A., Bogie, I., Talebi, B. Khosrawi, K., 2005. Stage 2 Exploration and Development, NW Sabalan Geothermal Field, Iran. Proceedings World Geothermal Congress 2005.

Bath, A.H., Edmunds, W.M., Andrews, J.N., 1978. Paleoclimatic trends deduced from the hydrogeochemistry of a Triassic sandstone aquifer, United Kingdom, Isotope Hydrology 1978, Vol. II, IAEA, Vienna (1979) 545–567.

Bikerman, M., 1968. The geology of the Roskruge Mountains: Arizona Geological Society Guidebook III, p. 183-191.

Blacet, P. M. and Miller, S. T., 1978. Reconnaissance geologic map of the Jackson Mountain quadrangle, Graham County, Arizona: U. S. Geological Survey Miscellaneous Field Studies Map MF-939.

Brown, D.E., 2007. Clifton Hot Springs, Arizona: GRED III Final Report, Arizona Geological Survey Contributed Report CR-07-A.

Buehrer, T.F., 1927. The radioactivity of the thermal waters of Castle Hot Springs, Arizona. American Journal of Science, May 1, 1927 Series 5 Vol. 13:445-449.

Chiu, T.C., Fairbanks, R.G., Cao L., Mortlock, R.A. 2007. Quaternary Science Reviews 26, 18–36.

Clark, Ian, and Fritz, Peter, 1997. Environmental Isotopes in Hydrogeology, pub CRC Press LLC, Fla. P.343.

Coney, P. J., 1978. The plate tectonic setting of southeastern Arizona: In Callender, J. F., Wilt, J. C., and Clemons, R. E., eds., Land of Cochise, New Mexico Geological Society Guidebook, 29th Field Conference, pp. 285290.

Coney, P.J. (1980a) Cordilleran metamorphic core complexes. Geol Soc Am Mem 153:3–6.

Coney, P.J. (1980b) Cordilleran metamorphic core complexes. Geol Soc Am Mem 153:7–31.

Covington, H.R., 1980, Subsurface Geology of the Raft River Geothermal Area, Idaho: Geothermal Resources Council, Transactions, Vol. 4, p. 113-1150.

Craig, Harmon, 1961. Isotopic variations in meteoric waters. Science 133:1702–1703Creasey, S.C., and Krieger, M.H., 1978. Galiuro volcanics, Pinal, Graham, and Cochise Counties, Arizona: Journal of Research, U.S. Geol. Survey, v. 6, p. 115-131.

Craig, Harmon, 1963, The isotopic geochemistry of water and carbon in geothermal areas, E. Tongiori, ed., in Spolette Conference on Nuclear Geology and Geothermal Areas, Spolette, 1963: Rome, Consiglio Nazionale delle Recerche, 17 p.

Creasey, S.C., Banks, N.G., Ashley, R.P., and Theodore, T.G., 1977. Middle Tertiary plutonism in the Santa Catalina and Tortolita Mountains, Arizona: Journal of Research, U.S. Geological Survey, v. 5, p. 705-71.

Creasey, S. C. and Krieger, M. H., 1978, Ga1iuro volcanics, Pinal, Graham, and Cochise Counties, Arizona: U. S. Geological Survey Journal of Research, Vol. 6, No.1, p. 115-131.

Crumpler, L. S., 1978, Report on the reconnaissance geologic mapping of the Springerville volcanic field, August, 1978, unpublished report at the University of Arizona, Tucson, Arizona, 2 p.

Cunningham, E. B., Long, A., Eastoe, C., and Bassett, R.L., 1998. Migration of Recharge Waters Downgradient from the Santa Catalina Mountains into the Tucson Basin Aquifer, Arizona. Department of Geosciences, University of Arizona, Tucson. Hydrogeology Journal (1998) 6:94–103.

Damon, P. E., and associates, 1966, Correlation and chronology of the ore deposits and volcanic rocks: Atomic Energy Commission Ann. Rept. No. 1966 COO-689-60, University of Arizona.

Damon, P.E., 1968. Application of the potassium-argon method to the dating of igneous and metamorphic rocks within the Basin and Ranges of the Southwest: Ariz. Geol. Soc. Guidebook III, p. 7-22.

Damon, P.E., and Mauger, R.L., 1966. Epiorogeny-orogeny viewed from the Basin and Range Province: Soc. Min. Eng. Trans., v. 235, p. 99-112.

Damon, P.E., Erickson, R.C., and Livingston, D.E., 1963. K-Ar dating of Basin and Range uplift, Catalina Mountains, Arizona: in Nuclear Geophysics, Nat'l. Acad. Sci.-Nat'l. Research Council Pub. 1075, p. 113-121.

Damon, P.E., Shafiqullah, M., and Lynch, D. J., 1978. Late Cenozoic landscape developments in the Basin and Range Province of Arizona in Smiley, T. L., Péwé, T.L., Nations, J.D., Schafer, J.P. (eds.), Landscapes of Arizona: The Geological Story (in press).

Darton, Nelson Horatio, 1920. Geothermal data of the United States, including many original determinations of underground temperature, USGS Bulletin: 701. 97 p.

Davidson, E. S., 1973. Geohydrology and water resources of the Tucson basin, Arizona: U. S. Geological Survey Water Supply Paper 1939-E., 81 p.

Davis, G. H., 1978. Laramide folding and faulting in southeastern Arizona: submitted for publication, American Journal of Science.

Davis, G. H., and Coney, P. J., 1979. Geologic development of the Cordilleran metamorphic core complexes: Geology, Vol. 7, p. 120-124.

Dellechaie, Frank, 1976. A Hydrochemical Study of the South Santa Cruz Basin near Coolidge, Arizona, in Proceedings of the Second United Nations Symposium on the Development and Use of Geothermal Resources, Volume I, pp. 330-348.Drewes, H., 1972. Cenozoic rocks of the Santa Rita Mountains southeast of Tucson, Arizona: U.S. Geological Survey Professional Paper 746, 66 p.

Dickinson, W.R., 1991. Tectonic setting of faulted Tertiary strata associated with the Catalina core complex in southern Arizona. Geol Soc Am Spec Pap 264: 1–106

Drewes, H., 1972, Structural geology of the Santa Rita Mountains, southwest of Tucson, Arizona: U. S. Geological Survey, Professional Paper 748, 35 p.

Drewes, H., 1976. Laramide tectonics from Paradise to Hells Gate, southeastern Arizona: Arizona Geological Society Digest, v. 10, p. 151-167.

Drewes, H., 1978. The Cordilleran orogenic belt between Nevada and Chihuahua: Geological Society of America Bulletin, v. 89, p. 641-657.

Druitt, C.E., 1976. Mean Annual Temperature Map, State of Arizona. Arizona Geological Survey, OG-17, 1 map sheet.

Eastoe, Chris, 2014. University of Arizona Geoscience Department. Personnel communication.

Eastwood, R. L., 1970. A geochemical petrological study of mid-Tertiary volcanism in parts of Pima and Pinal Counties, Arizona, Ph.D. dissertation: Tucson, University of Arizona, 212 p.

Ellis, A. J., and Mahon, W. A. J., 1977. Chemistry and geothermal systems: New York, Academic Press, 392 p.

Elston, W. E., 1958. Burro uplift, northeastern unit of sedimentary basin of southwestern New Mexico and southeastern Arizona: America

Sheridan, Satkin and Wohletz, 1980. Thermal Resource Evaluation at Castle Hot Spring, Arizona

Epis, R.C., and Chapin, C.E., 1975. Geomorphic and tectonic implications of the post-Laramide, late Eocene erosion surface in the southern Rocky Mountains: Geological Society of America Memoir 144, p. 45-74.

Eriksson, E., 1965. An account of the major pulses of tritium and their effect in the atmosphere. Tellus 17:118–130

Feth, J.H., Roberson, C.E., and Polzer, W.L., 1964. Sources of mineral constituents in water from granitic rocks, Sierra Nevada, California and Nevada: U.S. Geological Survey Water-Supply Paper 1535-1, 70 p.

Faure, Gunter, 1986. Principles of Isotope Geology., 2nd edition, Wiley & Sons.

Fleischmann, D.J., 2006. New Mexico Geothermal Report. Published by the Geothermal Energy Association (GEA) for the U.S. Department of Energy, Geothermal Energy Association, September.

Fournier, R.O., 1981. "Application of water geochemistry to geothermal exploration and reservoir engineering," chapter 4 in Geothermal Systems: Principles and Case Histories (L. Rybach and L. P. J. Muffler, eds.), Wiley New York, 109-143.

Fournier, R.O., 1989.Lectures on geochemical interpretation of hydrothermal waters. UNU Geothermal Training Programme, Iceland.

Fournier, R.O., and Potter, R.W. II, 1982. An equation correlating the solubility of quartz in water from 25 °C to 900 °C, at pressures up to 10000 bars. Geochim. Cosmochim. Acta, 46, 1969-1974.

Fridriksson, Thráinn and Ármannsson, Halldór, 2004. Application of Geochemistry in Geothermal Resource Assessments. Presented at Short Course on Geothermal Development in Central America – Resource Assessment and Environmental Management, organized by UNU-GTP and LaGeo, in San Salvador, El Salvador, 25 November – 1 December, 2007

Garrels, R.M., 1967. Genesis of some groundwater from igneous rocks in Abelson, PhD., ed. Researches in geochemistry, v.2, New York, John Wileys, p. 405-420.

Gat, Joel R. and Gonfiantini, R., 1981. Stable isotope hydrology: deuterium and oxygen-18 in the water cycle: a monograph prepared under the aegis of the IAEA/UNESCO Working Group on Nuclear Techniques in Hydrology of the International Hydrological Programme.

Gerlach, T., and others, 1975, Geothermal water resources in Arizona: Feasibility study: U.S. Dept. Interior Office Water Resources Research Proj. A-054-Ariz., University of Arizona.

Geyh, Mebus A., F. D'Amore, G. Darling, T. Paces, Z. Pang, and J. Šilar, 2000. Environmental Isotopes in the Hydrological Cycle Vol 4, Principals and Applications, printed by International Atomic Energy Agency,

Geyh, Mebus A., F. D'Amore, G. Darling, T. Paces, Z. Pang, and J. Šilar, 2000. Environmental Isotopes in the Hydrological Cycle Vol 4, Principals and Applications, printed by International Atomic Energy Agency,

Giardina, Jr., S. and Conley, J.N., 1978. Thermal Gradient Anomalies, Southern Arizona. Arizona Geological Survey, Oil & Gas (OG) -27, 49 p., scale 1:1,382,400, 3 sheets.

Giardina, S. Jr. and Conley, J.N., 1978. Thermal Gradient Anomalies, Southern Arizona. Arizona Oil and Gas Conservation Commission, Phoenix, Arizona.

Giggenbach, W.F., 1988. Geothermal solute equilibria. Derivation of Na-K-Mg-Ca geoindicators. Geochimica et Cosmochimica Acta, Volume 52, Issue 12, December 1988, Pages 2749–2765.

Giggenbach, W.F., 1991a. Chemical techniques in geothermal exploration, in UNITAR/UNDP Guidebook: Application of geochemistry in resources development, 119-144.

Giggenbach, W.F., 1991b. The composition of gases in geothermal and volcanic systems as a function of tectonic setting, in Water-Rock Interactions, Kharaka and Maest eds., Balkema Rotterdam, 873-878.

Giggenbach, W.F. and Goguel, R.L., 1989. Collection and analysis of geothermal and volcanic water and gas discharges, DSIR report CD 2401, 4th ed., Pentone, New Zealand.

Gillespie, J.B., and Bentley, C.B., 1971. Geohydrology of Hualapai and Sacramento Valleys, Mohave County, Arizona: U.S. Geological Survey Water-Supply Paper 1899-H, 37 p.

Gilluly, J., 1956. General Geology of central Cochise County, Arizona: U.S. Geological Survey Professional Paper 287,169 p.

Goff, F. E., 1979, "Wet" geothermal potential of the Kingman-Williams region, Arizona: Los Alamos Scientific Laboratory Informal Report LA-7757-MS, 25 p.

Gootee, B.F., Mahan, M.K., and Love, D.S., 2012. A Summary of Reported Elevated Salinity Concentrations for Groundwater Samples Collected in Arizona, AZGS Open-File Report 12-26, 23 p.

Grose, L. T., 1977, Geology in geothermal energy exploration [abs.]: American Association of Petroleum Geologists Bulletin, v. 61, no. 5.

Hahman,W.R., 1978. Low-temperature Geothermal Reservoir Site Evaluation in Arizona, OFR 78-01.

Hahman, W. R., Sr., 1979. Geothermal energy in Arizona. Geothermal Energy, in press. Harris, R.C. 1998. Bibliography of Geothermal Resources in the San Carlos-Safford-Duncan Nonpoint-Source Management Zone, Arizona, Arizona Geological Survey Open-File Report 98-6.

Hahman, W.R., Sr, Mancini, F., White, D., Chebab, M., Goldstone, L., and Weibel, B., 1980, Evaluation of geothermal energy in Arizona - Final report by Arizona Geothermal Planning Team - Volume 2 of 2, January 1 - December 31, 1979: U.S. Department of Energy and Four Comers Regional Development Commission, 61 p.

Hahman, W.R., Sr, Mancini, F., White, D., Chebab, M., Goldstone, L., and Weibel, B., 1980. Evaluation of geothermal energy in Arizona - Final report by Arizona Geothermal Planning Team - Volume 2 of 2, January 1 - December 31, 1979: U.S. Department of Energy, and. Four Comers Regional Development Commission, 61 p.

Haigler, Leon B., 1969. Geothermal Resources, in Mineral and Water Resources of Arizona, Arizona Bureau of Mines Bulletin 180, pp. 575-580.

Harshbarger, J. W., 1972, Overview of geothermal resources potential in Arizona: Field notes, Arizona Bureau of Mines, v. 2, no. 2, p. 9-12.

Harmon, Craig, 1961. Isotopic variations in meteoric waters. Science 133 (3465): pp. 1702–1703. doi:10.1126/science.133.3465.1702. PMID 17814749.

Harris, R.C., 1998. Bibliography of geothermal resources in the San Carlos-Safford-Duncan Nonpoint-Source Management Zone, Arizona. Arizona Geological Survey Open File Report, OFR-98-06, 7 p.

Harris, Raymond, 1998. Bibliography of Geothermal Resources in the San Carlos-Safford-Duncan Non-point Source Management Zone, Arizona.

Harris, R.C., 1997. Distribution of evaporites and implications for water quality in the San Carlos-Safford-Duncan Nonpoint-Source Management Zone: Arizona Geological Survey Open-File Report 97-3, 56 p.

Hayes, P. T., 1969, Geology and topography, in Mineral and Water Resources of Arizona: Arizona Bureau of Mines Bulletin, 180, p. 50.

Hayes, P.T., 1970. Cretaceous paleogeography of southeastern Arizona and adjacent areas: U.S. Geological Survey Professional Paper 658-B, 42 p.

Heindl, L. A., 1967. Groundwater in fractured volcanic rocks in southern Arizona: in Hydrology of fractured rocks-Dubrovnik symposium, 1965 proc. Vol. 2, International Association of Sci. Hydrol. pub.74, p. 503-513.

Hem, J.D., 1970. Study and Interpretation of the chemical characteristics of natural water, US Geological Survey Water Supply Paper 1473, reprinted 2005 by University Press of the Pacific, Honolulu, Hawaii

Hurst, Richard W., 2010. Isotopic Tracers in Groundwater Hydrology, Hurst & Associates Inc. and the University of Arizona's SAHRA Isotopes and Hydrology Web Site (http://www.sahra.arizona.edu/programs/isotopes/.. SWHydro V.2 N1, Feature 2.

Hem, John, D., 1950. Quality of Water of the Gila River Basin above Coolidge Dam, Arizona: Geological Survey Water-Supply Paper 1104, 230 p.

Hem, l.D., 1950. Quality of water of the Gila River Basin above Coolidge Dam, Arizona: U.S. Geological Survey Water Supply Paper 1104, 230 p.

Houser, B.B., 1990. Late Cenozoic stratigraphy and tectonics of the Safford, Tonto, and Payson basins, southeastern and central Arizona, in Gerhels, G.E., and Spencer, lE., Geologic excursions through the Sonoran Desert region, Arizona and Sonora: Arizona Geological Survey Special Paper 1, p. 20-24.

Houser, B.B., Richter, D.H., and Shafiqullah, M., 1985. Geologic map of the Safford quadrangle, Graham County, Arizona: U.S. Geological Survey Miscellaneous Investigations Series Map 1-1617, scale 1:48,000.

Janecke, S.U., 1986. Structural geology and tectonic history of the Geesaman Wash area, Santa Catalina Mountains, Arizona. M.S. thesis, University of Arizona, 151 pp

Kalin, R.M., 1994. The hydrogeochemical evolution of the groundwater of the Tucson basin with application to 3-dimensional groundwater flow modeling. Ph.D. dissertation, University of Arizona, 550 pp.

Kanda, Isaac, 2011. Conceptual Model Based on Preliminary Observation of Ongoing Geothermal Resource Appraisal at the Domes Well Field, Olkaria, Kenya, Geothermal Resources Council Transactions Vol. 35, p. 1467-1473.

Karingithi, Cyrus W., 2009. Chemical Geothermometers for Geothermal Exploration. Kenya Electricity Generating Company Ltd.

Kennedy, B.M., Christenson, B. W.; Van Soest, M. C., 2010. Helium Isotopes in Geothermal Exploration, American Geophysical Union, Fall Meeting 2010, abstract #V23D-04.

Knechtel, M.M., 1935. Indian Hot Springs, Graham County, Arizona: Wash. Academy. Sci. Jour., v.25, p. 409-413.

Kruger, J.M., Johnson, R.A. and Houser, B.B., 1995. Miocene-Pliocene half-graben evolution, detachment faulting and late-stage core complex uplift from reflection seismic data in south-east Arizona, Basin Research, v.7, p. 129-149.

Laney, R. L.; Hahn, Mary Ellen, 1986. Hydrogeology of the eastern part of the Salt River Valley area, Maricopa and Pinal Counties, Arizona. USGS Water-Resources Investigations Report: 86-4147.

Lepley, L.K., 1978. Landsat lineament map of Arizona with emphasis on Quaternary fractures, in Low Temperature Geothermal Reservoir Site Evaluation in Arizona, Bureau of Geology and Mineral Technology, Tucson, Arizona, p. 63-91.

Lepley, L.K., 1979. Skylab Lineament Map of Arizona with Tec- tonic Model and Exploration Guide for Geothermal Resources, 1:500,000 scale, in Geothermal Reservoir Site Evaluation in Arizona, W.R. Hahman, Sr., ed., Bureau of Geology and Mineral Technology, Tucson, Arizona, p. 92-148.

Libby, W.F., Arnold, J.R., 1949. Science 23(110), 678-680.

Libby, W.F., 1971. History of tritium. In: Moghissi AA, Carter MW (eds) Tritium. Messenger Graphics/Las Vegas Publishers, Las Vegas, pp 3–11

Lindgren, Waldemar, 1905. The Copper Deposits of the Clifton-Morenci District, Arizona: U.S. Geological Survey Prof. Paper 43, Pl. 1, 1:62,500.

Lindgren, Waldemar, 1905. Description of the Clifton Quadrangle Arizona: U.S. Geological Survey Geological Atlas, Folio 129, 1:62,500.

Lindquist, J.C., 1992. Tritium analysis of groundwater to determine stream-channel recharge rates in the Tucson Basin.

Livington, D. E., Maucer, R. L., and Damon, P. E., 1968. Geochronology of the emplacement, enrichment, and preservation of Arizona porphyry copper deposits: Economic Geology, Vol. 63, p. 30-36.

Livingston, D. E., Mauger, R. L., and Damon, P. E., 1968. Geochronology of the emplacement, enrichment, and preservation of Arizona porphyry copper deposits: Econ. Geol., v. 63, p. 30-36.

Loring, A. K., 1976, The age of Basin-Range faulting in Arizona, in Tectonic Digest: Arizona Geological Society Digest, v. 10, p. 229-257.

Mann, Larry J., 1980. Maps showing hydrologic conditions in the San Francisco River area, Greenlee County, Arizona, 1978; a reconnaissance study: Open-File Report 80-441, 2 maps; 75 x 68 cm.

Mariner, R. H., et al., 1977. Chemical, Isotopic, and Gas Compositions of Selected Thermal Springs in Arizona, New Mexico, and Utah: U.S. Geological Survey Open File Report 77-654, 42 p.

Mariner, R.H. and Janik, C.J., 1995. Geochemical data and conceptual model for Steamboat Hills geothermal system, Washoe County, Nevada, Geothermal Resource Council Transactions.

Marjaniemi, D., 1968. Tertiary volcanism in the northern Chiricahua Mountains, Cochise County, Arizona: Arizona Geological Society Guidebook III, p. 209-214.

Maturgo, M., Zaide-Delfin, Layugan, D. and Catane, D., 2000. Characteristics of The Volcanic-Hydrothermal System In Mt. Labo, Philippines: Implications To Development, Proceedings World Geothermal Congress 2000.

Mauger, R. L., Damon, P. E., and Livingston, D. E., 1968. Cenozoic argon ages on metamorphic rocks from the Basin and Range Province: American Journal of Science, v. 266, p. 579-58.

McKay, W.A., 1981. Hydrogeochemical inventory and analysis of thermal springs in the Black Canyon-Hoover Dam area, Nevada and Arizona: Geothermal Resources Council, Transactions, vol. 5, p. 185-187.

Meinzer, O. E., 1924, Origin of thermal springs in Nevada, Utah, and southern Idaho: Journal of Geology, v. 32, p. 29.

Menges, C. M., Pearthree, P. A., and Calvo, S., 1982. Quaternary faulting in southeast Arizona and adjacent Sonora, Mexico (a.bs): Abstracts, 78th annual meeting Cordilleran Section, The Geological Society of America, April 19-21, 1982, Anaheim, California, p. 215.

Minissale, A. Duchi, V., Kolois, N., and Totaro, G., Verruchi, C. 1989. Geothermal Characteristics of Greek thermal springs. J. Volcanol. Geoth. Res. 39, pp.1-16.

Mohrbacher, C.J., 1984. Mountain-front recharge to the Tucson basin from the Santa Catalina Mountains. M.S. thesis, University of Arizona, 87 pp.

Morrison, R. B., 1969. Cenozoic rocks, in Mineral and Water Resources of Arizona: Ariz. Bur. Mines Bull. 180, p. 43-44.

Morrison, R. B., Menges, C. M., and Lepley, L. K., 1981, Neotectonic maps of Arizona: in Stone C. and Jenny, J. P., eds., Arizona Geological Society Digest, Vol: 13, p. 179-183.

Motzer, E.M., 2005. Age Dating Groundwater. Online Report. 2200 Powell St, Suite 225, Emeryville, CA 94608, pp4.

Moyer, T. C., 1982, The volcanic geology of the Kaiser Spring area, S. E. Mohave County, Arizona; Unpub.M. S. thesis, Arizona State University.220 p.

Muffler, L. J. P. and M. Guffanti (eds), 1979. Assessment of geothermal resources in the United States - 1978. US Geol. Surv., Circ. 790.

Norton and Gerlach, 1975. Nations Symposium on the Development and Use of Geothermal Resources, vol. 2, p. 1217-1229.

O ´Dochartaigh, B.E., MacDonald, A.M., Darling, W.G., Hughes, A.G., Li, J.X., Shi, L.A., 2010. Determining groundwater degradation from irrigation in desert-marginal northern China. Hydrol J 18:1939–1952

Olmsted, F.H., 1980. Temperature logs of wells and test wells in the Yuma area, Arizona and California, U.S.G.S. Open-file Report 80-335, 300 p.

Olson, M.C., 1982. Mountain-front recharge to the Tucson basin from Tanque Verde Canyon, Arizona. M.S. thesis, University of Arizona, 124 pp.

Oppenheimer, J. M. and Sumner, J. S., 1981. Gravity modeling of the basins in the Basin and Range Province Arizona: in Stone C. and Jenny, J. P., eds, Arizona Geological Society Digest,-Vol. 13, p. 111-115 with 1:1,000,000 scale, depth to bedrock map.

Owen-Joyce, S.J. and C.K. Bell, 1983. Appraisal of water resources in the Upper Verde River Area: Yavapai and Coconino Counties, Arizona: Arizona Department of Water Resources Bulletin 2, U.S. Geological Survey: Phoenix, AZ, 219 p., 3 plates.

Pashley, E.F., 1966. Structure and stratigraphy of the central, northern, and eastern parts of the Tucson basin. PhD dissertation, University of Arizona, 273 pp.

Peterson, R.C., 1968. Structural study of the East end of the Catalina fore range, Pima County, Arizona. PhD dissertation, University of Arizona, 105 pp

Poole, D. R., 1986. Aquifer geology of alluvial basins of Arizona, in T. W. Anderson and A. Ivan Johnson, editors, Regional Aquifer Systems of the United States; Southwest Alluvial Basins of Arizona, AWRA Monograph No. 7, American Water Resources Association, Bethesda, MD. pp. 27-36.

Powell and Cumming, 2010. Spreadsheets for Geothermal Water and Gas Geochemistry. Proceedings, Thirty-Fifth Workshop on Geothermal Reservoir Engineering, Stanford University, Stanford, California, February 1-3, 2010. SGP-TR-188

Rankama, Kelvervo and Sahama, Th. G., 1950. Geochemistry, Chicago Univ. Chicago Press, 912 p.

Rehrig, W.A., and Heidrick, T.L., 1976. Regional tectonic stress during the Laramide and late Tertiary intrusive periods, Basin and Range Province, Arizona: Ariz. Geol. Soc. Digest, v. 10, p. 205-2.

Rigby, Alan, 2014. Personal Communication. University of Utah Nobel Gases Laboratory

Robertson, F.N., 1991. Geochemistry of groundwater in alluvial basins of Arizona and adjacent parts of Nevada, New Mexico, and California. (Geological Survey professional paper; 1406-C.

Sauck, W. A. and Sumner, J. S., 1970. Residual aeromagnetic map of Arizona: Department of Geosciences, The University of Arizona.

Scarborough, R.B., and Peirce, H.W., 1978. Late Cenozoic basins of Arizona, in Callender, J.F., Wilt, J.C., and demons, R.E., eds., The Land of Cochise: New Mexico Geological Society field conference, 29th, Guidebook, p. 253-259.

Shafiqullah, M., Damon and other 1980. K-AR geochronology and geologic history of Southwestern Arizona and adjacent areas, in Jenny, J.P. and Stone, C. eds., Studies in Western Arizona: Arizona Geological Society Digest, vol. 12, p. 201-260.

Shafiqullah, M., Damon, P. E., and Peirce, H. W., 1976. Late Cenozoic tectonic development of Arizona Basin and Range Province [abs.]: 25th Intl. Geol. Congress, v. 1, p. 99.

Shafiqullah, M., Damon, P.E., Lynch, D.J. and Kuck, P.H., 1978. Mid-Tertiary Magmatism in Southeastern Arizona, New Mexico Geological Society Guidebook, 29th Field Conference, Land of Cochise, 1978.

Sheridan, M., Satkin, R.L., and Wohletz, K.H., 1980. Thermal Resource Evaluation at Castle Hot Spring, Arizona. Arizona State University Department of Geology. Arizona Geological Survey Open-File Report 80-5.

Siler, Drew L., Faulds, James E., Mayhew, Brett, and McNamara, David, 2014. Advancements in 3D Structural Analysis of Geothermal Systems, Search and Discovery Article #120141.

Siler, Drew L. and Faulds, James E., 2013. Play-Fairway Analysis for Geothermal Exploration: Examples from the Great Basin, Western USA. Abstract, Geological Society of America, 2013 GSA Annual Meeting in Denver: 125th Anniversary of GSA (27-30 October 2013) Denver, Colorado, USA, PP. No. 282-6

Silver, L. T., 1978. Precambrian formations and Precambrian history in Cochise County, Southeastern Arizona: in Land of Cochise, 29th Field Conference, New Mexico Geological Society Guidebook, p. 157-163.

Simpson, E.S., Thorud, D.B., Friedman, I., 1970. Distinguishing seasonal recharge to groundwater by deuterium analysis in southern Arizona. International Association of Hydrology, Pub. 92:112–121.

Sonny, Romain, 2010. Groundwater flow, heat and mass transport in geothermal systems of a Central Alpine Massif, PhD thesis to the faculty of Sciences of the University of Neuchâtel.

Stearns, N. D., and others, 1937. Thermal springs in the United States: U.S. Geol. Survey Water-Supply Paper 679-B.

Stone, C., and Witcher, J.C., 1983. Geothermal energy in Arizona; Final Report: Tucson, University of Arizona, Arizona Bureau of Geology and Mineral Technology Open-File report 83-12, 398 p.

Stone, Claudia, 1981. A Preliminary Assessment of the Geothermal Resource Potential of the Yuma Area, Arizona. Arizona Geological Survey Open-File Report 81-04.

Stone, Claudia, 1980. Springerville Geothermal Project Geology, Geochemistry, Geophysics Final Report, Arizona Geological Survey Open-File Report 80-04.

Stone, Claudia, Jones, Nile O., and Campbell, Alice, 1980. Preliminary Geothermal Assessment of the Yuma Area, Arizona, Arizona Geological Survey Open-File Report 80-13.

Stute, Martin, and Deák, Jozsef, 1989. Environmental Isotope Study (14C, 13C, 180, D, Noble Gases) on Deep Groundwater Circulation Systems in Hungary With Reference to Paleoclimate RADIOCARBON, VOL 31, No. 3, 1989, P III-XII.

Stuiver and Polach, 1977. Radiocarbon 19(3), 355-363.

Suemnicht, G.A., 1977. The geology of the Canada del Oro Headwaters, Santa Catalina Mountains, Arizona. University of Arizona, M.S. thesis, 108 pp

Swan, M. M., 1982. Influence of pre-Cretaceous structure upon late Cretaceous-Tertiary magmatism in southern Arizona and New Mexico (abs): Abstracts, 78th annual meeting Cordilleran Section, The Geological Society of America, April 19-21, 1982, Anaheim, California, p. 238.

Swanberg, C.A., Morgan, P., Stoyer, C.R., and Witcher, J.C., 1977. An appraisal study of adjacent areas in New Mexico and Utah and their value for desalination and other uses: New Mexico Energy Institute Tech. Compilation Rept. NME 1-6, 76 p.

Swanberg, C. A., and Morgan, P., 1978/79. The linear relation between temperatures based on the silica content of groundwater and regional heat flow: A new heat flow map of the United States: Pure and Applied Geophysics, vol. 117, p. 227-241.

Swanberg, C.A., 1975. The Mesa Geothermal Anomaly, Imperial Valley, California: a comparison and evaluation of results obtained from surface geophysics and deep drilling, in Proceedings, Second United

Swanberg, C.A., 1977. An appraisal study of the geothermal resources of Arizona and adjacent areas in New Mexico and Utah, and their value for desalinization and other uses: New Mexico Energy Institute report No 6, 76 p.

Swanberg, C.A., et a1. 1977. An Appraisal Study of the Geothermal Resources of Arizona and Adjacent Areas in New Mexico and Utah and Their Value for Desalination and Other Uses: New Mexico Energy Institute Report No.6, 76 p.

Thorman, C. H., 1981. Geology of the Pinaleño Mountains, Arizona a preliminary report: in Stone C. and Jenney, J. P. eds o , Arizona Geological Society Digest, Vol. 13, p. 5-11.

Tit1ey, S. R., 1976. Evidence for a Mesozoic linear tectonic pattern in southeastern Arizona: in Tectonic Digest, Arizona Geological Society Digest, Vol. X, p. 71-101.

Truesdell, A. H., Nathenson, M., Rye, R. O. 1977. The effects of subsurface boiling and dilution on the isotopic compositions of Yellowstone thermal waters. J. Geophys. Res. 82: 3694-3704.

Truesdell, A. H., and Hulston, J. R., 1980. Isotopic evidence on environments of geothermal systems, in P. Fritz and J. Ch. Fontes, eds., Handbook of environmental isotope geochemistry: New York, Elsevier Scientific Publishing Co., v. 1. 546 p.

Turner, G. L., 1962. The Deming axis, southeastern Arizona, New Mexico and Trans-Pecos, Texas: New Mexico Geological Society Guidebook-Mogollon Rinl, 13th Field Conference, 1962, p. 59-71.

Waring, G.A., 1915. Revised by Blankenship, R.R., and Bentall, R., 1965, Thermal springs of the United States and other countries of the world-a summary: US Geological Survey Professional Paper 491, 383 p.

Waring, G.A., revised by Blankenship, R.R., and Bentall, R., 1965, Thermal springs of the United States and other countries of the world-a summary: US Geological Survey Professional Paper 491, 383 p.

Webb, M. D.; Genereux, D. P.; Solomon, D. K., 2008. The Chemical and Isotopic Signature of Old Groundwater and Magmatic Solutes in a Costa Rican Rainforest: Evidence From Carbon, Helium, and Chlorine. American Geophysical Union, Fall Meeting 2008, abstract #H51C-0823

White, R.S. 1976. The determination of seasonal variations in groundwater recharge by deuterium and oxygen-18 analysis for the Tucson basin, Arizona. M.S. thesis, University of Arizona, 45 pp.

White, W.M., 2010. NOBLE GASES AND EVOLUTION OF THE ATMOSPHERE, Lecture 25, Spring 2003. Cornell University, Earth and Atmospheric Sciences 656, Isotope Geochemistry.

White, D. E., and Brannock, W. W., 1950, The sources of heat and water supply of thermal springs, with particular reference to Steamboat Springs, Nevada: Trans. Am. Geophys. Union, v. 31, no. 4, p. 566-574.

Wikipedia, 2014. Website accessed online at http://en.wikipedia.org/wiki/Isotope_geochemistry.

Wilson, E. D., Moore, R. T., and Cooper, J. R., 1969. Geologic map of Arizona: Arizona Bureau of Mines and U.S. Geological Survey.

Wilson, E.D., and Moore, R.I., 1959. Structure of the Basin and Range province in Arizona: Arizona Geological Society Southern Arizona Guidebook 2, p. 89-98.

Witcher, J.C., 1979a. Proven, potential and inferred geothermal resources of Arizona and their heat contents. Arizona Geological Survey Open File Report, OFR-79-05, 1 map sheet, map scale 1:500,000, 67 p.

Witcher, J. C., 1979b. A geothermal reconnaissance study of the San Francisco River between Clifton, Arizona and Pleasanton, New Mexico: State of Arizona Bureau of Geology and Mineral Technology Open-File Report, 18 p.

Witcher, J.C. 1979c. A Progress Report of Geothermal Investigations in the Clifton Area., Arizona Geological Survey.

Witcher, J.C. 1979d. Geothermal Reservoir Site Evaluation in Arizona progress report, Arizona Geological Survey OFR 79-2.

Witcher, J.C., 1981a. Geothermal resource potential of the Safford-San Simon basin, Arizona: Arizona Bureau of Geology and Mineral Technology Open-File Report 81-26, 131 p., 4 sheets, scale 1:250,000.

Witcher, J. C., 1981b. Geothermal energy potential of the lower San Francisco River region, Arizona: Arizona Bureau of Geology and Mineral Technology Open-File Report 81-07, 141p, 3 sheets, scale 1:250,000.

Witcher, J.C., 1982. Exploration for Geothermal Energy in Arizona Basin and Range, A Summary of Results and Interpretation of Heat Flow and Geochemistry Studies in Safford Basin, Arizona. AZGS OFR 82-05.

Witcher, J.C. and Stone, C., 1982. Geothermal Energy in Arizona, Arizona Geological Survey.

Witcher, J.C., 2008. Drilling and Exploration Plan, Geothermal Well Greenhouse-1, Willcox Greenhouse, Private Fee Minerals, Willcox, Arizona. AOGCC well permit 981, file.

Wright, J. J., 1971, The occurrence of thermal ground water in the Basin and Range province of Arizona, in Hydrology and Water Resources in the Southwest: Arizona Section American Water Resources.

Wynn, 1981. Principal facts for gravity stations and base-station net in the Silver City one-degree by two degree quadrangle, Arizona and New Mexico: U.S. Geological Survey Open-File Report OF-81-0040, 141 p.

Young, D.P., 1988. The history of deformation and fluid phenomena in the top of the Wilderness Suite, Santa Catalina Mountains, Pima County, Arizona. M.S. thesis, University of Arizona, 144 pp

Young, H.W. and Lewis, R.E., 1982. Hydrology and Geochemistry of Thermal Groundwater in Southwest Idaho and North-Central Nevada. USGS Prof. Paper 1044-J.

APPENDICES

APPENDIX A: NPS Permit and Annual Reporting

APPENDIX B: Laboratory Data

APPENDIX C: Summary of Results Tables

APPENDIX D: Powell & Cumming Geothermometer Workbook